Sapienza University of Rome Doctoral School of Neuroscience

PhD Program of Psychobiology and Psychopharmacology

Mechanisms of memory formation and consolidation in hippocampal and cortical pyramidal mouse neurons

Cicle XXV

Student: Sandra Colazingari

Tutor: Prof. Arturo Bevilacqua

Academic Year 2012/2012

CONTENTS

Abstract

The roles of hippocampus and cortex in recent and remote memory processing is well assessed and the association of experience-dependent behavioural modifications with hippocampal and anterior cingulate cortical (ACC) neuron morphological changes at different time points after contextual fear conditioning has been characterised. Although the association between such morphological modifications and biochemical changes related deserves further characterisation. Here, we have previously observed that during the formation of recent contextual fear memory, hippocampal CA1 neurons display morphological changes in parallel with rapid accumulation of EphrinB2, a cell adhesion factor known, in association with its receptor(s), to influence synaptic plasticity and the dynamics of dendritic spines. To investigate whether this process may represent a general marker of induced neuronal plasticity, we studied the conversion of recent -to-remote memory, which ultimately depends on an increase in dendritic spine number of pyramidal neurons of the anterior cingulate cortex (ACC), by analysing the effect of contextual fear conditioning on EphrinB2 levels in these neurons. To this end, we determined dendritic complexity and EphrinB2 levels 24 hours (recent), 7 days (imtermediate) and 36 days (remote) after conditioning in C57BL/6N mice. We observed that EphrinB2 accumulation parallels the increase in spine density of CA1 neurons of conditioned mice, at the recent and intermediate time point, subsequently decreasing at the remote time point. In addition, a similar parallel pattern was observed for neuronal EphrinB2 levels and dendritic complexity in the

ACC, which were both increased at the remote time point. The increase in EphrinB2 levels observed in the hipppocampus 24 hr post conditioning and in the ACC 36 days after was prevented by post-training anisomycin treatment. On the contrary, late anisomycin treatmen (24 days post conditioning) didn't prevent EphrinB2 increase in the cortex. These results suggest that accumulation of EphrinB2 is involved in memory-associated cellular modifications detected in both the hippocampus and ACC, and may therefore represent a more general biochemical marker of conditioning-induced neuronal rearrangements.

Chapter 1 – Learning, memory and underlying processes

1.1 Learning and memory

Memory is one of the most fundamental mental functions. It is the basis for thinking, feeling, perceiving, learning and is strongly involved in behavior. Without memory we would be capable only of reflexes and stereotyped behaviors, and for such reason learning and memory are subjects of intensive study in the field of neuroscience.

We define memory as a behavioral change caused by an experience, and define learning as a process(es) for acquiring memory. According to these definitions, there are different types of memory. One distinction, for instance, is that between declarative and procedural memory. In fact, some memories, such as those concerning events and facts, are available to our consciousness and thus defined as *declarative memory.* A different type of memory, called *procedural memory,* is not available to our consciousness and is needed, for example, to use a previously learned skill. Declarative memory and procedural memory are independent and can both be improved through exercise and practice.

In addition to memory as a result of complex activities, seen only in relatively intelligent animals, learning may occur as a result of *habituation* or classical conditioning, seen in many species. In any case, memory requires alterations to occur in the brain. The most popular candidate site for memory storage are synapses, where neurons communicate. Changes in the transmission efficacy at a synapse (synaptic and neuronal plasticity) have been considered to be the bases of memory. A particular pattern

of synaptic usage or stimulation, called the *conditioning stimulation,* is believed to induce synaptic and neuronal plasticity. Many questions remain to be answered, such as how synaptic plasticity is induced and how synaptic plasticity is implicated in learning and memory. Many studies concerning these issues are now in progress.

1.1.1 Associative and non-associative learning

At the beginning of the twentieth-century, Ivan Petrovič Pavlov and Edward Lee Thorndike defined two different types of non declarative learning, *associative* and *non-associative learning*. Non- associative learning involves repeated exposures to a single event and does not reflect learning of a relationship among multiple events (Pavlov, 1927).

Some exaples of non-associative learning are *habituation* and *sensitisation*. Eric kandel was one of the first to study the neural basis of habituation and sensitization based on his experiments on gill withdrawal of the seaslug *Aplysia californica* in the 1970s (see for example, Kandel et al., 2007).

Habituation is characterised by a progressive decrease in behavioral responses to a repeated stimulus. An animal first responds to a stimulus, but if it is neither rewarding nor harmful the animal reduces subsequent responses. Habituation is stimulus specific and training on one stimulus does not generalize to other stimuli unless the test stimuli are perceptually similar to the first. Dishabituation is the recovery of responsiveness to a stimulus that has undergone habituation training due to the recent occurrence of a more intense stimulus, detect as new.

Sensitization is the increase in responsiveness to a stimulus due to the exposition to another harmful stimulus. The potentiated startle response procedure nicely illustrates

the concept. In this situation, startle responding to the first presentation of an auditory stimulus (e.g., tone) is assessed

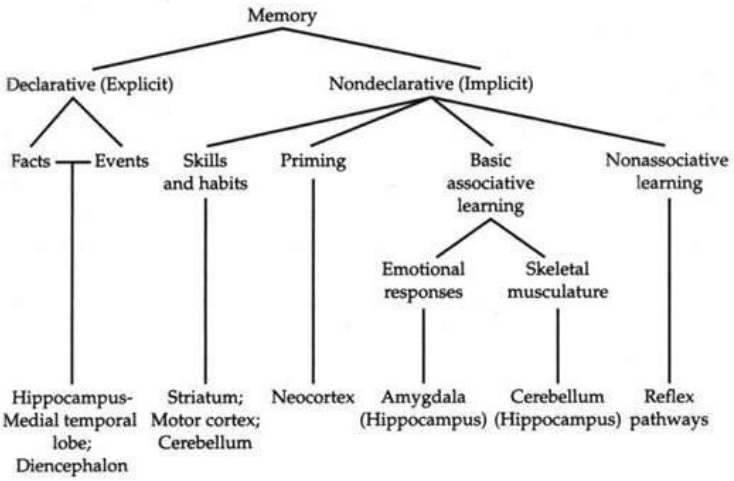

Fig 1.1 - Different types of long term memory. Richard F. Thompson, The brain. A Neuroscience Primer, 3rd edition, New YorkWorth Publishers, 2000, p. 365.

in two groups of rats. In the control group, the baseline level of responding is determined by simply presenting the tone to the rats and measuring the startle response. In the second group, experimental group, startle responding to the tone is assessed some time after presentation of some sensitizing event (like electric foot shock). The startle response in this group is increased relative to that seen in the control group.

In the associative learning, subject learn an association between two stimuli (classical conditioning) or a behavior and a stimulus (operant conditioning). Classical conditioning was described for the first time by Pavlov at the beginning of the twentieth-century, while studying

digestive process in dogs. He discovered that the simple viewing of meat makes a dog salivate, a reflexive response to food. He called meat the unconditioned stimulus (US) and salivation the unconditioned response (UR). Then Pavlov tried to ring a bell before presenting the meat. The first few times there was no UR, but after several pairings of the bell and food view, the dog learned that the bell was a cue indicating food presentation and began to salivate even without seeing the meat. In this example, the bell represented a conditioned stimulus (CS) and salivation to the ring was the conditioned response (CR) (Pavlov; 1927).

In classical conditioning, an organism learns to associate different stimuli. After repeatedly pairing between a US (which that elicits a response without conditioning) with another previously neutral stimulus (a CS, which does not normally evoke the response) the subject learns that the first stimulus is a cue for the second one and produces a CR. Temporal contiguity is necessary to obtain a conditioned response: the subject learns that the CS cames immediately before the US and this cen be generalized to a variety of stimuli and responses.

Pavlov then studied other fenomena linked to classical conditioning, such as extinction. Extinction is observed when the CR is no longer induced by a CS when this is presented repeatedly without pairings to a US. After successful conditioning, a dog's response to the bell can be extinguished by repeatedly ringing the bell but not presenting the food. The simplest explanation of extinction is that as the CS is presented without the in the absence of the US, the animal gradually "unlearns" the CS–US association which is known as the associative loss theory. However there is some fear restoration such as spontaneous recovery. The dog has not completely forgotten the association between the bell and the food. If the

experimenter waits a day after extinction training, the dog may have a spontaneous recovery of the conditioned response and salivate again to the bell (Pavlov, 1927).

Operant conditioning was first discovered by Edward Thorndike and subsequently studied by Burrhus Frederic Skinner. He believed that the best way to understand behavior is to look at the causes of an action and its consequences. The behavior of all animals is guided by its consequences. Operant conditioning is goal-oriented behavior. It is a process by which humans and animals learn to behave in such a way as to obtain rewards and avoid punishments. Reinforcement and punishment are the core tools of operant conditioning: the first one is a consequence that causes a behavior to occur with greater frequency; on the other hand, punishment is a consequence causing a behavior to occur less frequently. Skinner studied operant conditioning by conducting experiments using rats placed in a "*Skinner Box*". The box contains a lever in the side so that as the animal moves around the box, it would accidentally hit it. As the immediate consequence of such accident, a food pellet drops into a container next to the lever. The rats quickly learns to knock the lever after a few times of being put in the box. The consequence of receiving food (positive reinforcement) if they pressed the lever ensured that they would repeat the action again and again. By use of a similar box, Skinner also showed how negative reinforcement works: he subjected rats to an unpleasant electric current that ran in the floor of a skinner box and that would stops when a lever was pressed. The rats quickly learned to go straight to the lever after a few times of being put in the box. The consequence of escaping the electric current ensured that they would repeat the action again and again. Punishment is defined as the opposite of reinforcement since it's conseguence is to weaken or eliminate a response rather

than increase it. Like reinforcement, punishment can work either by directly applying an unpleasant stimulus like a shock after a response or by removing a potentially rewarding stimulus (Skinner, 1953; 1974).

1.1.2 Long and short term memory

Distinction between long and short term memory (LTM and STM) was introduced for the first time by Atkinson and Shiffrin (1968). According to their model called "the dual-store memory model", memories can reside in the short-term "buffer" for a limited time as their association are strengthened and transferred to LTM. Generally, STM keeps memories for a period of several seconds to a minute, until they are forgotten or transferred to the LTM. The capacity of STM is very limited: George A. Miller (1956) showed that the capacity of short-term memory was 7±2 item. Later experiments estimates that the capacity of short-term memory are lower, 4–5 items, but can be increased through a process called chunkings (Cowan, 2001). Although people can retain only about four different units in short-term memory, chunking can greatly increase a person's recall capacity. For example, in recalling a phone number of 10 digits, the person could chunk the digits into three groups: the first three digits, then the second three-digit chunk, and, last, a four-digit chunk. This method of remembering phone numbers is more effective than remembering a string of 10 digits.

On the contrary, the capacity of LTM can be incredibly large. It can store many quantities of information for potentially unlimited duration. For instance, people can remember a random seven-digit number, stored in the STM, only for a few seconds before forgetting. On the other hand, they can remember telephone numbers, stored in LTM, for many years through repetition. Short-term memory depends

on transient patterns of neuronal communication, instead LTMs are supported by more stable and permanent changes in neural connections. The transfer of items from short-term to long-term memory is called consolidation.

The multi-store model of Atkinson and Shiffrin has been criticised for being too simplistic. In 1975, Baddeley proposed an alternative model introducing the concept of "working memory", which, unlike STM, consist of three specific and active components: the central excutive, the phonological loop and the visuo-spatial sketchpad. Afterwards, the episodic buffer was added to this model. The central executive channels information to the three component processes: the phonological loop, the visuo-spatial sketchpad, and the episodic buffer. The phonological loop is responsible of the articulatory process: stores auditory information by silently rehearsing sounds or words in a continuous loop. The visuospatial sketchpad stores visual and spatial information. The episodic buffer is dedicated to integrate visual, spatial and verbal information across the other three domains. The episodic buffer is also assumed to have links to long-term memory and semantical meaning (Baddeley, 2000).

1.1.3 Declarative and procedural memory

Respect to the multi-store model of Atkinson and Shiffrin, LTM is also believed to be actually made up of multiple subcomponents, such as declarative memory (or explicit memory) and procedural memory (or implicit memory). Declarative memory refers to all memories that are consciously available and is divided in: episodic memory that refers to memory for specific event and semantic memory that includes memory for knowledge such as meaning of words and other concepts, unrelated to specific experiences. The notion of semantic memory was

first introduced by Endel Tulving, when he introduced a proposal to distinguish between episodic memory and what he termed semantic memory (Tulving, 1973).

Procedural memory refers to memory necessary to do things, used objects or do repetitive movements, such as use a pen or drive a car. Procedural memory guides the processes we perform and most frequently resides below the level of conscious awareness (Squire, 1987; Knowlton et al., 1996).

The process of learning and memory storage of explicit memory can be divided in four different step:

Encoding: the process through which facts and events are elaborated to be stored by being converted into a construct that can be stored within the brain and recalled later from short term or long term memory (Jensen and Lisman, 2005).

Consolidation: During consolidation transient memory become persistent and stable. It involves persistent changes in molecular structures that alter synaptic trasmission between neurons, for instance long-term potentiation (LTP). Consolidation of STM into LTM presumably involves two processes at the molecular level: synaptic consolidation and system consolidation (Dudai 2006).

Storage: refers to the process through which acquired memory traces are manteined in different brain structures.

Retrieval: refers to the process of recalling information that is stored in memory.

Declarative memories are encoded by the hippocampus, entorhinal cortex and perirhinal cortex, but consolidated and stored elsewhere. The precise location of storage is unknown but recent observations suggest that cortical areas are involved in such allocation process (Restivo et al., 2009; Colazingari et al., manuscript in preparation). Implicit memory involves the cerebellum, amygdala and the striatum. (Thompson and kim, 1996; Squire, 2004).

1.1.4 Memory systems and localization in the brain

Until the 19th century, memory was assigned to the whole cortex without any specialization. First evidences that different forms or aspects of learning and memory involve different brain systems came from Wilder Panfield's studies. He stimulated the brain of patients with electrical probes and observed their responses. In this way he could more accurately target the areas of the brain responsible of different effects and create maps of the sensory and motor cortices of the brain (cortical homunculus) (Panfield, 1952). He also reported that stimulation of the temporal lobes could lead to vivid recall of memories. Other evidences of specific localization of memory in the brain came from the case of a patient, named H.M. studied by Milner. The left and right medial temporal lobes of this patient were surgically removed. After the surgery, he suffered from severe anterograde amnesia, in particular he was impaired in his ability to form new semantic knowledge (Scoville and Miller, 1957). He could not commit new events to his explicit memory, although his working memory and procedural memory were intact. H.M. was influential not only for the knowledge he provided about memory impairment and amnesia, but also because it allowed a good understanding of how particular areas of the brain may be linked to specific processes. In particular, his apparent ability to complete tasks that require recalls from procedural memory and short term memory but not long term episodic memory, suggests that retrieval from these memory systems may be mediated, at least in part, by different areas of the brain (Milner et al., 1968; Milner, 1972).

Similarly, the fact that H. M. only had problems with long term memory but with an intact short term memory, clearly demonstrate that these two phenomena are supported by different hardware. Furthermore, the fact that H. M. had

intact memories from his childhood, but could not remember anything new shows that the structures in which memories are stored are different from those in which they are encoded, and hippocampus probably plays a role in the latter. H. M.'s heavy impairment in certain spatial tasks provides further evidence for the association of the hippocampus with spatial memory (Kolb and Whishaw, 1996).

There are other dissociations discovered on H. M., for instance about motor and skill learning. Milner trained H. M. on a mirror-drawing task. This task involves tracing some figure on the paper by only seeing the mirror image of the drawing. Normal people are initially pretty bad at this task, but they can get better with training. H. M. had a normal learning curve for this task. On later days, even though he denied having performed the task previously, he retained his skill, showing nearly normal improvement from session to session. H. M. was able to learn the procedures necessary to perform this cognitive skill, even though he did not have any declarative memory of performing the task. The distinction between procedural and declarative learning may be one dichotomy to explain these findings (Milner, 1972).

Current views recognize a number of different forms or aspects of learning and memory involving different neural systems in the brain. On the other hand it is likely that under normal conditions many or all of these brain–memory systems are engaged to some degree in most learning situations. Thus, explicit memories for experience involve the hippocampus medial temporal lobe system and implicit basic associative learning and memory involves the cerebellum, amygdala, and other systems. Under normal conditions, however, many of these brain–memory systems are engaged to some degree in learning situations. But each

of these brain systems is learning something different about the situation (Thomson and Kim, 1996).

1.2 Hippocampus and memory

1.2.1 Hippocampal anatomy

The hippocampus is a component of the limbic system and plays important roles in consolidation of information from short-term memory into long-term memory and in spatial navigation. It is closely associated with the cerebral cortex and is composed of three main parts: the Ammon's horn, the dentate gyrus (DG) and the subiculum. The Ammon's horn area (cornu Ammonis, CA) is further divided into CA1, CA2 and CA3 areas. The DG is a tightly packed layer of small granule cells instead the CA areas are all filled with densely packed pyramidal cells similar to those found in the neocortex (Amaral and Lavenex, 2006). The cortical region adjacent to the hippocampus is known collectively as the parahippocampal gyrus (or parahippocampus) (Eichenbaum et al., 2007). It includes the entorhinal cortex (EC) and the perirhinal cortex. Within the hippocampus, the flow of information from the EC is largely unidirectional, with signals propagating through:

- perforant path: the EC axons project densely to the granule cells in the DG.
- mossy fibers path: the DG cell axons (called mossy fibers) pass on the information from the EC to the apical dendrite of CA3 pyramidal cells.
- Schaffer collaterals path: the CA3 axons pass signals to the CA1 layer. Pyramidal cells of CA1 send their axons to the subiculum and deep layers of the EC.

The perforant path-to-DG-to-CA3-to-CA1 was called the trisynaptic circuit by Per Oskar Andersen (Andersen et al.,

1971).

In addition to the EC, hippocampus receives imputs from other cortical regions such as retrosplenial cortex and

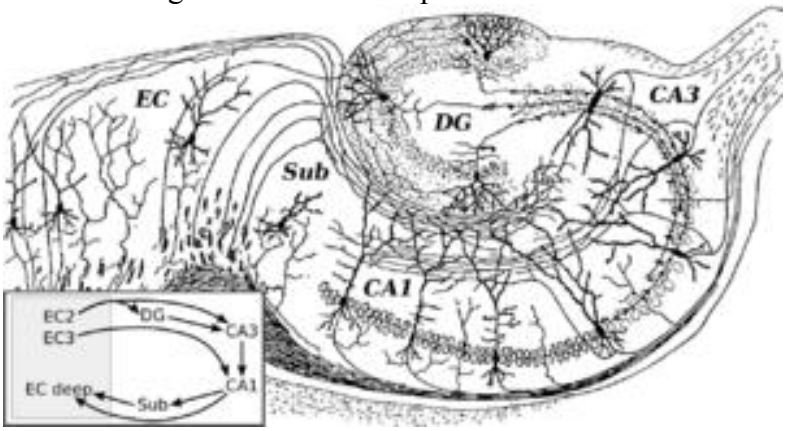

Fig. 1.2 - Hippocampal circuits. (Santiago Ramon y Cajal (1911) Histologiedu Systeme nerveux de l'Homme et des Vertebres Paris: A. Maloine)

cingulate gyrus. Moreover, the hippocampus also receives a number of subcortical inputs. These inputs include the amygdala (specifically the anterior amygdaloid area, the basolateral nucleus, and the periamygdaloid cortex), the thalamus, the hypothalamic areas, the supramammillary and retromammillary regions, the ventral tegmental area, the raphe nuclei (the nucleus centralis superior and the dorsal raphe nucleus), the nucleus reticularis tegmenti pontis, the dorsal tegmental nucleus, and the locus coeruleus.

Hyppocampal neurons use glutamate as the excitatory neurotransmitter and GABA as the inhibitory neurotransmitter (Megías et al., 2001) The hippocampus receives modulatory inputs from the serotonin,

norepinephrine and dopamine systems. A very important projection comes from the medial septal area, which sends cholinergic and GABAergic fibers to all parts of the hippocampus (Wilson et al., 1994).

1.2.2 Hippocampus and memory

Ever since the description of the well-known amnesic patient H.M. by Scoville and Milner, intense research has focused on defining the role of the hippocampus in declarative memory and acquisition of new memories.

There is now a consensus that the human hippocampus is involved in episodic memory (O'Keefe and Nadel, 1978; Squire and Alvarez, 1995; Eichenbaum and Cohen, 2001). A number of studies have been reported in which animals were trained at different times before the hippocampal formation or the fornix were experimentally damaged (Ramos, 1998; Squire et al., 2001). Animals with hippocampal damage typically have impaired memory for information learned just before and after surgery, but not for information learned more remotely.

These findings suggest that the hippocampus (and related structures) is necessary for memory storage and retrieval for only a limited time after learning. Initially, the hippocampus serves to encode and consolidate memory and to reactivate memory for retrieval. Over time and through a process of reorganization, the connections among the cortical regions are progressively strengthened until the cortical memory can be reactivated and retrieved independently of the hippocampus (Squire and Alvarez, 1995).

The hippocampus was also linked to emotional regulation by Papez in 1937, who hypothesized that increased anxiety and aggression following rabies infection could be attributed to damaged hippocampal circuits. The Papez circuit was ultimately linked to memory formation, rather than the

control of emotionality, but this work established a connection between negative emotion and the hippocampus.

Moreover the hippocampus has been studied extensively for its role in spatial learning and navigation. The spatial theory was initially proposed by O'Keefe and Nadel. In 1970s they discovered 'place cells', neurons in the rat hippocampus that appeared to show activity related to the rat's location within its environment (O'Keefe and Nadel, 1978).

O'Keefe and co-workers continued to investigate this question, despite skepticism from other scientist, and there is now almost universal agreement that spatial coding plays an important role in hippocampal function.

The discovery of place cells led to a theory that the hippocampus might act as a cognitive map, a neural representation of the layout of the environment (O'Keefe and Nadel, 1978). Several lines of evidence support this hypothesis. Many observation showed that without a fully functional hippocampus, humans may not remember where they have been and how to get where they are going (Chiu et al., 2004). Studies with animals have shown that an intact hippocampus is required for initial learning and long-term retention of some spatial memory tasks, particularly ones that require finding the way to a hidden goal (Morris et al., 1982; Sutherland et al., 1982; 2001; Clark et al., 2005).

1.3 Plasticity

Synaptic plasticity is the ability of chemical synapses to change their strength in response to their use or disuse of transmission over synaptic pathways (Hughes, 1958).

The first scientist suggesting plasticity in the number and strength of neural connections as the physical basis of learning and the support of memory was Santiago Ramón y Cajal, whose intuition led him to infer the function of the

nervous system from its morphology (Ramòn y Cajal, 1891).

In 1949 the psychobiologist Donal O. Hebb proposed the Hebbian theory according to which an increase in synaptic efficacy arises from repeated and persistent pre-synaptic stimulation of the post-synaptic neuron. Therefore simultaneous activation of cell pairs leads to pronounced increases in their inter-synaptic strength (Hebb, 1949).

In 1966, Terje Lømo observed for the first time that brief trains of electrical stimuli increased the efficacy of synaptic transmission between the perforant path and the granular cells of the hippocampal dentate gyrus in anesthetized rabbits. Some years later, in 1973, Lømo and the British scientist Timothy Bliss discovered that a moderately high frequency of stimulation in the same hippocampal pathway produced a stable and lasting increase of the synaptic responses, which was named LTP (long-term synaptic potentiation) (Bliss and Lømo, 1973). Further studies confirmed LTP, not only as a lasting, but also as a quick-induction phenomenon, with associative and stimuli-specificity features which made it a good candidate for a cellular mechanism of learning and memory.

Nowadays LTP is widely considered one of the major cellular mechanisms that underlies learning and memory (Cooke and Bliss, 2006).

1.3.1 Long term potentiation

Long-term potentiation (LTP) is one of different mechanisms underlying synaptic plasticity and consist of a long-lasting enhancement in signal transmission between two neurons that results from stimulating them with trains of high frequency electrical stimuli.

LTP has been observed in different neural structures, such as the cerebral cortex, cerebellum, amygdala (Clugnet

and LeDoux, 1990). Molecular mechanisms of LTP are different in the different areas of the brain. Infact, LTP in the Schaffer collateral pathway of the hippocampus is NMDA receptor-dependent instead LTP in the mossy fiber pathway is NMDA receptor-independent (Harris and Cotman, 1986).

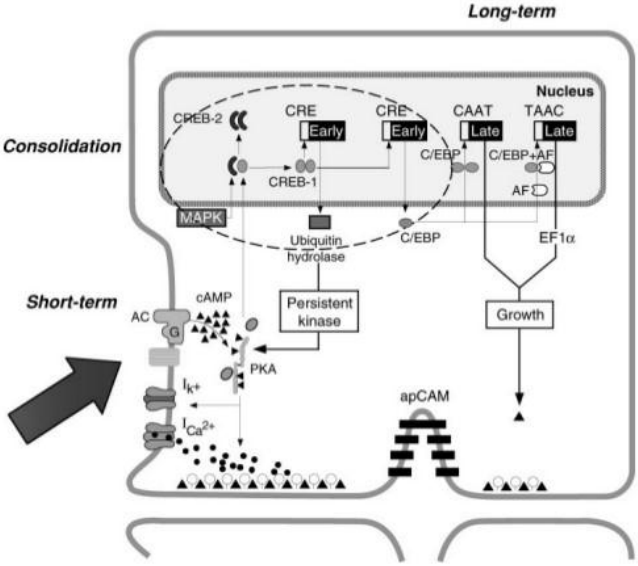

Fig 1.3 - The standard model long LTP. (Dudai et al., 2002)

The CA1 area of the hippocampus has become the prototypical site of mammalian LTP studies and is characterize by a specific signalling pathways. Synapses activation generates a rapid (time of milliseconds) pre-synaptic releasing of glutamate which activates ionotropic AMPA receptors (AMPAr) in the post-synaptic membrane, producing an influx of Na^+ which depolarizes the post-synaptic neuron (Lamprecht and LeDouxand, 2004; Xia and Storm, 2005; Penzes et al., 2008). Subsequently, that local

post-synaptic depolarization allows N-methyl-D-aspartate receptors (NMDAr) to remove the Mg^{2+} ions that block them, thus giving rise to a large influx of Ca^{2+} in the post-synaptic neuron through the NMDAr channels themselves. This massive Ca^{2+} influx activate several protein kinases such as calcium/calmodulin-dependent kinases (CaMKs), calcium/phospholipid-dependent kinase (PKC), cAMP-dependent kinase (PKA), or extracellular signal-regulated kinase (ERK). Moreover some protein phosphatases, like PP1, can also serve as negative regulators (Yong-Seok and Silva, 2009). PKA activation in turn activates CREB (cAMP response element binding protein) transcription factor and the synthesis and availability of other transcription factors in the neuronal nucleus such as c-fos, ARC, c-jun and other early genes (West et al., 2002; Abel, and Nguyen, 2008; Zheng and Keifer, 2009). Activation of CaMKs, and of CamKII in particular, induces within minutes from the NMDAr opening morphological changes in the neuronal cytoskeleton, so that new dendritic spines or persistent enlargements of existing spine heads are produced (Park et al., 2006). All these events culminate in synaptic remodeling and neuronal plasticity, which is assumed to make the trace stable.

1.3.2 Dendritic spines and plasticity

Dendritic spines are branched protoplasmic extensions which are the major site of excitatory synaptic transmission in the vertebrate brain. Dendritic spines are small protrusions from the dendrite surface with head volumes ranging from 0.01 μm^3 to 0.8 μm^3 that are first formed in early postnatal life, shaped up by the animal's experience, and maintained into adulthood. Spines are classified by their shape in "thin", "stubby", "mushroom" and "branched".

There is a continuum of shapes between these categories. Time-lapse imaging of spine dynamics visualized with genetically engineered fluorescent proteins revealed that the spines are not static, but actively move, and alter their morphology continuously even in the adult brain, reflecting

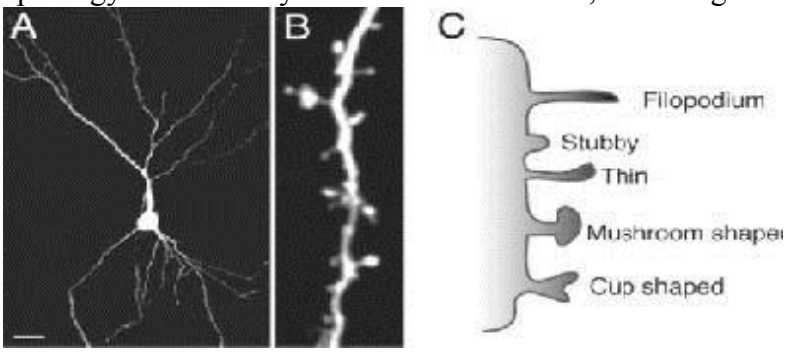

Fig 1.4 - Different shapes of dendritic spine. (Lippman and Dunaevsky, 2005).

the plastic nature of synaptic connections (Matus, 2000; Holtmaat et al., 2005). Spines with strong synaptic contacts typically have a large spine head, which connect to the dendrite via a membranous neck. The variable spine shape and volume is thought to be correlated with the strength and maturity of the synapse it bears.

Different experimental research on the initiation and maintenance of synaptic plasticity, particularly in CA1 pyramidal neurons of the hippocampus, have shown that certain types of learning, as well as artificially induced LTP, can produce increases or morphological changes in dendritic spines giving rise to new synapses or strengthening existing ones, which could constitute the main structural basis of memory (Matsuzaki et al., 2004; Harvey et al., 2007). Morphological alteration of excitatory synapses is one of the most important and efficient cellular mechanisms

underlying plasticity of neural functions (Engert et al., 1999).

The cytoskeleton of dendritic spines is particularly important in neuronal plasticity; without a dynamic cytoskeleton, spines would be unable to rapidly change their volumes or shapes in responses to stimuli. The cytoskeleton of dendritic spines is primarily made of filamentous (F) actin. Spine maintenance and plasticity depend on different factors. Actin regulators, small GTPases such as Rac, RhoA and CDC42, rapidly modify spine cytoskeleton and morphology (Pak et al., 2003); activity of NMDAr is involved in spine growth and stability (Fischer et al., 2000; Lin et al., 2004) and low levels of AMPAr activity is necessary to maintain spine survival.

1.4 Ephrins and spines

New spines grow before establishing a synaptic contact, so an important question is to understand how they select their partner and stimulate their differentiation into a presynaptic terminal. Adhesion molecules, like cadherins and ephrins, are likely candidates to contribute to this process (Arikkath et al., 2008; Rao et al., 1998, Kullander and Klein, 2002). Ephrin ligands and their Eph receptors are highly expressed in the developing nervous system, where they have well-known roles in the establishment of neuronal connectivity by guiding axons to the appropriate targets and regulating the formation of synaptic connections (Pasquale, 2005; Poliakov et al., 2004; Luo and Flanagan, 2007).

In mammals, Eph receptors are divided in two classes: EphA, with nine members and EphB, with five members (Klein, 2009), respectively binding EphrinAs (five members) and EphrinBs (three members), with the exception of EphA4, which can bind both A and B type ligands (Pasquale, 2008). A distinctive feature of Eph-ephrin

complexes is their ability to generate bidirectional signals that affect both the receptor expressing and ephrin-expressing cells (Pasquale, 2005). Eph receptor "forward" signaling depends on the tyrosine kinase domain, which mediates autophosphorylation as well as phosphorylation of other proteins, and on the associations of the receptor with

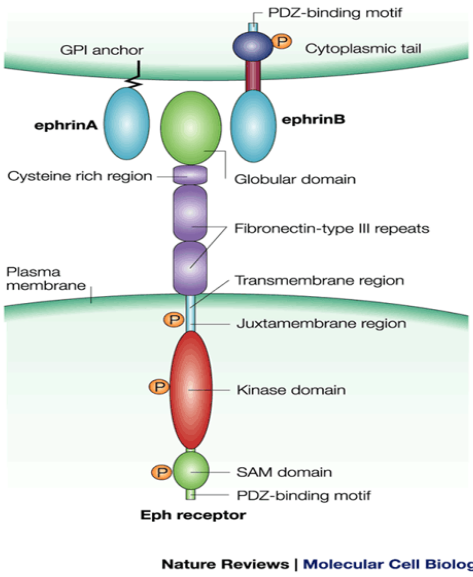

Fig 1.5 - Rapresentative Eph-Ephrin complex.(Kullander and Klein, 2002)

various effector proteins. Ephrin-B "reverse" signaling also depends in part on tyrosine phosphorylation of the ephrin cytoplasmic region (mediated by Src family kinases and some receptor tyrosine kinases) and on associated proteins. Most Eph receptors and the B-type ephrins also have a carboxy-terminal PDZ domain-binding site, which is particularly important for the physiological functions of

ephrinB (Egea and Klein, 2007). Activity of EphrinBs and EphB receptors, in particular, has been directly associated to molecular mechanisms of synaptic plasticity. In cultured rat hippocampal or cortical neurons, for instance, EphB receptors have been shown to be expressed postsynaptically and to interact with presynaptic EphrinBs, regulating initial steps in the formation of synaptic connections (Rao et al., 1998; Dalva et al., 2000). In particular, the interaction of postsynaptic EphB receptors with EphrinB2 potentiates activity of glutamate NMDA receptors suggesting a possible pathway for the involvement of these factors in synaptic plasticity (Takasu et al., 2002). At the same time, EphrinBs/EphB receptors may also act in a reverse fashion as observed in the hippocampus, where EphrinB ligands are expressed postsynaptically suggesting their involvement in the regulation of synaptic transmission and plasticity by interaction with presynaptic receptors (Grunwald et al., 2001). In situ RNA hybridisation data show that, while EphrinB1 expression is barely detectable in CA areas, both EphrinB2 and EphrinB3 are strongly expressed in CA1, and at a much lesser extent in CA3 (Grunwald et al., 2001). At these synapses, EphrinB2 and EphrinB3 have been found to functionally interact with NMDA receptors, being functionally necessary for LTP and LTD development, as demonstrated in genetically modified mice (Grunwald *et al*., 2004). Interestingly, immunohistochemical analysis of EphrinB2 in the hippocampus has revealed a uniform distribution of the factor in the neuronal layer of all CA areas (Migani et al., 2007). This observation, in strong contrast to previous in situ RNA hybridisation results, suggests the possibility that mechanisms of post-transcriptional regulation act on expressed mRNAs to control proper levels of the factor depending on cell activity, such as rapid translation of Ephrinb2 mRNA as a

consequence of synaptic and neuronal plasticity.

1.5 Consolidation of memory

Consolidation is the progressive post-acquisition stabilization of long term memory, as well as the memory phase(s) during which such presumed stabilization takes place (Dudai, 2002). It has long been suggested that fresh memories need time to stabilize, and that often, such traces are prone to interference by distracting stimuli, injuries, or toxins which, however, lose their effectiveness along with time.

The term "consolidation" is attributed to Muller and Pilzecker, who showed, in a series of studies carried out between 1892 and 1900, that memory takes time to fixate (Muller and Pilzecker 1900). Their evidence was based on systematic search for the laws that govern the acquisition and retrieval of verbal material. They discovered that the correct recalling of the target material is improved during the first few minutes after training, and that new stimuli presented during the first minutes after training tend to impair the recalling of target material. They suggested that there is a post-training interval during which associations consolidate in memory.

A few years later, Burnham further elaborated this idea. He suggested that the processes of organization and assimilation of memory need time to take place (Burnham, 1903). Burnham's "time" actually refers to two different types of consolidation kinetics: fast, such as unveiled by the studies of Muller and Pilzecker, and slow, such as unveiled by the observations of residual premorbid memory in global amnesics. This temporal dichotomy suggests that the generic term "consolidation" conceals two different types of processes and mechanisms: the synaptic consolidation,

which take place within the first minutes-to-hours after learning and is hippocampal-dependent, and system consolidation, which takes much longer and in which memories that initially depend on the hippocampus undergo reorganization and become hippocampal-indipendent

1.5.1 Synaptic consolidation

Synaptic consolidation has been described in all species both *in vivo* and in *in vitro* cultured neurons. According to the standard model of synaptic consolidation, memory traces can exist in at least two forms: short-term and labile, long-term and stable (Hebb, 1949). The short-term trace may mature into a long-term form or decay. The physiological conditions giving rise to the long-term form are not yet fully identified but long term memory is the conseguence of two or more inputs, including neuromodulatory ones, that promote synaptic consolidation (McGaugh, 2002). Information leads to modification of synaptic proteins by activation of intracellular signal transduction cascades, activation of transcription factors, modulation of gene expression at synapses and cell body, reorganization of synaptic proteins including membrane receptors and cytoskeletal elements, all together culminating in synaptic remodeling and growth, which is assumed to make the trace stable (Park et al., 2006). The activation, expression, and function of certain transcription factors and early genes is an essential part of the cascade of events occurring transiently immediately after training, and can be disrupted by several types of agents, like inhibitors of protein synthesis. The process involves not only the synapse but also the cell body and nucleus and similar ubiquitous intracellular signaling cascades, such as the cAMP and the mitogen-activated protein kinase (MAPK) cascades, are recruited, and at the end of the process cellular remodeling and growth occur

(Deisseroth et al., 1996; Bailey et al., 2004).

1.5.2 System consolidation

According to the standard model of consolidation, long-term memories depend on the hippocampus and related structures for their encoding (recent memory). The stabilization of these internal representations is assumed to involve synaptic consolidation, which is achieved within minutes-to-hours. In

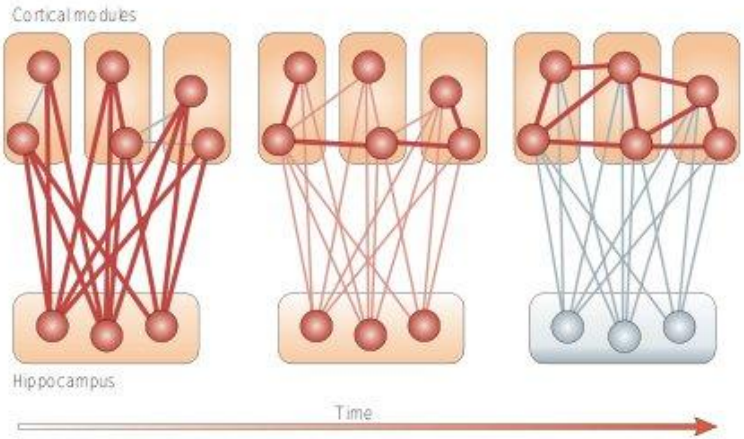

Fig 1.6 - Standard model of system comunication (Frankland and Bontempi, 2005)

parallel, a process of system consolidation is initiated. In this process memory traces reorganize over a period of weeks, shifting to the neocortex (i.e. the anterior cingulate cortex, ACC, Restivo et al., 2009), so that at the end of the process the neocortex can independently maintain the specific memories (remote memory). What triggers system consolidation is still unknown, but the hypothesis is that, upon recurrent activation of hippocampal trace over time,

the hippocampus sends synaptic messages to neocortical neurons, triggering synaptic consolidation.

Many evidences support the theory of system consolidation. Infact the temporally graded retrograde amnesia in many human patient is most often associated with damage to the medial temporal lobe, including the hippocampus; on the other hand, flat extensive retrograde amnesia usually involves damage to neocortex in the lateral and anterior temporal lobe (Squire et al., 2001). Furthermore, amnesic patients with lesions in the medial temporal lobe can still remember remote autobiographical events in great detail (Bayley and Squire., 2002).

Moreover, selective lesions in the hippocampal formation or entorhinal cortex in laboratory animals, including mice, rats, rabbits and monkeys, produce postlesion temporally graded amnesia in several types of memory tasks, extending for weeks (Zola-Morgan and Squire 1990, Kim and Fanselow 1992, Cho et al. 1993, Kim et al. 1995, Clark et al. 2002).

1.6 Conceptual framework of the present study

As discussed in the first chapter, the roles of hippocampus and cortex in recent and remote memory processing is well assessed and the association of experience-dependent behavioural modifications with morphological changes in hippocampal and anterior cingulate cortical (ACC) neuron at different time points after contextual fear conditioning, has been characterized (Restivo et al., 2009).

In particular,

a) the role of hippocampus in recent memory formation, with particular reference to spatial learning, is well defined (Zola-Morgan and Squire 1990; Martin and Clark, 2007; Squire and Bayley, 2007), and modifications in synaptic

plasticity and cellular morphology of hippocampal pyramidal neurons have been extensively described (. Leuner et al., 2003; Restivo et al., 2006). These changes are believed to depend on learning-induced pathways of protein synthesis (Bailey et al., 2004). However, the nature of such pathways and molecular mechanisms underlying memory formation, with particular reference to the expression of factors that may be directly involved in neuronal rearrangements, is still not well understood; and

b) in spite of the existing information on the sequential alterations of hippocampal and ACC neurons following memory consolidation and remote memory formation, still little is known regarding its cellular/molecular bases.

As already discussed, EphrinBs and EphB receptors are involved in dendritic spines morphogenesis in coltured neurones and post sinaptic EphrinB2 is required for hippocampal LTP (Contractor et al., 2002; Grunwald et al., 2001), suggesting its involvement in the regulation of synaptic transmission and plasticity by interaction with presynaptic receptors. In light of this pattern of activity and of *in situ* mRNA/immunohistochemical protein localization of EphrinB2 in mouse hippocampal neurons (Grunwald et al., 2004; Migani et al. 2007), we have therefore hypothesised that changes in expression of such cellular adhesion factor may occur upon memory formation and consolidation, representing a cellular/molecular marker of learning-induced neuronal responses.

We have therefore approached such hypothesis in two sequential steps:

1) to shed light into the nature of mechanisms of memory formation we subjected male C57BL/6N mice to contextual and cued fear conditioning and evaluated its behavioural, morphological and biochemical effects 24 hr later. Contextual fear conditioning was performed on two

experimental groups: conditioned and pseudoconditioned. We analyzed changes in neuronal morphology by Golgi-Cox staining in CA1 pyramidal neurons of conditioned, pseudoconditioned and naïve mice and EphrinB2 expression by western blot and immunohistochemistry, to characterize possible variation of such factor in association with morphological changes detected;

2 – since Western blot and immunohistochemical analysis of hippocampal EphrinB2 distribution revealed a specific increase in the pyramidal neurons of the CA1 area of conditioned mice (see chapter 4), we have investigate whether this increase may represent a more general effect of induced neuronal plasticity and studied the conversion of recent-to-remote memory, which ultimately depends on an increase in dendritic spine number of pyramidal neurons of the anterior cingulate cortex (ACC) (Restivo et al., 2009), by analyzing the effect of contextual fear conditioning on EphrinB2 levels in these neurons. To this end, we determined dendritic complexity and EphrinB2 levels 24 hours (recent), 7 days (intermediate) and 36 days (remote) after conditioning/pseudoconditioning in male C57BL/6N mice; and

3 – finally, to better characterise memory-associated variations in neuronal EphrinB2 levels we performed intra-hippocampal infusion of the inhibitor of translation anisomycin. Specifically, we first determined whether animal conditioning and the observed EphrinB2 increase along with the increase in spine density detected at the recent and remote time point were prevented by immediately post-training anysomicin infusion in the hipocampus. We then evaluated whether a similar effect was obtained by late (24 days post-training) hippocampal infusion of anisomycin, in order to establish a time-dependent role of the hippocampus on remote memory

consolidation and morphological changes/EphrinB2 increase observed in the ACC 36 days post-conditioning.

Chapter 2 – Materials and methods

2.1. Animals

Six-week-old, male C57BL/6N mice (Charles River Italia, Calco) were used in all experiments. Animals were housed in a temperature-controlled facility (22°C ± 1°C) on a 12/12 hr light/dark cycle for 7 days, inside standard mouseroom cages with unlimited access to food and water. Animal weights at the beginning of experiments ranged from 26 to 30 g. All experimental procedures were conducted according to the official European guidelines for the care and use of laboratory animals (86/609/EEC) and the Italian legislative decree 116/92.

2.2 Cellular and molecular mechanisms of recent memory formations in pyramidal hippocampal neurons

For this study we employed the following materials and methods.

2.2.1 Contextual and Cue fear-conditioning protocol

For this procedure, each mouse was placed in a transparent Plexiglas cage (28 cm × 28 cm × 10 cm, $L \times W \times H$) with a grid floor made of stainless steel rods (conditioning chamber), inside an experimental room (room 1). After 2 min of free exploration, 12 animals (from now on named *conditioned*) were exposed to a conditioned stimulus (CS) consisting of a tone (80 dB, 2000 Hz, 20 s) and to a subsequent unconditioned stimulus (US) consisting of an electric shock (0.3 mA, 1 s), provided immediately after the CS. Mice were left in the cage without additional stimuli for a total time of 5 min. Twelve control mice (from here on

named *pseudoconditioned*) were maintained in the cage for a total of 5 min without any stimulus. Activity of each mouse was recorded as described for the open field test. Responses measured consisted of time of immobility (freezing), i.e., a complete lack of movement except for those relative to breathing, expressed in seconds.

Contextual fear memory was tested on 6 animals of both *conditioned* and *psudoconditioned* groups 24 h after the conditioning session. To this end, each mouse was placed in the conditioning chamber inside room 1 for 5 min. During the test, animals were not subject to any stimulus. Activity, recorded as described for the conditioning session, was analysed in the first 2 min of the test.

One hour after the contextual test session, tested mice were placed in a cue test cage, consisting of a transparent Plexiglas cage (28 cm × 28 cm × 35 cm, $L \times W \times H$) with a plain floor and shaped in a triangle by a diagonal black plastic wall, inside a different experimental room (room 2) with different lights. After 2 min of free exploration, each mouse was exposed to the same tone (80 dB, 2000 Hz) used for the contextual fear-conditioning session for the remaining 3 min of the test. Activity was recorded and assayed as described for the previous tests. Responses measured consisted of time of freezing, expressed in seconds, during the initial 2 min and the remaining 3 min of the test.

2.2.2 Animal perfusions and brains preparation

Twenty-four hours after the conditioning session, 6 animals of each experimental group, for a total of 18, were anesthetised with chloral hydrate (400 mg/kg, i.p.) and perfused intracardially with ice-cold 0.1 M phosphate-buffered saline (PBS, pH 7.4). Since non-significant interhemispheric differences have been so far reported in the

assessment of neuronal morphology upon conditioning (i.e., Restivo et al., 2009), we dissected the brains, cut them in two halves along the central fissure, and processed one half for morphological analysis, the other half for *Western blot* and/or immunohistochemical analysis of EphrinB2. Distribution of right/left hemispheres was balanced among groups.

2.2.3 Golgi-Cox staining and sections preparation

Variations in neuronal morphology at recent and remote memory time points were assessed by Golgi-Cox staining, as described by Glaser and Van der Loos (1981). Dissected hemispheres of conditioned and pseudoconditioned animals were impregnated with a 1% potassium dichromate, 1% mercuric chloride, 0.8% potassium chromate solution and stored in the dark at room temperature for 6 days. After transfer to a 30% sucrose solution for 2 days, they were finally sectioned using a vibratome. Coronal sections (150 □m thick) were mounted on gelatinised slides, stained according to the method described by Gibb and Kolb (1998) and cover slipped with Eukitt.

2.2.4 Quantification of neuronal morphological parameters

Spine density was measured on pyramidal neurons located in the CA1 region of the dorsal hippocampus, in the lateral amygdala and in layers II/III of the ACC, defined according to the Franklin and Paxinos (2001) atlas, with a light transmission microscope (Leica DMLB, Leica Microsystems GmbH, Wetzlar, Germany) equipped with an image analysis device and software for morphological analyses and three-dimensional reconstruction system (Neurolucida, MicroBright Fields, Inc., Colchester, VT, USA). Neurons were first identified under low

magnification (200×) in the appropriate sections and selected for further analysis according to the following criteria: presence of at least three dendrites without obvious truncations; complete and dark impregnation along the entire length of all dendrites; relative isolation from neighbouring impregnated neurons (Vyas et al., 2002). Quantitative assessments of complete dendritic structure and spine density of six neurons per animal were then performed under higher magnification (1000×) by an experimenter blind to the experimental conditions. Spine density of the dendritic trees were quantified tracing the entire apical and basal dendrites. As for spine density assessment, segments of 25 μm were sampled on apical and basal dendrites starting 50 μm from the cell body. On each dendrite, all protrusions with or without bulbous expansions were counted as spines if they were in direct continuity with the dendritic shaft and were used for calculation of spine density. Spine density was automatically calculated by dividing the counted number of spines by the measured dendrite length. At the same time, a precise Sholl analysis was performed by referring spine densities among branch orders and among circular distances from the soma. Values obtained for all neurons from a given animal were averaged to a single value.

2.2.5 Western blot analysis of EphrinB2

Dissected hemispheres from 3 animals of *conditioned, pseudoconditioned* and control groups were rapidly placed on ice. The whole cortex and the dorsal hippocampus were carefully removed and homogenised in RIPA lysis buffer (Harlow et al., 1988) containing a commercial mixture of protease and phosphatase inhibitors (Sigma–Aldrich, Milano, Italia). Samples were subsequently centrifuged at 10,000 × *g* for 30 min a 4 °C to remove cell debris.

Concentration of soluble protein in the supernatants was determined by the standard Bradford colorimetric assay (Bradford, 1976). Aliquots containing 60 μg protein of each sample were diluted in Laemmli sample buffer, boiled at 100 °C for 5 min and subject to 8% polyacrylamide gel electrophoresis in the presence of 0.1% SDS. Coloured molecular weight markers (Sigma–Aldrich, Milano, Italia) were used as size references. Electrophoretic separation was performed for 2 h under a field of 15 V/cm. Proteins were then transferred to a nitrocellulose membrane in a Tris-glycine-methanol buffer, under a 150 mA current applied for 2 h. Finally, the membrane was soaked in protein blocking solution, consisting of a 3% bovine serum albumin (BSA) in a Tris-buffered saline (TBS), for 1 h at RT, and processed for identification of EphrinB2 by use of a specific polyclonal goat antibody (Neuromics, Edina, MN, USA, catalogue number: GT15026), diluted 1/1000 in blocking solution. This antibody was chosen among other commercially available antibodies for both Western blot and immunohistochemical analysis (see below), in light of its proven specificity for EphrinB2 and lack of cross-reactivity with other EphrinB members (Migani et al., 2007). The membrane was incubated with the primary antibody or a control solution overnight at 4 °C, washed with blocking solution three times for 10 min and finally incubated for 1 h at RT with a horseradish peroxidase (HRP)-conjugated, rabbit secondary anti-goat antibody (Sigma–Aldrich, catalogue number: A5420) diluted 1/5000 in blocking solution. The membrane was washed with blocking solution three times for 5 min, processed for immunoreactivity detection by a HRP-driven chemiluminescence reaction (Pierce Thermo Scientific, Rockford, IL, USA) and exposed to Kodak XAR-5 autoradiographic film. After EphrinB2 analysis, each membrane was incubated at 55 °C for 5 min

in a 2% SDS, 100 mM β-mercaptoethanol, 62.5 mM Tris–HCl pH 6.7 solution to detach bound antibodies, washed in PBS and processed as described above, using a mouse monoclonal primary antibody specific for β-actin (Santa Cruz Biotechnology, Heidelberg, Germany, catalogue number: sc-8432), diluted 1/1000 and a HRP-conjugated goat secondary anti-mouse antibody (Santa Cruz Biotechnology, catalogue number: sc-2005), diluted 1/5000. Films were scanned and subjected to a densitometric measure of their intensity, which is proportional to the amount of specific antibody-bound protein present in each sample, by use of an image analysis software (ImageJ, Rasband, W.S., U.S. National Institutes of Health, USA, http://imagej.nih.gov/ij/).

2.2.6 Western blot analysis of EphA4 receptor

Protein extracts were also processed for EphA4 receptor analysis. Nitrocellulose filters containing electrophoresed proteins were first subject to analysis of EphA4 receptor by use of a specific polyclonal antibody (Santa Cruz Biotechnology, catalogue number: sc-921) diluted 1/500 in blocking solution, and subsequently of b-actin, as described above. Scans and image analysis were performed accordingly.

2.2.7 Immunohistochemical analysis of EphrinB2

Histochemical evaluation of EphrinB2 content of dorsal hippocampus and amygdala of three animals of each experimental group, i.e. *conditioned, pseudoconditioned* and control (*naive*), was performed by the procedure described by Migani et al. (2007). Dissected hemispheres were rapidly soaked in 4% paraformaldehyde (PFA) in PBS and fixed overnight at 4 °C. They were then transferred to 30% sucrose in PBS, embedded in cutting medium and rapidly

frozen at −20 °C. Sections were prepared at −20 °C using a Leitz cryostat (Leica Microsystem GmbH, Wetzlar, Germany). Forty micrometre-thick coronal sections were singularly placed in cell culture wells in 0.5% NaN_3 in PBS and stored at 4 °C until use. Immunohistochemistry was performed simultaneously on free-floating serial sections relative to the hippocampus and amygdala. Sections were post-fixed overnight in 4% PFA in PBS at 37 °C to reduce non-specific immunostaining. After three washes for 5 min in PBS at RT, sections were treated with 3% H_2O_2 in PBS to inhibit endogenous peroxidase activity, washed twice for 10 min in PBS at RT and then incubated in 10% rabbit serum, 5% BSA in PBS (blocking solution), for 18 h at RT to increase the specific staining/background ratio. Sections were incubated at RT with goat primary EphrinB2 specific antibody (Neuromics, Edina, MN, USA, catalogue number: GT15026), diluted 1/400 in blocking solution for 2 h, under gentle rocking, and washed three times in blocking solution for 20 min at RT. They were finally incubated at RT with a rabbit secondary biotin-conjugated anti-goat antibody (Santa Cruz Biotechnology, catalogue number: sc-2774; Sigma–Aldrich, catalogue number: B7014), diluted 1/1000. After three further 10 min washes at RT with PBS, antibody binding was revealed by a biotin–streptavidin–peroxidase system (ABC, Vector Laboratories, Burlingame, CA, USA) and visualised by 5 min incubation in diaminobenzin (DAB)–metal complex (Vector Laboratories, Burlingame, CA, USA). Sections were rinsed in PBS and mounted on glass slides, dehydrated by immersion in increasing alcohol concentrations, treated with xylene and finally mounted with Permount (Sigma–Aldrich). Images were recorded by a digital camera connected to a Nikon 80i (Nikon Italia, Torino, Italia) microscope and a personal computer, and

analysed using ImageJ software (Rasband, W.S., U.S. National Institutes of Health, USA, http://imagej.nih.gov/ij/). Illumination and recording settings were kept constant throughout the observations. Images were converted to greyscale and scanned. Quantitative immunohistochemical analyses of different hippocampal regions and of the amygdala were performed on 200× images, calculating optical density (OD) according to the formula $OD = -\log 10(I/I_0)$, where I indicates the intensity of transmitted light and I_0 the intensity of incident light (Isoda et al., 2010). At least six sections per animal were analysed; in each of them six fields (100 µm diameter) per region were sampled. For a more detailed analysis of hippocampal CA1 areas, the OD values were sampled on 400× images of at least twelve individual neuronal cell bodies per animal. Values obtained for each sample in a given animal were averaged to a single value.

2.2.8 Statistical analyses

Results were expressed as means ± SEM. Behavioural performances, relative to 6 *conditioned* and 6 *pseudoconditioned* animals, were subject to analysis of variance (ANOVA). Differences in spine densities and branch node numbers were evaluated on 6 animals per group (*conditioned, pseudoconditioned* and control) by a two-way ANOVA. Post-hoc analyses were conducted by Tukey honestly significant differences (HSD) analysis. Apical and basal dendritic compartments were considered separately. Densitometry of Western blot scans, relative to 3 animals per group (*conditioned, pseudoconditioned* and control), was analysed by one-way ANOVA. Immunohistological data, relative to 3 animals per group (*conditioned, pseudoconditioned* and control), were evaluated by two-way ANOVA, followed by post-hoc HSD

analysis. Correlation analysis of EphrinB2 immunoreactivity and apical dendritic spine density of hippocampal CA1 neurons was performed by calculating Spearman's rank correlation coefficient rho. Statistical analyses were performed using R: a language and environment for statistical computing (R development core team, R foundation for statistical computing, ISBN 3-900051-07-0, 2008, Vienna, Austria, http://www.R-project.org).

2.3 Cellular and molecular mechanisms of remote memory formations in pyramidal hippocampal and anterior cingulate cortex neurons

For this study we employed the following materials and methods.

2.3.1 Contextual fear-conditioning protocol

For the training session, each mouse (12 mouse for each experimental groups) was placed in a conditioning chamber consisting of a transparent Plexiglas cage (17 x 17 x 25 cm, L x W x H) with a grid floor made of stainless steel rods, for a total of 7 min. After 2 min of free exploration, *conditioned animals* were exposed to a series of five non signaled electric footshocks (0.7 mA, 2 sec; 1 min interval between two consecutive shocks) (Restivo et al., 2009). P*seudoconditioned* mice were exposed to the context for a total time of 7 min but were not subjected to any shock. Activity of each mouse was recorded by a video camera fixed over the chamber and connected to a personal computer. The time of immobility or freezing, a complete lack of movement except for breathing, observed in the first 2 min of the session (baseline freezing) was calculated and

expressed as percent time (Labrie et al., 2008).

Contextual fear memory was tested on 6 animals of both *conditioned* and *psudoconditioned* groups 24 hr (early time point), 7 days (intermediate time point) or 36 days (late time-point) after the conditioning session (p.c.). To this end, each mouse was placed in the conditioning chamber for 5 min, without being exposed to any stimulus. Activity was recorded as described for the conditioning session and freezing time was calculated as percent of freezing observed during the 5 min memory test subtracted of the previously calculated baseline freezing (Labrie et al., 2008). Animals used in behaviour experiments (36) were never tested twice.

2.3.2 Surgery

Six Animals for each experimental groups (*saline* or *anisomycin* mice) were anesthetised with chloral hydrate (400 mg/kg, i.p.) and implanted bilaterally with stainless steel cannulae above the stratum pyramidale of the dorsal CA1 region of the hippocampus according to the Franklin and Paxinos (2001) atlas, using the following coordinates: AP, -1.8 mm, ML, +/- 1.5 mm, DV: -0.9. The correct placement of the infusion cannulae was verified post-mortem by standard histological procedures (Barros et al., 2000) and only mice with cannula tips correctly located were included in this study.

Post-training intra-hippocampal infusion of anisomycin were performed immediately after the conditioning session, late (24 days) intra-hippocampal infusion were performed 24 days later.

Anisomycin (Sigma) was dissolved in equimolar HCL, diluted with 0.9% NaCl and adjusted to pH 7.4 with NaOH for a final concentration of 160 mg/ml. The intrahippocampal dose was 80mg/0.5 ml per side. Saline animals received equivolume of the vehicle (pH 7.4).

2.3.3 Golgi-Cox staining and sections preparation

Variations in neuronal morphology at remote memory time points were assessed by Golgi-Cox staining, as described previously.

2.3.4 Quantification of neuronal morphological parameters

Spine density was measured on pyramidal neurons located in the CA1 region of the dorsal hippocampus and in layers II/III of the ACC, defined according to the Franklin and Paxinos (2001) atlas, with a light transmission microscope (Leica DMLB, Leica Microsystems GmbH, Wetzlar, Germany) as described previously.

2.3.5 Western blot analysis of EphrinB2

The dorsal hippocampus and the ACC area (defined according to the Franklin and Paxinos atlas, 2001) of hemispheres from three animals of each experimental group were carefully removed by punching and then homogenised in RIPA lysis buffer (Harlow and Lane, 1988) and processed as described previously.

2.3.6 Immunohistochemical analysis of EphrinB2

Histochemical evaluation of EphrinB2 content of pyramidal neurons located in the dorsal hippocampus and ACC of three animals of each experimental group was performed as described previously.

2.3.7 Statistical analyses

Results were expressed as means ± SEM. Behavioural performances, relative to 6 *conditioned* and 6 *pseudoconditioned* animals at each time point (24 hr, 7 days, 36 days) and 6 *saline* and 6 *anisomycin* animals for each

experimental point, were subject to analysis of variance (ANOVA). Differences in spine densities and branch node numbers were evaluated on 6 animals per group *(conditioned, pseudoconditioned*) at each time point, by a two-way ANOVA. Post-hoc analyses were conducted by Tukey Honestly Significant Differences (HSD) analysis. Apical and basal dendritic compartments were considered separately. Immunohistological data, relative to 3 animals per group at each experimental point, were evaluated by two-way ANOVA, followed by post-hoc HSD analysis. Statistical analyses were performed using R: A language and environment for statistical computing (R development core team, R foundation for statistical computing, ISBN 3-900051-07-0, 2008, Vienna, Austria. http://www.R-project.org).

Chapter 3 - Results

3.1 Cellular and molecular mechanisms of recent memory formations in pyramidal hippocampal neurons

3.1.1 Conditioned mice showed strong contextual and cued fear response

When reexposed to the experimental context during the memory retrieval session 24 hr post-conditioning, *conditioned* mice showed greater freezing responses (i.e., the percent of time spent in immobility) than *pseudoconditioned* mice during the first 2 min of the test session (*conditioned* animals: 38 ± 9.9 s; *pseudoconditioned* animals: 14.1 ± 1.1 s; training condition effect, $F_{1,10} = 5.76$; $p < 0.05$) (Fig. 3.1).

When exposed to a different context, *conditioned* and *pseudoconditioned* animals showed similar exploration activity during the first two minutes of the test session, prior to administration of the tone. On the contrary, during the final three minutes of the test session, in which animals were subjected to a continuous tone, a greater freezing response was observed in *conditioned* animals (61.84 ± 6.5 seconds vs. 30.96 ± 1.7 seconds of *pseudoconditioned* animals; training condition effect, $F_{1,10} = 20.91$; $p < 0.01$) (Fig. 3.1).

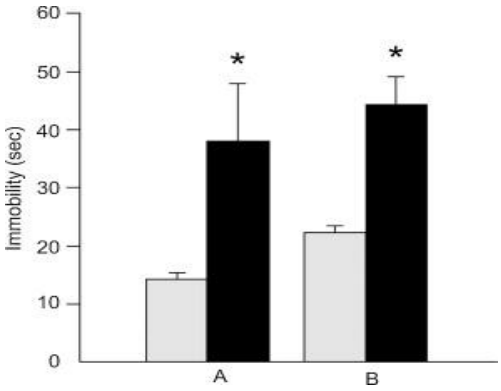

Fig. 3.1 - Behavioural responses to context and cued fear conditioning. Freezing time, expressed in seconds, during the first 2 min of the conditioning test (A) and during the last 3 min of the cue test (B), relative to *pseudoconditioned* (□) and *conditioned* (■) animals (mean ± SEM).

3.1.2 Contextual fear conditioning promotes a rapid increase in dendritic spine density of hippocampal CA1 and lateral amygdala neurons

Density of dendritic spines was measured in apical and basal dendrites of hippocampal CA1 pyramidal neurons and lateral amygdala pyramidal neurons from *conditioned*, *pseudoconditioned* and *control* (naive) mice. While no differences were observed in spine density of basal dendrites of hippocampal neurons in the three experimental conditions, structural rearrangements were observed on apical dendrites of neurons from *conditioned* mice (training condition effect: $F2,26= 2.172$; $p < 0.01$) (Fig. 3.2)

Differences in spine density were also observed on basal and apical dendrites of lateral amygdala neurons from *conditioned* mice (training condition effect: basal spines, $F2,14= 3.303$; $p< 0.001$; apical spines, $F2,16= 1.759$; $p < 0.05$) (Fig. 3.3).

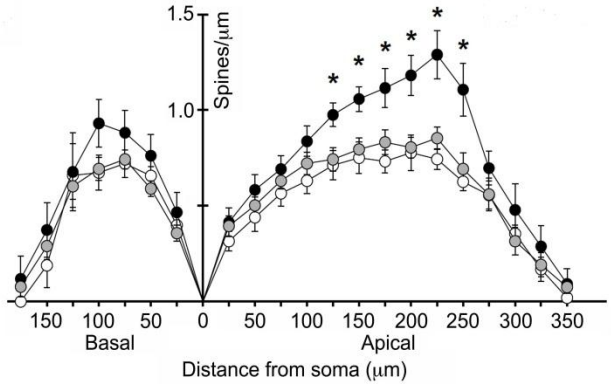

Fig. 3.2. - Dendritic spines of pyramidal CA1 hippocampal neurons. Values represent the mean number ± SEM of dendritic spines/µm counted on 25 µm dendritic segments, relative to basal (left panel) and apical (right panel) dendrites of pyramidal CA1 hippocampal neurons from *control(○)*, *pseudoconditioned(○)* and *conditioned(●)* animals. Single asterisks indicate difference between *conditioned* and *pseudoconditioned*/*control* animals, $p < 0.01$.

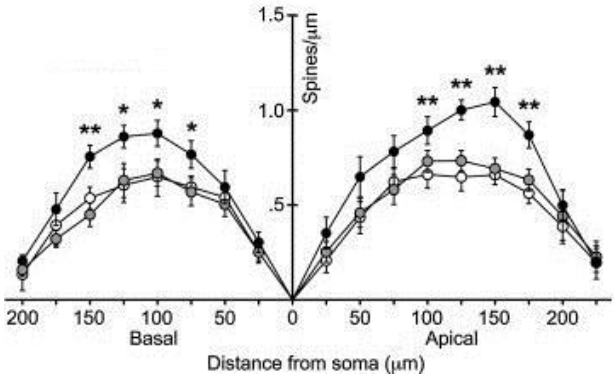

Fig 3.3 - Dendritic spines of pyramidal lateral amygdala neurons.Values represent the mean number ± SEM of dendritic spines/µm counted on 25 µm dendritic segments, relative to basal (left panel) and apical (right panel) dendrites of pyramidal lateral amygdala neurons from *control(○)*, *pseudoconditioned(○)* and *conditioned(●)* animals. Asterisks indicate differences between *conditioned* and *pseudoconditioned/control* animals: *$p < 0.05$; **$p < 0.01$.

3.1.3 Contextual fear conditioning for recent memories is associated with an increase in EphrinB2 levels.

Contextual fear conditioning is associated with a rapid increase in levels of EphrinB2 in the hippocampus. Presence of EphrinB2 in the hippocampus and whole cortex of *conditioned*, *pseudoconditioned* and *naive* mice was measured by Western blot analysis and subsequent densitometry, normalised by comparison with ubiquitous β-actin. A single, broad band of molecular mass slightly smaller than 40 kDa, as described for EphrinB2 (Holland et al., 1996), was detected in protein extracts from both the hippocampus and the cortex (Fig.3.4). Densitometric measurements showed a strong increase in EphrinB2 levels in the hippocampi of *conditioned* vs. *pseudoconditioned*/ *control* mice (training condition effect, $F2, = 20.063$; $p < 0.01$), while no differences were observed in the cortices (Fig.3.5). When presence of EphA4 receptor was analysed in the same conditions, no variations were observed in either structure of *conditioned* and *pseudoconditioned*/*control* animals (Fig.3.6).

Contextual fear conditioning is associated with a rapid increase in levels of EphrinB2 in the CA1 area of the hippocampus. The increase in EphrinB2 levels in the hippocampi of conditioned mice was further investigated by immunohistochemical analysis in different areas of such structure, namely CA1, CA3 and dentate gyrus (DG) (Fig.3.7A). The same analysis was performed on the amygdalas, the involvement of which in fear conditioning was evaluated by the cued test. Presence of EphrinB2 was observed in the pyramidal cell layer of CA1 and CA3 areas and in the granular layer of DG of all animals, confirming

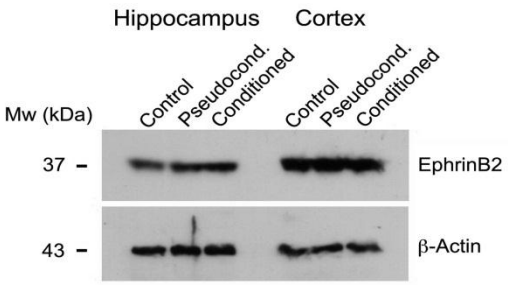

Fig 3.4 - Representative Western blot of EphrinB2 in protein extracts from the hippocampus and the cortex of *control, pseudoconditioned* and *conditioned* animal.

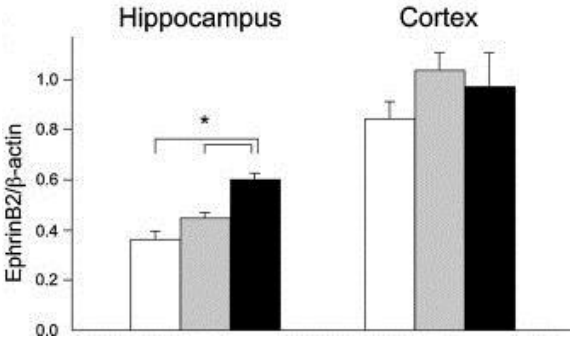

Fig 3.5 - Densitometric analysis of EphrinB2/β-actin abundance in the hippocampus and the cortex of *control* (□), *pseudoconditioned* (⧈) and *conditioned* (■) animal. Values represent the mean value ± SEM of extracts from three animals/group. Asterisk indicates difference between *conditioned* and *pseudoconditioned*/*control* animals, $p < 0.001$.

results of Migani et al. 2007. As for presence of such factor in the amygdala, EphrinB2 positive small cells were observed both in the lateral and basolateral nuclei, as already reported by Migani et al. 2007. Analysis of optical density values of *conditioned* vs. *pseudoconditioned*/*control* animals (Fig. 3.7B) showed an increased abundance of EphrinB2 in the CA1 area (training condition effect, (F2,6= 6.41; p<0.05), but not in other hippocampal areas nor in the amygdala. In addition, when the CA1 area of mice belonging to the three experimental groups was observed in detail (Fig. 3.8A), positive cell distribution was similar. In these neurons, EphrinB2 was localized in the neuronal cell bodies and apical dendrites, independently of the experimental group. Finally, when cell staining of pyramidal neurons in the hippocampi of *conditioned* animals was compared to that displayed by both *pseudoconditioned* and *control* animals by analysis of optical density (Fig. 3.8B), it was found to be substantially enhanced (F2,6=60.8, p<0.001), suggesting an increase in EphrinB2 expression of individual cells.

A correlation analysis of EphrinB2 immunoreactivity with neuronal morphology revealed the existence of a positive relationship between EphrinB2 levels and apical dendritic spine density of pyramidal neurons of the CA1 area of the hippocampus (Spearman's rank correlation rho=0.9; p<0.05).

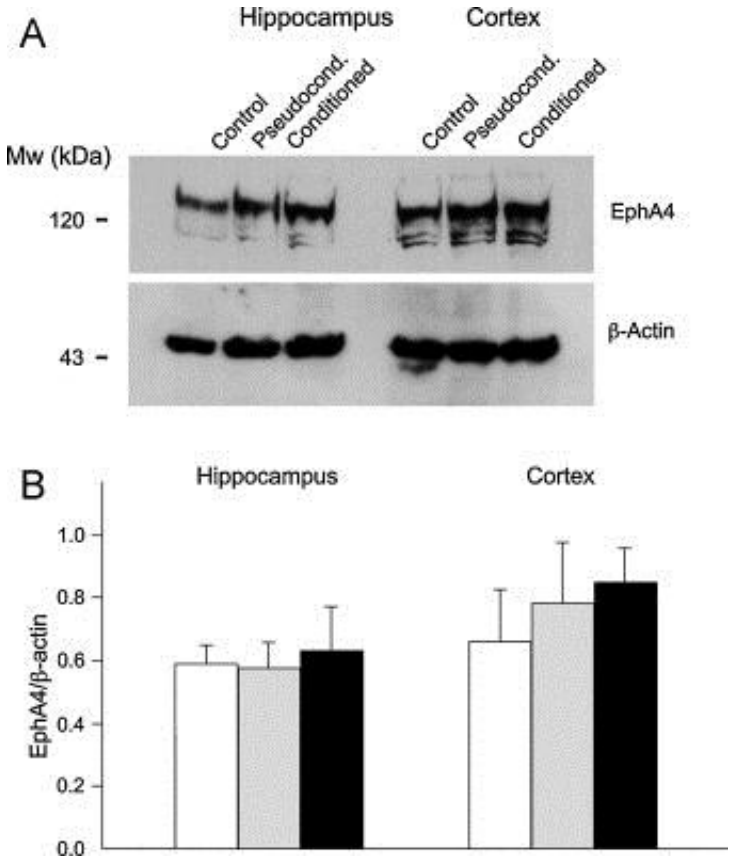

Fig 3.6 - (A) Representative Western blot of EphA4 in protein extracts from the hippocampus and the cortex of *control, pseudoconditioned* and *conditioned* animal. (B) Densitometric analysis of EphA4/β-actin abundance in the hippocampus and the cortex of *control* (□), *pseudoconditioned* (□) and *conditioned* (■) animal. Values represent the mean value ± SEM of extracts from three animals/group.

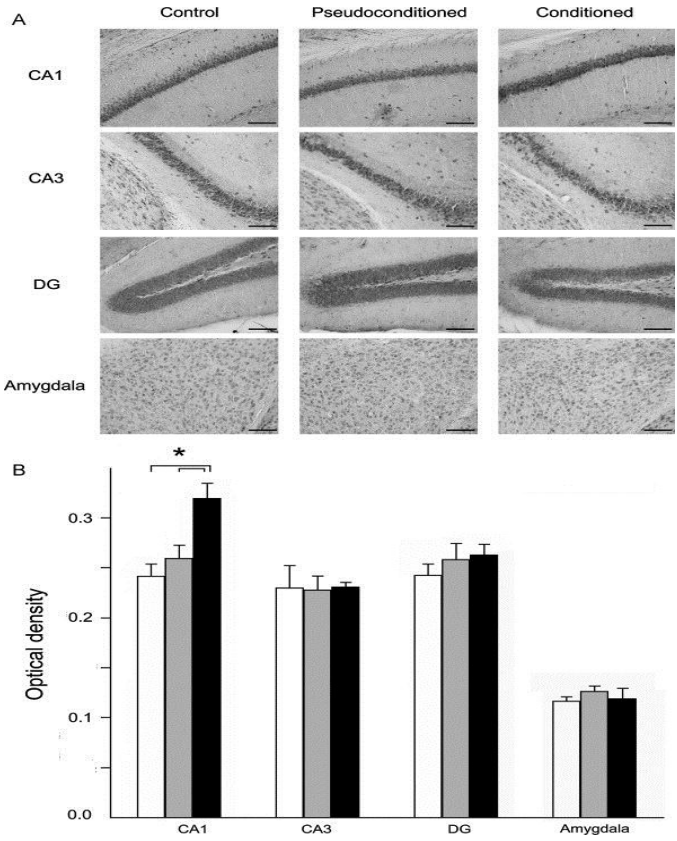

Fig 3.7 - (A) Representative immunohistochemical localization of EphrinB2 in hippocampal areas CA1, CA3 and DG, and the amygdala of *control, pseudoconditioned* and *conditioned* animals. Bars, 100 μm. (B) Densitometric analysis of EphrinB2 in the hippocampus and amygdala of *control* (□), *pseudoconditioned* (□) and *conditioned* (■) animals. Values represent the mean value ± SEM of 3 animals/group. Asterisk indicates difference between *conditioned* and *psedoconditioned*/*control* animals, $p < 0.05$.

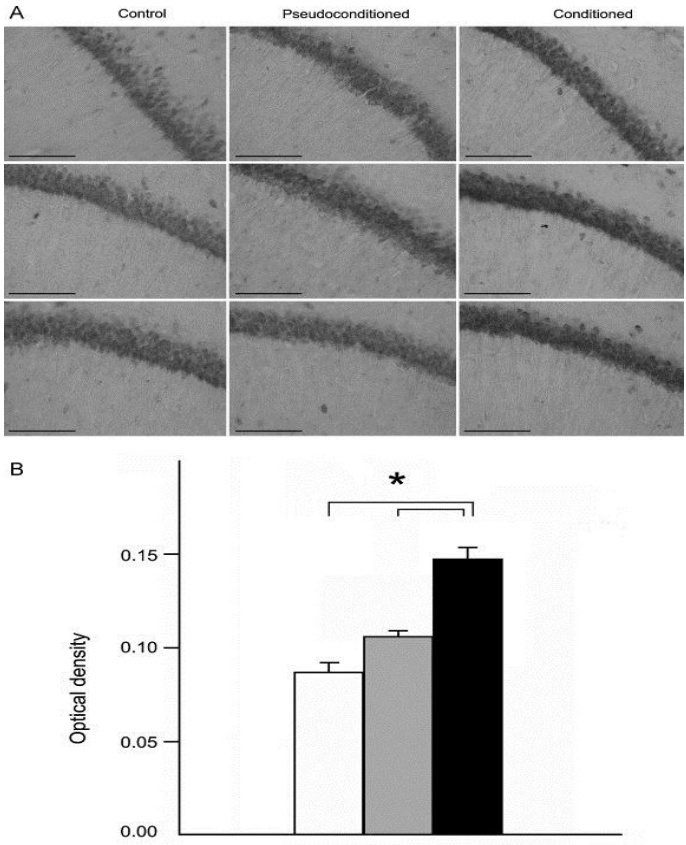

Fig 3.8 - (A) Representative immunohistochemical localization of EphrinB2 in hippocampal CA1 neurons of *control, pseudoconditioned* and *conditioned* animals. Bars, 100 μm. (B) Densitometric analysis of EphrinB2 in individual CA1 neurons of *control* (□), *pseudoconditioned* (□) and *conditioned* (■) animals. Values represent the mean value ± SEM of 3 animals/group. Asterisk indicates difference between *conditioned* and *pseudoconditioned*/*control* animals, $p < 0.001$.

3.2 Cellular and molecular mechanisms of remote memory formations in pyramidal hippocampal and anterior cingulate cortex neurons

3.2.1 Conditioned mice show strong contextual fear responses during the recent and remote memory tests.

Contextual fear memory tests for recent and remote memory were performed 24 hr, 7 days or 36 days post conditioning (p.c.). *Conditioned* mice showed greater freezing responses relative to *pseudoconditioned* ones at each retention interval (24 hr, $F(1,10)= 77.459$, $p< 0.001$; 7d, $F(1,10)= 80.676$ $p< 0.001$; 36d, $F(1,10)=9.835$, $p< 0.01$). Immobility: 24 hr, pseudoconditioned: 6.63% vs conditioned: 49.5%; 7 d, pseudoconditioned: 7.26% vs conditioned: 54.19%, 36 d, pseudoconditioned: 3.01% vs conditioned: 43.7% (fig. 3.9).

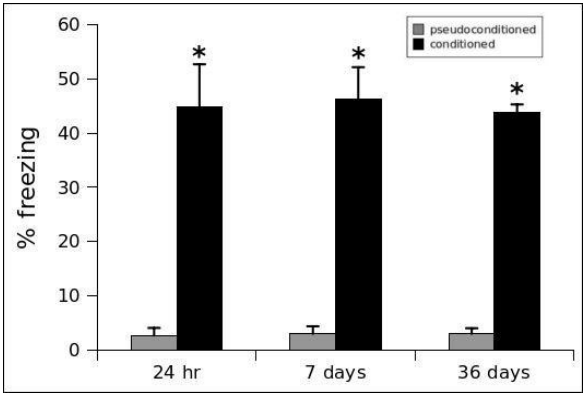

Fig 3.9 - Behavioural responses to context fear conditioning, expressed as percentage of freezing time, at different retention intervals. Asterisk indicates significant difference between groups: 24 hr, p=0.0034; 7 d, p=0.0019; 36 d, p=0.0061.

3.2.2 Contextual fear memory consolidation is associated with a time-dependent spine growth in the hippocampus and ACC.

Postconditional changes in neuronal morphology were analyzed in *conditioned* and *pseudoconditioned* mice at each time point. Dendritic spine density was evaluated by Golgi-Cox-staining in hippocampal and ACC pyramidal neurons. *Conditioned* mice exhibited a significant increase in spine density on apical and basal dendrites of CA1 neurons 24 hr after conditioning compared with *pseudoconditioned* mice. This increase was still evident 7 days after conditioning section but was only transient, since hippocampal apical spines density measured 36 days after conditioning was similar in *conditioned* and *pseudoconditioned* mice (Fig. 3.10-3.15) (24 hr, Apical: $F(1,10)= 4.900$, $p< 0.01$; Basal: $F(1,6)= 2.396$, $p< 0.05$; 7 d, Apical: $F(1,10)= 2.167$, $p< 0.05$). An inverted pattern was observable in the ACC. At the recent time point (24 hr), apical and basal spine densities were similar in *conditioned* and *pseudoconditioned* mice. These values, however, were significantly higher in the *conditioned* than in the *pseudoconditioned* group at the remote time point (36 d) (fig. 3.10-3.15), (Apical: $F(1,10)=2.960$, $p= 0.0059$; Basal: $F(1,6)=4.884$, $p= 0.0004$).

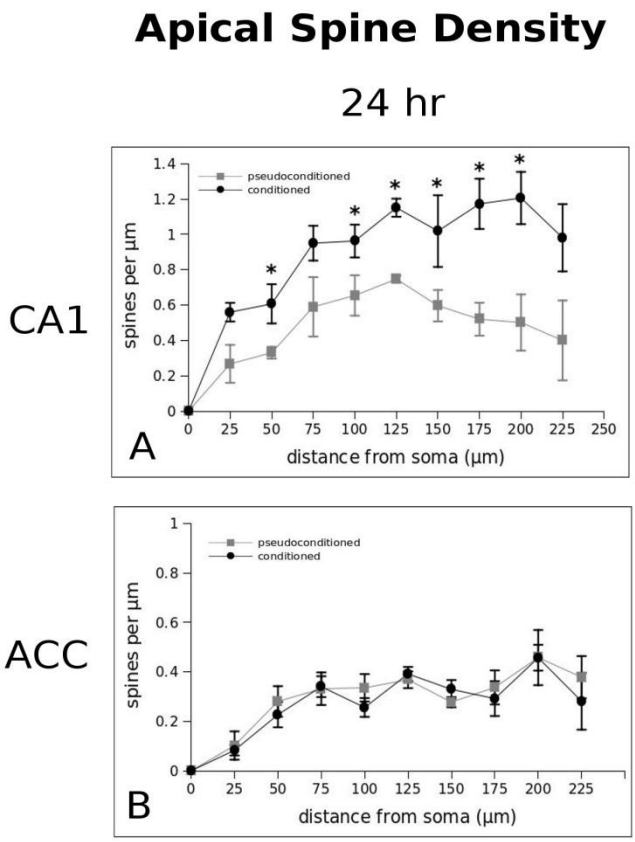

Fig 3.10 - Apical dendritic spine densities of pyramidal CA1 hippocampal (A) and ACC neurons (B) 24 hr p.c.. Values represent the mean number ± SEM of dendritic spines/µm counted on progressive 25 µm dendritic segments, relative to apical dendrites. Asterisks indicate differences between *conditioned(●)* and *pseudoconditioned(□)* animals: $p < 0.05$.

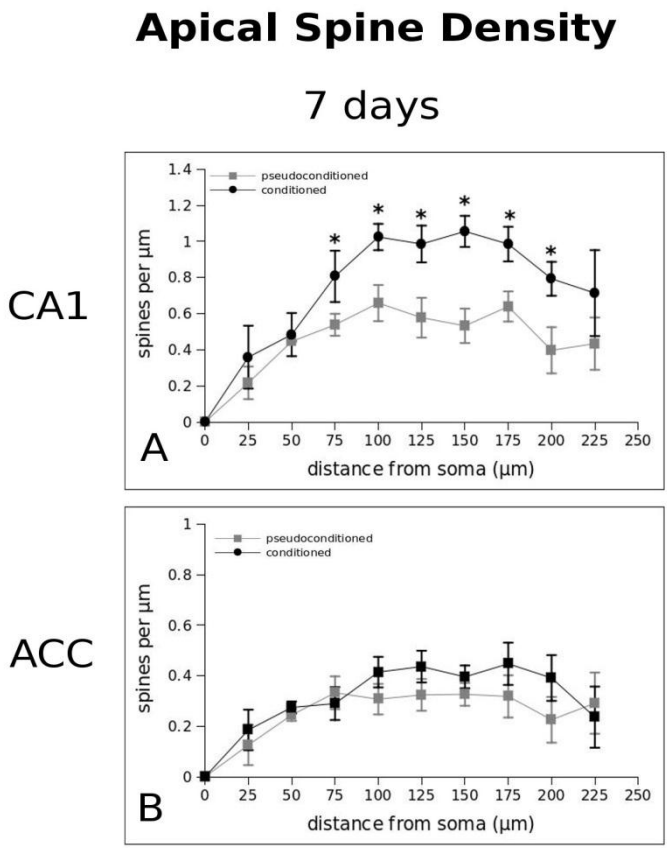

Fig 3.11 - Apical dendritic spine densities of pyramidal CA1 hippocampal (A) and ACC neurons (B) 7 days p.c.. Values represent the mean number ± SEM of dendritic spines/µm counted on progressive 25 µm dendritic segments, relative to apical dendrites. Asterisks indicate differences between *conditioned(●)* and *pseudoconditioned(□)* animals: $p < 0.05$.

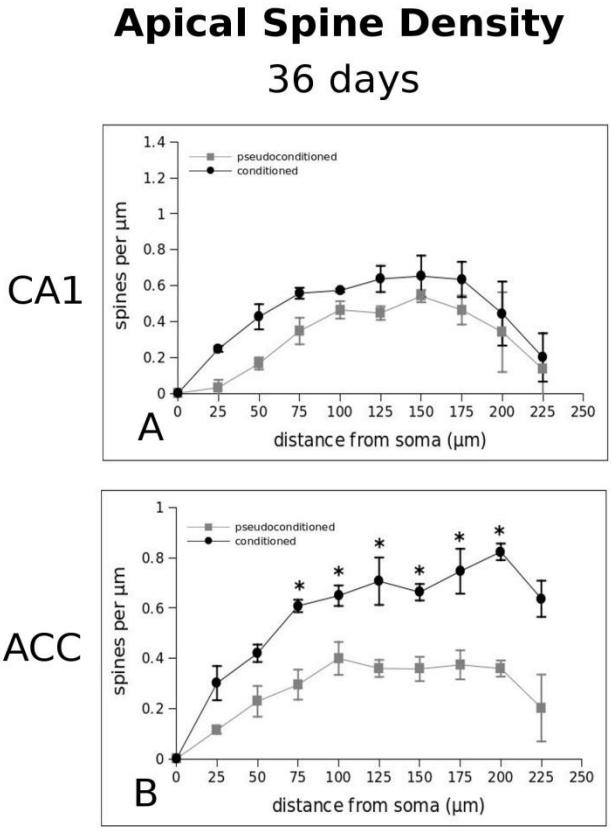

Fig 3.12 - Apical dendritic spine densities of pyramidal CA1 hippocampal (A) and ACC neurons (B) 36 days p.c.. Values represent the mean number ± SEM of dendritic spines/µm counted on progressive 25 µm dendritic segments, relative to apical dendrites. Asterisks indicate differences between *conditioned(●)* and *pseudoconditioned(□)* animals: $p < 0.05$.

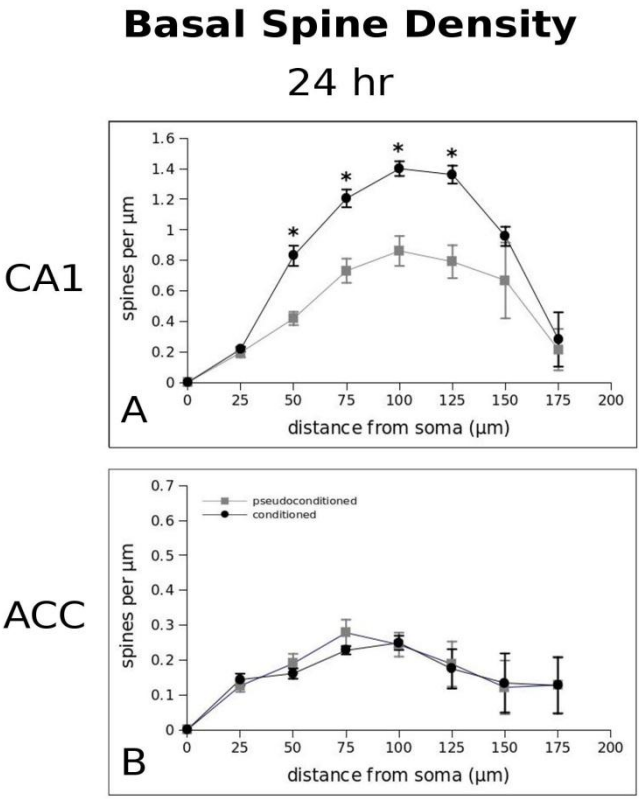

Fig 3.13 - Basal dendritic spine densities of pyramidal CA1 hippocampal (A) and ACC neurons (B) 24 hr p.c.. Values represent the mean number ± SEM of dendritic spines/µm counted on progressive 25 µm dendritic segments, relative to basal dendrites. Asterisks indicate differences between *conditioned(●)* and *pseudoconditioned(□)* animals: $p < 0.01$.

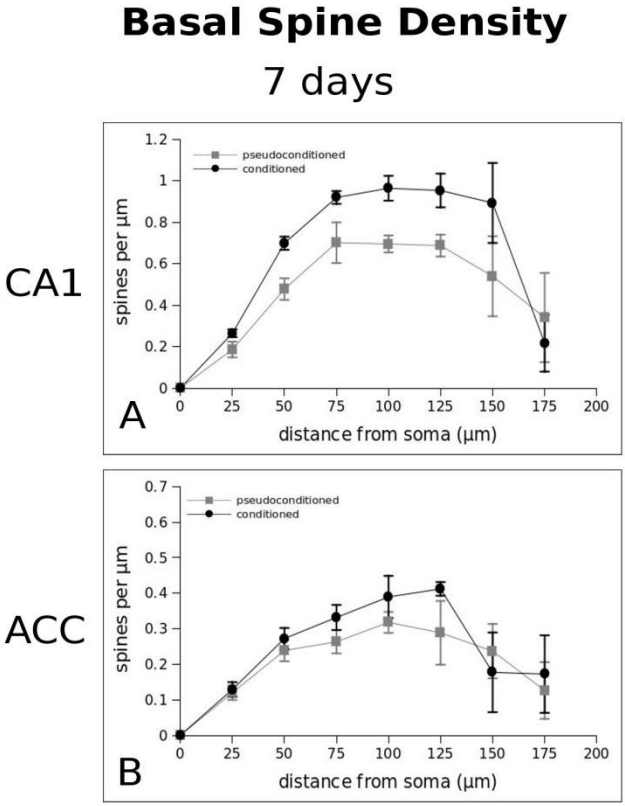

Fig 3.14 - Basal dendritic spine densities of pyramidal CA1 hippocampal (A) and ACC neurons (B) 7 days p.c.. Values represent the mean number ± SEM of dendritic spines/µm counted on progressive 25 µm dendritic segments, relative to basal dendrites. Asterisks indicate differences between *conditioned(●)* and *pseudoconditioned(□)*animals: $p < 0.01$.

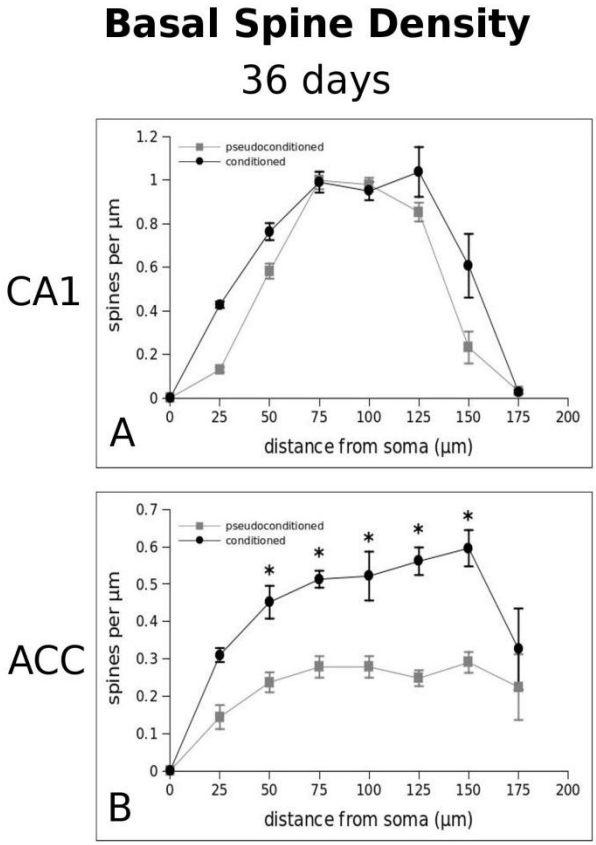

Fig 3.15 - Basal dendritic spine densities of pyramidal CA1 hippocampal (A) and ACC neurons (B) 36 days p.c.. Values represent the mean number ± SEM of dendritic spines/µm counted on progressive 25 µm dendritic segments, relative to basal dendrites. Asterisks indicate differences between *conditioned(●)* and *pseudoconditioned(□)* animals: $p < 0.01$.

3.2.3 Variations in EphrinB2 levels reflected morphological results

Levels of EphrinB2 in the hippocampus and ACC of *conditioned* and *pseudoconditioned* mice was analysed by Western blot and immunoistochemistry at each time point.

A rapid accumulation of EphrinB2 was observed in the CA1 area of conditioned mice in parallel with the increase in spine density, 24 hr after conditioning. At this time point, levels of this ligand were significantly higher in *conditioned* than in *pseudoconditioned* mice (fig. 3.16A-C3; ($F(1,4)=10.885$, $p<0.05$; OD: pseudoconditioned: 0.13 ± 0.003 vs conditioned: 0.24 ± 0.019) (fig. 3.17A-B; $F(1,4=159.34$, $p<0.001$). This increase was still evident after 7 days (fig. 3.16D-F; $F(1,4)=17.418$, $p<0.05$; OD: pseudoconditioned: 0.12 ± 0.007 vs conditioned: 0.19 ± 0.007) (fig. 3.17A-B; $F(1,4)=9.075$, $p<0.05$) and decreased at the remote time point (Fig. 3.16G-I; 3.17A-B) (OD: pseudoconditioned 0.13 ± 0.01 vs conditioned: 0.12 ± 0.008). As for morphological results, changes of EphrinB2 levels in the ACC showed an inverted pattern compared to CA1 areas. There were no significant differences in the ACC between the two groups, 24 hr and 7 days after conditioning (fig. 3.18A-F; 3.19), but a significant increase was observed in the levels of EprinB2 in the ACC of *conditioned* mice compared to *pseudoconditioned* ones, after 36 days (fig. 3.18G-I; 3.20; $F(1,4)=25.441$, $p< 0.01$; OD: pseudoconditioned: 0.16 ± 0.007 vs conditioned: 0.27 ± 0.015) (Fig. 3.19A-B; $F(1,4)=26.783$, $p<0.001$). Moreover, immunohistochemical analysis of the CA3 area showed no differences between the two groups at each experimental time (fig. 3.21).

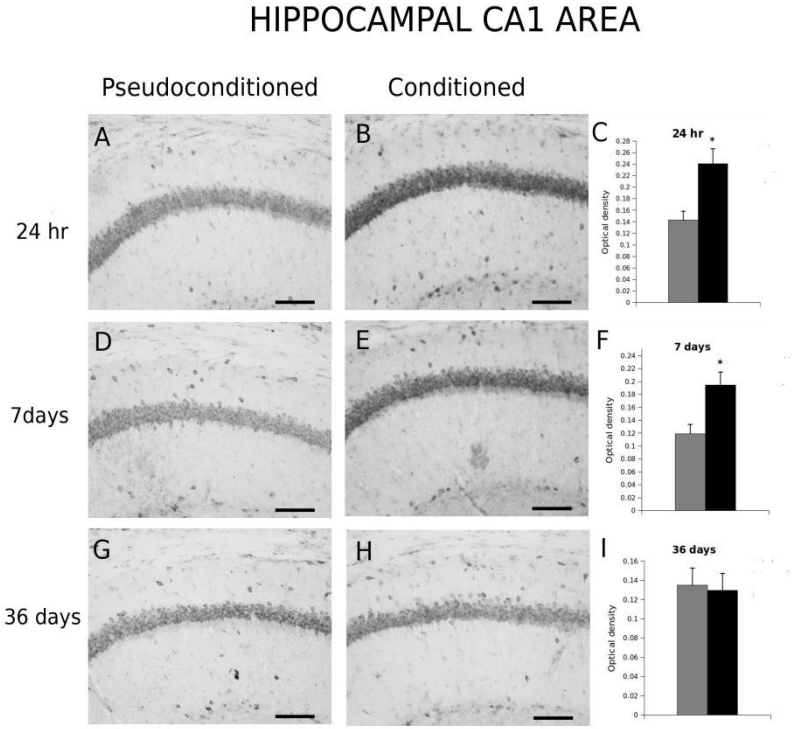

Fig 3.16 - (A, B, D, E, G, H):Representative immunohistochemical localization of EphrinB2 in hippocampal CA1 area of *pseudoconditioned (□) and conditioned (■)* animals at each retention interval. Bars, 100 μm. (**C, F, I**): Densitometric analysis of CA1 EphrinB2 immunoreactivity of *pseudoconditioned* and *conditioned* animals 24 hr, 7d and 36d p.c.. Values represent the mean value ± SEM of 3 animals/group. Asterisk indicates difference between *conditioned* and *pseudoconditioned* animals, $p < 0.05$.

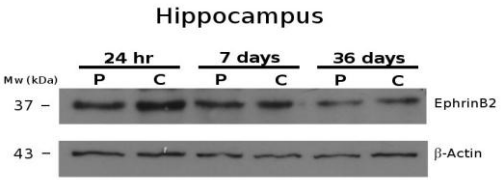

Fig 3.17A - Representative western blot analisys of EphrinB2 in the hippocampus of *pseudoconditioned* and *conditioned* animals at each retention interval.

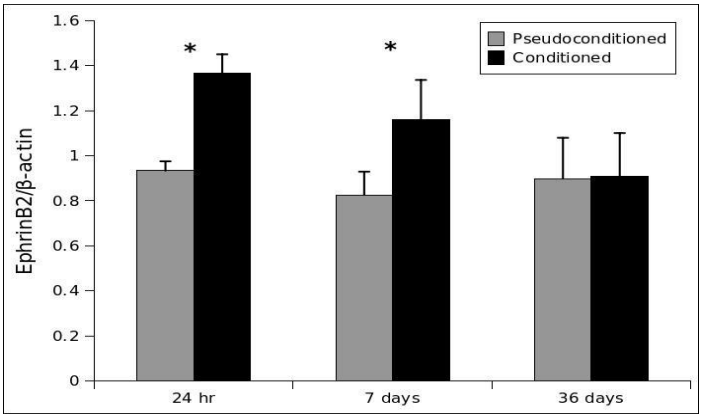

Fig 3.17B - Densitometric analysis of EphrinB2/β-actin abundance in the hippocampus of *pseudoconditioned* (□) and *conditioned* (■) animal at each retention interval. Values represent the mean value ± SEM of extracts from three animals/group. Asterisk indicates difference between *conditioned* and *pseudoconditioned* animals, $p < 0.05$.

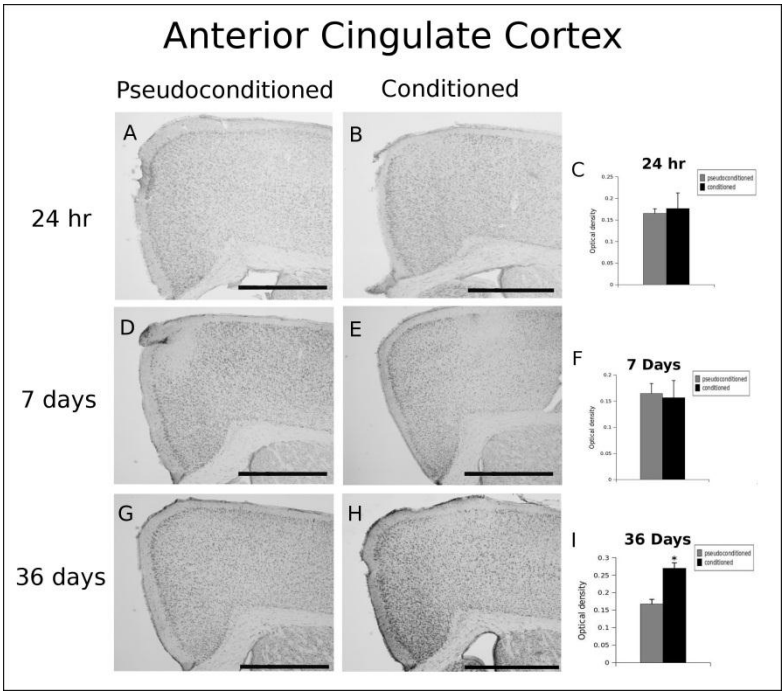

Fig 3.18 - (A, B, D, E, G, H): Representative immunohistochemical localization of EphrinB2 in the ACC of *pseudoconditioned (□) and conditioned (■)* animals at each retention interval. Bars, 1000 μm. (**C, F, I**): Densitometric analysis of EphrinB2 immunoreactivity relative to the ACC of *pseudoconditioned* and *conditioned* animals 24 hr, 7d and 36 d p.c.. Values represent the mean value ± SEM of 3 animals/group. Asterisk indicates difference between *conditioned* and *pseudoconditioned* animals, $p < 0.01$.

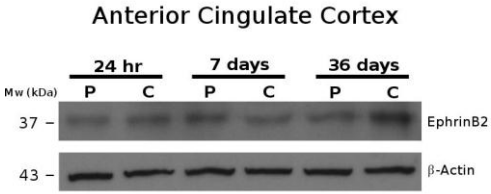

Fig 3.19A - Representative western blot analisys of EphrinB2 in the ACC of *pseudoconditioned* and *conditioned* animals at each retention interval.

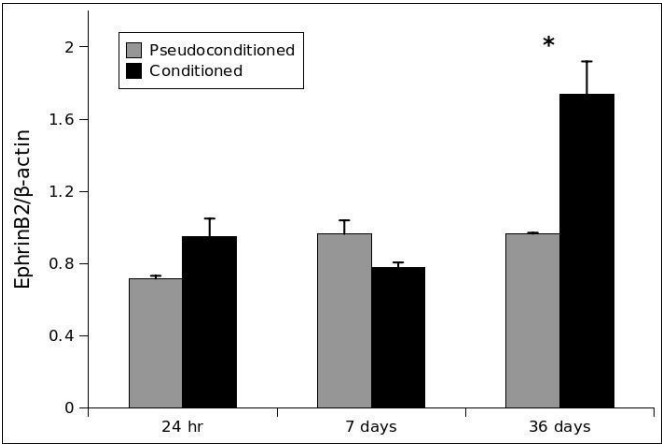

Fig 3.19B - Densitometric analysis of EphrinB2/β-actin abundance in the ACC of *pseudoconditioned* (□) and *conditioned* (■) animal at each retention interval. Values represent the mean value ± SEM of extracts from three animals/group. Asterisk indicates difference between *conditioned* and *pseudoconditioned* animals, $p < 0.001$.

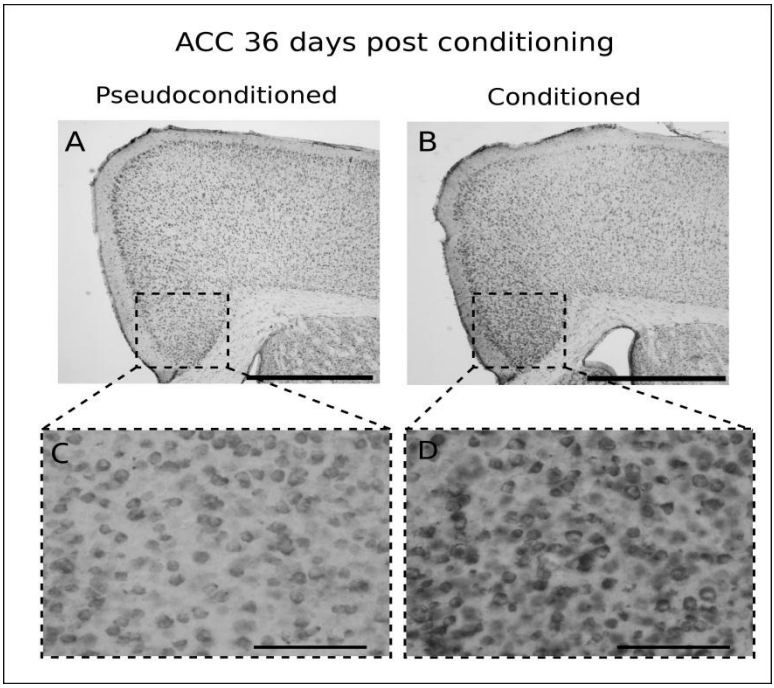

Fig 3.20 - Representative immunohistochemical localization of EphrinB2 in the ACC of *pseudoconditioned* and *conditioned* animals 36d p.c., at (**A, B**) low magnification (bars, 1000 μm) and (**C, D**) high magnification (bars, 100 μm).

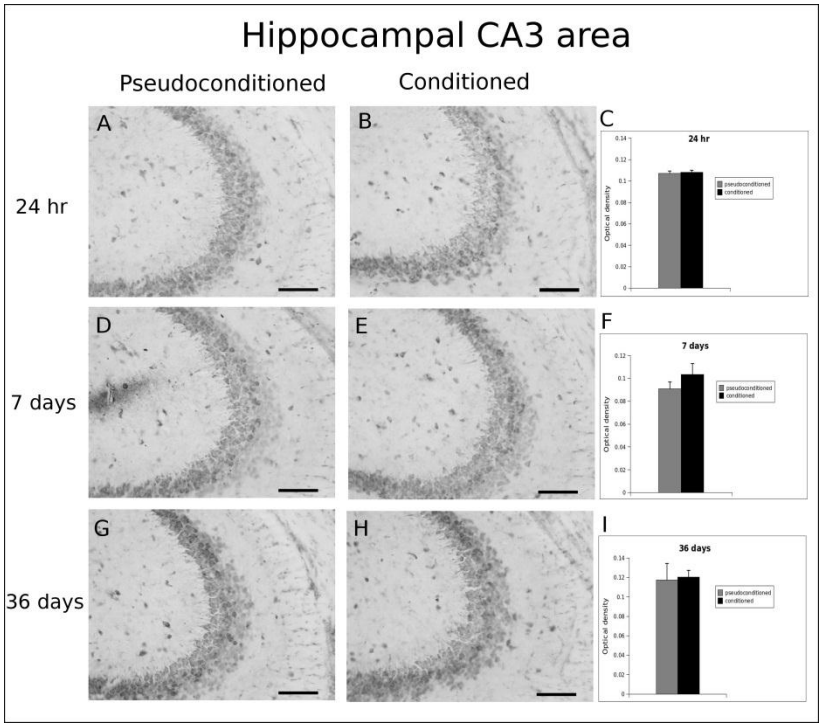

Fig 3.21 - (A, B, D, E, G, H): Representative immunohistochemical localization of EphrinB2 in hippocampal CA3 area of *pseudoconditioned (□) and conditioned (■)* animals at each retention interval. Bars, 100 μm. (**C, F, I**): Densitometric analysis of CA3 EphrinB2 immunoreactivity of *pseudoconditioned* and *conditioned* animals 24 hr, 7d and 36d p.c.. Values represent the mean value ± SEM of 3 animals/group. Asterisk indicates difference between *conditioned* and *pseudoconditioned* animals, $p < 0.05$.

3.2.4 The increase in EphrinB2 levels was prevented by anisomycin treatment

Post-training intra-hippocampal infusion of the translation inhibitor anisomycin prevents contextual fear memory consolidation. Conditioned mice, treated with *anisomycin* immediately post training, showed lower freezing responses relative to conditioned mice infused with *saline* (control group) during the memory test, 24 hours and 36 days post conditioning (fig. 3.22; 3.23) (24 hr: $F(1,10)= 4.021$; $p<0.001$; 36d: $F(1,10)= 16.574$; $p< 0.01$).

Post-training, intra-hippocampal infusion of anisomycin abolishes morphological changes (Fig. 3.24-3.25) (apical dendritic spines: $F(1,9)= 2.509$, $p<0,05$; basal dendritic spines: $F(1,6)= 2.572$, $p<0,05$) and biochemical changes (fig. 3.26) observed in hippocampal pyramidal neurons 24 hr after conditioning. No effect of the infusion were observed in saline control group (fig. 3.24, 3.25, 3.26)

Moreover post-training infusion of this translation inhibitor prevented morphological changes (Apical spines: $F(1,9)= 4.584$; $p<0.01$; Basal spines: $F(1,6)= 5.563$; $p<0.01$) and EphrinB2 increase observed in the ACC area at the remote time point (36 days p.c.) (Fig. 3.27; 3.28; 3.29).

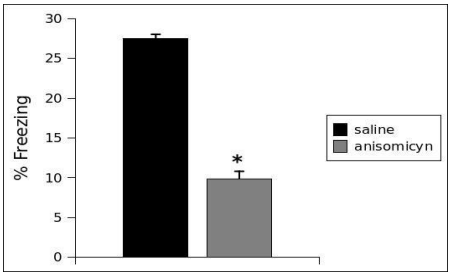

Fig 3.22 - Behavioural responses to context fear conditioning, expressed as percentage of freezing time, 24 hr after intra-hippocampal anisomicyn infusion. Asterisk indicates significant difference between groups: $p< 0.001$)

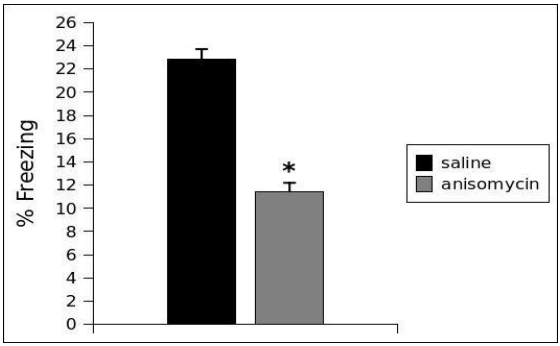

Fig 3.23 - Behavioural responses to context fear conditioning, expressed as percentage of freezing time, 36 days after intra-hippocampal anisomicyn infusion. Asterisk indicates significant difference between groups: $p< 0.01$).

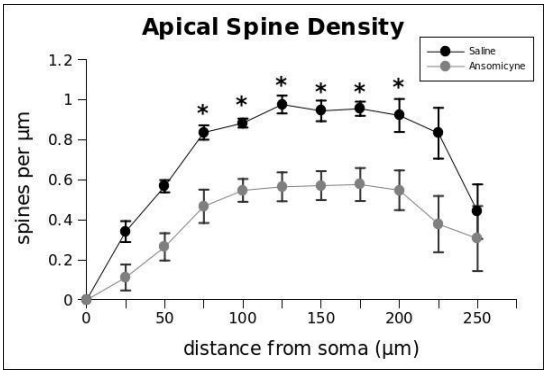

Fig 3.24 - Apical dendritic spine densities of pyramidal CA1 hippocampal neurons 24 hr after intra-hippocampal anisomicyn infusion. Values represent the mean number ± SEM of dendritic spines/µm counted on progressive 25 µm dendritic segments, relative to apical dendrites. Asterisks indicate differences between *saline* and *anisomycin* animals: $p< 0.05$

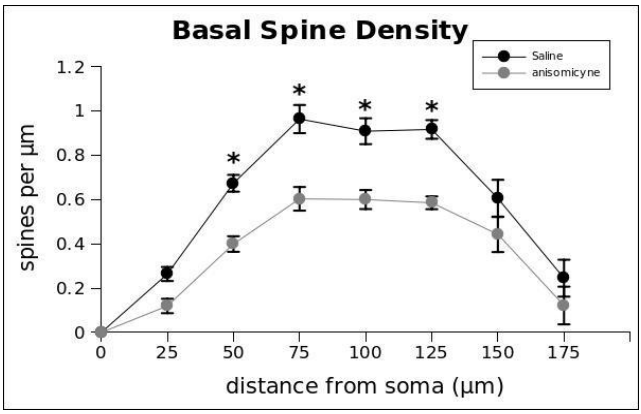

Fig 3.25 - Basal dendritic spine densities of pyramidal CA1 hippocampal neurons 24 hr after intra-hippocampal anisomicyn infusion. Values represent the mean number ± SEM of dendritic spines/µm counted on progressive 25 µm dendritic segments, relative to basal dendrites. Asterisks indicate differences between *saline* and *anisomycin* animals: $p < 0.05$.

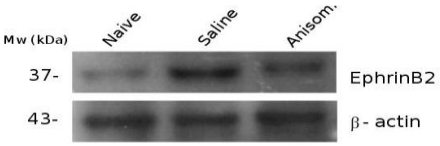

Fig 3.26 - Representative Western blot analisys of EphrinB2 in the hippocamus of *naïve, saline* and *anisomycin* animals 24 hr after intra-hippocampal anisomicyn infusion**.**

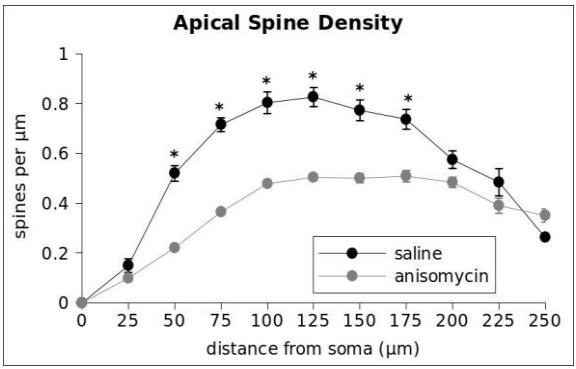

Fig 3.27 - Apical dendritic spine densities of ACC pyramidal neurons 36 days after intra-hippocampal anisomicyn infusion. Values represent the mean number ± SEM of dendritic spines/µm counted on progressive 25 µm dendritic segments, relative to apical dendrites. Asterisks indicate differences between *saline* and *anisomycin* animals: $p < 0.01$

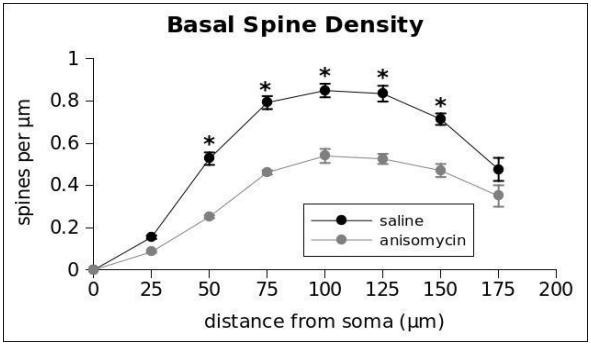

Fig 3.28 - Basal dendritic spine densities of ACC pyramidal neurons 36 days after intra-hippocampal anisomicyn infusion. Values represent the mean number ± SEM of dendritic spines/µm counted on progressive 25 µm dendritic segments, relative to basal dendrites. Asterisks indicate differences between *saline* and *anisomycin* animals: $p < 0.01$

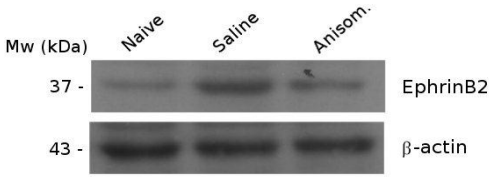

Fig 3.29 - Representative western blot analisys of EphrinB2 in the ACC of *naïve, saline* and *anisomycin* animals 36 days after intra-hippocampal anisomicyn infusion**.**

3.2.5 Late anisomycin treatment didn't prevent EphrinB2 increase in the cortex

Precedent experiments showed that early bilateral intra-hippocampal infusion of anisomycin completely abolished late (36 days) development of dendritic spine growth in ACC neurons of conditioned mice. Infact, conditioned mice receiving anisomycin infusion immediately post training exhibited less spines on ACC neurons than the *saline* group and didn't show increase in EphrinB2 level (Fig. 3.27, 3.28, 3.29).

Conversely, mice receiving intra-hippocampal infusion of anisomycin 24 days postconditioning did not show any reduction in freezing time compared with saline conditioned mice during the remote memory test (Fig. 3.30). Moreover late hippocampal infusion did not prevent conditioned mice to show an increase in spine density on ACC neurons 36 days postconditioning and in EphrinB2 level (Fig. 3.31, 3.32, 3.33).

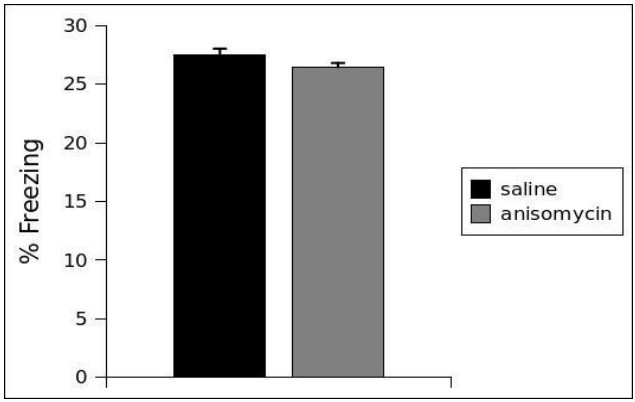

Fig 3.30 - Behavioural responses to context fear conditioning, during the remote memory test (36 days p.c.) of mice receiving intra-hippocampal infusion of anisomycin 24 days postconditioning.

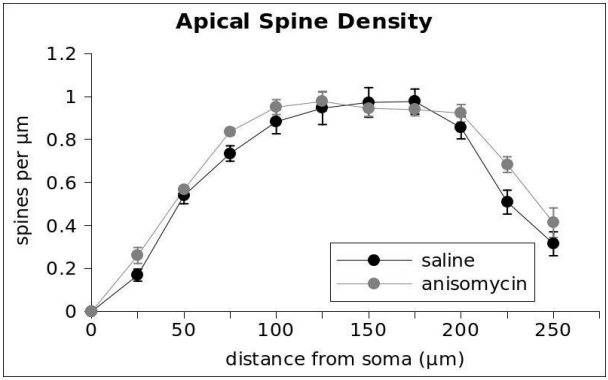

Fig 3.31 - Apical dendritic spine densities of ACC pyramidal neurons at the remote time point (36 days p.c.) of mice receiving intra-hippocampal infusion of anisomycin 24 days postconditioning. Values represent the mean number ± SEM of dendritic spines/µm counted on progressive 25 µm dendritic segments, relative to apical dendrites.

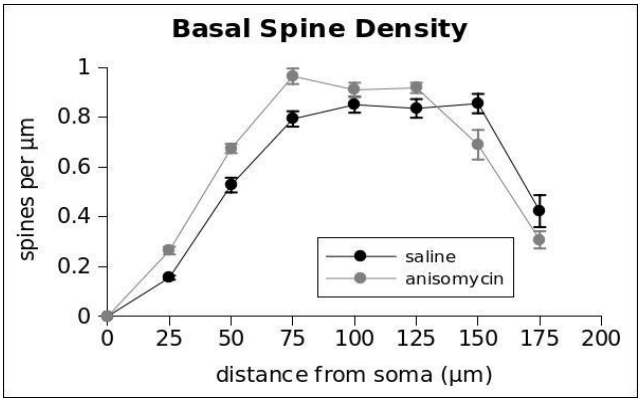

Fig 3.32 - Basal dendritic spine densities of ACC pyramidal neurons at the remote time point (36 days p.c.) of mice receiving intra-hippocampal infusion of anisomycin 24 days postconditioning. Values represent the mean number ± SEM of dendritic spines/µm counted on progressive 25 µm dendritic segments, relative to basal dendrites.

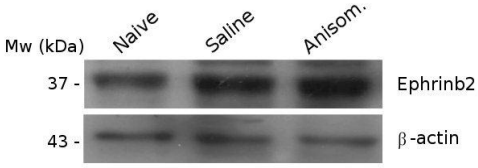

Fig 3.33 - Representative western blot analisys of EphrinB2 in the ACC of *naïve, saline* and *anisomycin* at the remote time point (36 days p.c.) of mice receiving intra-hippocampal infusion of anisomycin 24 days postconditioning.

Chapter 4 - Discussion and Conclusions

4.1 Cellular and molecular mechanisms of recent memory formations in pyramidal hippocampal neurons

Modulation of synaptic strength and structure is the fondamental mechanism by witch implicit and explicit memory are encoded and stored. Recent studies suggest this synaptic growth and formation of new connections depend on stable changes in neurons that maintain long-term memory based on learning-induced pathways of protein synthesis. However, little is known about molecular anc cellular mechanisms that initiate and maintain the structural changes (Bailey and kandel 2004, Bliss et al, 2003), in spite of the substantial amount of data produced on morphological modifications of neurons involved in memory formation and consolidation (Leuner et al., 2003; Knafo et al., 2004; Restivo et al., 2006).

Previous studies have shown the activation of some signalling pathways during the formation of contextual fear memory in the CA1 area of the hippocampus and in the lateral amygdala. Specific protein khinase such as PKA (Isiega et al., 2006), PKC (Tronson et al., 2008) and CaMKII (Silva, 2003) control this signalling and the transcription of immediate early genes like c-fos and Arc (Radulovic et al., 1998; Matsuo et al., 2008). Other pathways, including translation of specific protein products, have not been described yet.

To shed light into this complex process, we investigated possible changes induced by fear conditioning in expression of EphrinB2, a cell-to-cell adhesion factor involved in synaptic plasticity (Grunwald et al., 2004; Migani et al.,

2007; Liebl et al., 2003), and the association of these changes with conditioning-dependent behavioural and cellular modifications.

Ephrin ligands and their tyrosine kinase receptors are "guidance" proteins involved in development, abundantly expressed in the developing brain, that have been also shown to play a role in adult neural plasticity. They are known to influence neuronal plasticity and the dynamics of dendritic spines in the adult brain. By interaction with their receptors, EphrinBs, in particular, appear to be involved in both LTP (Contractor et al., 2002) and LTD (Grunwald et al., 2001) maturation processes (Henderson et al., 2001) of hippocampal neuron synapses. In the present study, we have focused our attention on EphrinB2, a factor expressed both presynaptically and postsynaptically, as observed in hippocampal connections: presynaptic EphrinB2 regulate initial steps in the formation of synaptic connections by inducing interaction of postsynaptic EphB receptors with NMDA glutamate receptors (Rao et al., 1998; Dalva et al., 2000). In addiction, clustering of postsynaptic EphB2 receptors may enhance interaction with presynaptic Ephrins and increase glutamate release (Klein, 2009). In hippocampal CA1 and CA3 neurons, EphrinB2 is also expressed on postsynaptic membranes and is functionally necessary for LTP and LTD (Grunwald et al., 2004). Moreover, in the hippocampus, EphrinB2 mRNA is abundant in CA1 neurons but poorly expressed in CA3 and DG neurons (Grunwald et al., 2001; 2004). In contrast to such uneven mRNA distribution, Migani et al. (2007) observed similar levels of EphrinB2 protein in neuronal cell bodies of CA1, CA3 and DG. These observations suggest that specific mechanisms may control EphrinB2 synthesis at the translational level, making of such factor a good candidate as a protein product readily induced by

conditioning via *de novo* translation of stored messages.

In this work we provide evidence that changes in spine density and dendrite complexity occur in hippocampal neurons during the formation of recent contextual fear memory and, consistent with the hypothesis of Bailey et al. (2004), that such changes are associated to an increase in the levels of EphrinB2 observed in these cells.

We first subjected mice to contextual and cued fear conditioning test and observed strong fear conditioning responses. The formation of aversive memory was associated with an increase in dendritic spine density in the CA1 hippocampal region and the lateral amygdala, confirming the involvement of the hippocampus and the amygdala in such behavioural paradigm (Huff et al., 2006). The increase in spine density in lateral amygdala neurons was observed in both basal and apical neurons, as already reported (Vyas et al., 2002). In hippocampal pyramidal neurons, spine density increase was limited to apical dendrites. However, for these cells, previous reports have described a certain variability in conditioning-dependent modifications, depending on the specific learning task or the experimental procedures employed (Leuner et al., 2003; Knafo et al., 2004; Restivo et al., 2009).

Since our main objective was to investigate the role of the hippocampus in contextual fear memory, we then analyzed presence of EphrinB2 in such structure and compared it to that found in the whole cortex of conditioned, pseudoconditioned and naive mice by Western blot. Contextual fear conditioning was associated with a rapid increase in levels of EphrinB2 in the hippocampus of conditioned mice, while no differences were observed in the cortices, coherently with the theory that recent memory relies on hippocampal rather than on cortical activity (Restivo et al., 2009). This result represents the first report

of a cell adhesion factor rapidly induced upon conditioning in the structure responsible for spatial learning.

We also analyzed cellular localization of EphrinB2 in the hippocampus and, in light of what observed in behavioural experiments, compared it to that found in the amygdala. We observed a clear distribution of such factor in the pyramidal neuron layer of the CA1 and CA3 and in the granular layer of DG as reported by Migani et al. (2007). A detailed analysis of EphrinB2 immunoreactivity allowed us to localize the factor in neuronal cell bodies and apical dendrites. Whether this factor is also present in basal dendrites was not clear and remains to be elucidated. Quantitative measurements were performed as described in different reports relative to a number of products, including cannabinoid receptors (Suárez et al., 2009), PKC (Ferri et al., 2006), 5-HT (Isoda et al., 2010), the apoptotic protein 14-3-3theta/tau, GFAP and α-internexin (Tang et al., 2002).

Conditioned animals showed increased levels of EphrinB2 in the CA1 area but not in other hippocampal areas, respect to pseudoconditioned and naive mice. This increase was found to be correlated with rise in spine density observed in CA1 apical dendrites, by Spearman's rank correlation analysis, suggesting an association of EphrinB2 abundance with mechanisms that leads the formation of new dendritic spines. In the hippocapus, EphrinB2 mRNA is more abundant in the CA1 area than in the CA3 and DG (13-14), in contrast with the protein distribution that is similar in the three different areas (Migani et al., 2007). This observation suggest the hypothesis that the observed rapid increased of such factor in the CA1 area of conditioned mice is the result of conditioning-induced translation of stored mRNAs. If confirmed, this observation would make EphrinB2 a good candidate among protein factors quickly induced by

conditioning and probably involved in mechanisms of new spine growth. This, in turn, is consistent with the established view that new protein synthesis is required to maintain the persistence of synaptic strengthening and weakening, independently of transcription (Kang et al., 1996; Huber et al., 2000; Cracco et al., 2005; Pfeiffer and Huber, 2006).

In spite of the increase in spine density observed in lateral amygdala of conditioned mice, immunohistochemical analysis didn't show changes in EphrinB2 levels of conditioned mice. This result suggest that, although such structure is clearly involved in the emotional learning of fear conditioning, molecular mechanisms underlying its plasticity may not involve the same adhesion factors observed in the hippocampus.

We also analyzed possible changes in the abundance of EphA4, a putative receptor for EphrinB2, in consequence of fear conditioning. However, no differences were found in the hippocampus and cortex under defferent conditions, suggesting that the increase in amout found for EprinB2 is specific and, if EphA4 covers a role(s) in neuronal plasticity, this does not depend on new synthesis. This pattern, however, deserves futher study.

Our results on conditioning-induced increase in EphrinB2 abundance in CA1 neurons suggest a possible role for such factor in changes in neuronal structure, although not excluding a similar role for other EphrinBs and/or different cell-to-cell adhesion factors. They may therefore represent the basis for further molecular studies of cell plasticity in the nervous tissue.

4.2 Cellular and molecular mechanisms of remote memory formations in pyramidal hippocampal and anterior cingulate cortex neurons

To investigate whether the increase in EphrinB2 levels may represent a process of induced neuronal plasticity in the hippocampus and other brain structures, we studied the conversion of recent to remote memory, which ultimately depends on an increase in dendritic spine density of pyramidal neurons of the anterior cingulate cortex (ACC) (Restivo et al.,2009), by analyzing the effect of contextual fear conditioning on EphrinB2 levels in these neurons.

Long-term memories depend on the hippocampus for their encoding (recent memory), as established by the standard theory of memory consolidation. The stabilization of the memory trace is assumed to involve synaptic consolidation, which is achieved within minutes-to-hours. In parallel, a process of system consolidation is initiated in which memory traces reorganize over a period of weeks, shifting to the neocortex (i.e. the anterior cingulate cortex, ACC), so that at the end of the process the neocortex can independently maintain the specific memories (remote memory). It is not yet known what triggers system consolidation, but the hypothesis is that over time, upon recurrent activation of the hippocampal trace, the hippocampus send synaptic messages to neocortical neurons, and these messages trigger synaptic consolidation locally (Dudai, 2002; Squire et al., 2004). According to this model, we determined dendritic complexity and EphrinB2 levels 24 hours (recent), 7 days (imtermediate) and 36 days (remote) after conditioning/pseudoconditioning in the hippocampus and ACC of mice. As aspected, contextual fear memory consolidation was associated with a time-dependent

spine growth in the hippocampus and ACC. Conditioned mice exhibited a significant increase in spines density on CA1 pyramidal neurons 24 hr and 7 days after conditioning and in ACC neurons 36 days after conditioning.

We observed that in conditioned mice, EphrinB2 accumulation parallels the increase in spine density of CA1 neurons at the recent and intermediate time points p.c., and the subsequent decrease at the remote time point. In addition, a similar parallel pattern is observed for EphrinB2 levels and dendritic complexity in ACC neuron, which are both low at the recent and intermediate time points but are increased at the remote time point p.c.. These results support the hypothesis that accumulation of EphrinB2 is involved in memory-associated cellular modifications detected in both the hippocampus and ACC, and may therefore represent a biochemical marker of conditioning-induced cell rearrangements observed in different neuronal types.

The theory of system consolidation attributes a central role to the early activation of hippocampal-cortex circuits for the recruitment of cortical networks in the storage of remote memory (Bontempi et al., 1999; Dudai, 2002; Frankland and Bontempi, 2005). As a conseguence, an early hippocampal lesion or intra-hippocampal infusion of an inhibitor of protein syntesis would prevent remote memory storage and morphological and biochemical changes associated to memory consolidation (Restivo et al., 2009). On the contrary, the same manipulation performed after the end of hippocampal-cortical communication, namely 24 days p.c., as reported (Restivo et al., 2009), would result ineffective in such inhibition.

To analyze this issue we performed immediately post-training intra-hippocampal infusions (early infusions) of the inhibitor of translation anisomycin to block hippocampal-cortex communication. We then examined conditioning

induced performances, morphological changes and EphrinB2 levels 24 hr later in the hippocampus and after 36 days in the ACC. As expected, we observed a disruption in recent and remote memory in parallel with inhibition of the increase in spine density observed in the hippocampus and ACC, respectively at 24 hr and 36 days p.c.. Furthermore, the early hippocampal infusions prevented consolidation-induced EphrinB2 increase observed in the hippocampus after 24 hr and also in the ACC at the remote time point, suggesting a strong relationship between morphological changes and increase in EphrinB2 levels detected.

We also performed late hippocampal infusions of anisomycin, 24 days p.c. to confirm the transient nature of hippocampal-cortical communication. Our results support previous observations, since mice subjected to late intra-hippocampal infusion showed normale increases in EphrinB2 abundance and the associated rise in spine density in ACC neurons.

These findings strongly suggest a role for EphrinB2 ligand in neuronal plasticity and dendritic spine formation not only in the hippocampus, during recent memory consolidation but also in the ACC during remote memory stabilization.

Taken together, our results can be summarized as follows:

a) the hippocampus directly controls memory consolidation processes occurring in the ACC;

b) this control occurs early after conditioning and acts via formation of new synaptic connections;

c) the cortical response to such influence results in similar neuronal modifications;

d) both processes occur in association to an increase in the cellular amount of the cell-to-cell adhesion factor EphrinB2;

e) both processes occur according to mechanisms depending on new protein synthesis taking place in hippocampal neurons early after conditioning;

f) the role of protein synthesis in ACC neuronal modifications, although made likely by these observations, remains to be elucidated.

References

Abel T, Nguyen PV (2008) Regulation of hippocampus-dependent memory by cyclic AMP-dependent protein kinase. Prog Brain Res, 169, pp. 97–115

Amaral, D; Lavenex P (2006) "Ch 3. Hippocampal Neuroanatomy". In Andersen P, Morris R, Amaral D, Bliss T, O'Keefe J. The Hippocampus Book. Oxford University Press.

Andersen P, Bliss TV, Skrede KK. (1971) Unit analysis of hippocampal population spike. Exp Brain Res. 13(2):208-21.

Arikkath J, Reichardt LF (2008) Cadherins and catenins at synapses: roles in synaptogenesis and synaptic plasticity. Trends Neurosci, 31:487-494.

Atkinson RC, Shiffrin RM. (1968) Human memory: a proposed system and its control processes. In: Spence KW, Spence JT (eds). The psychology of learning and motivation: advances in research and theory. New York: Academic Press; vol. 2, pp. 89-195.

Baddeley and Godden (1975) Context-dependent memory in two natural enviornments: on land and underwater.

Baddeley AD (2000) "The episodic buffer: a new component of working memory?". Trends in Cognitive Science 4 (11): 417–23.

Barros, DM, Izquierdo LA, Mello e Souza T, Ardenghi PG, Pereira P, Medina JH, Izquierdo I (2000) Molecular signalling pathways in the cerebral cortex are required for retrieval of one-trial avoidance learning in rats. Behavioural Brain Research, 114, 183–192.

Bailey CH, Kandel ER, Si K (2004) The persistence of long-term memory: a molecular approach to self-sustaining changes in learning-induced synaptic growth. Neuron;44:49–57.

Bayley PJ, Squire LR. (2002). Medial temporal lobe amnesia: gradual acquisition of factual information by nondeclarative memory. J. Neurosci. 22:5741–48

Bliss TV, Lømo T (1973) Long-lasting potentiation of synaptic transmission in the dentate area of the anesthetized rabbit following stimulation of the perforant path. J Physiol. 232(2):331-56.

Bliss TV, Collingridge GL, Morris RG (2003) Introduction. Long-term potentiation and structure of the issue. Philos Trans R Soc Lond B Biol Sci. Apr 29;358(1432):607-11.

Bontempi B, Laurent-Demir C, Destrade C, Jaffard R (1999) Time-dependent reorganization of brain circuitry underlying long-term memory storage. Nature 400:671–75

Bradford MM (1976) A rapid and sensitive method for the quantitation of microgram quantities of protein utilizing the principle of protein-dye binding. Anal Biochem, 72, pp. 248–254

Burnham WH (1903) Retroactive amnesia: illustrative cases and a tentative explanation. Am. J. Psychol. 14:382–96

Chiu YC, Algase D, Whall A (2004) Getting lost: directed attention and executive functions in early Alzheimer's disease patients. Dement Geriatr Cogn Disord 17 (3): 174–80.

Cho YH, Beracochea D, Jaffard R (1993) Extended temporal gradient for the retrograde and anterograde amnesia produced by ibotenate entorhinal cortex lesions in mice. J. Neurosci. 13:1759–66

Clark RE, Broadbent NJ, Zola SM, Squire LR (2002) Anterograde amnesia and temporally graded retrograde amnesia for a nonspatial memory task after lesions of hippocampus and subiculum. J. Neurosci. 22:4663–69

Clark RE, Broadbent NJ, Squire LR (2005) Hippocampus and remote spatial memory in rats. Hippocampus 15 (2): 260–72

Contractor A, Rogers C, Maron C, Henkemeyer M, Swanson GT, Heinemann SF (2002) Trans synaptic Eph receptor–ephrin signaling in hippocampal mossy fiber LTP. Science, 296 (5574), pp. 1864–1869

Cooke SF, Bliss TV (2006) Plasticity in the human central nervous system. Brain 129 (Pt 7): 1659–73.

Cowan, N. (2001) The magical number 4 in short-term memory: A reconsideration of mental storage capacity. Behavioral and Brain Sciences 24: 97–185.

Clugnet MC, LeDoux JE (1990). Synaptic plasticity in fear conditioning circuits: induction of LTP in the lateral amygdala by stimulation of the medial genicolate body. J Neurosci 10 (8): 2818–24

Cracco JB, Serrano P, Moskowitz SI, Bergold PJ, Sacktor TC (2005) Protein synthesis-dependent LTP in isolated dendrites of CA1 pyramidal cells. Hippocampus, 15, pp. 551–556

Dalva MB, Takasu MA, Lin MZ, Shamah SM, Hu L, Gale NW, Greenberg ME (2000). EphB receptors interact with NMDA receptors and regulate excitatory synapse formation? Cell, 103 (6) , pp. 945–956

Deisseroth K, Bito H, Tsien RW (1996) Signaling from synapse to nucleus: postsynaptic CREB phosphorylation during multiple forms of hippocampal synaptic plasticity. Neuron 16:89–101

Dudai Y (2002) Memory from A to Z. Keywords, Concepts and Beyond. Oxford: Oxford Univ. Press

Dudai Y (2006) Reconsolidation: the advantage of being refocused. Curr Opin Neurobiol. Apr;16(2):174-8. Epub Mar 24.

Egea J, Klein R (2007) Bidirectional Eph-ephrin signaling during axon guidance.Trends Cell Biol. May;17(5):230-8.

Eichenbaum H, Yonelinas AP, Ranganath C (2007) The medial temporal lobe and recognition memory. Annu Rev

Neurosci 30: 123–52.

Eichenbaum H, Cohen NJ (2001) From conditioning to conscious recollection. Oxford University Press, New York.

Engert F, Bonhoeffer T (1999) Dendritic spine changes associated with hippocampal long-term synaptic plasticity. Nature, 399:66-70.

Ferri P, Cecchini T, Ambrogini P, Betti M, Cuppini R, Del Grande P, Ciaroni S (2006) Alpha-tocopherol affects neuronal plasticity in adult rat dentate gyrus: the possible role of PKCdelta. J Neurobiol, 66 (8) , pp. 793–810

Fischer M, Kaech S, Wagner U, Brinkhaus H, Matus A (2000) Glutamate receptors regulate actin-based plasticity in dendritic spines. Nat Neurosci, 3 , pp. 887–894

Frankland PW, Bontempi B (2005) The organization of recent and remote memories. Nat Rev Neurosci 6:119 –130.

Franklin KBJ, Paxinos G (2001)The mouse brain in stereotaxic coordinates. (2nd ed.) Academic, San Diego

R. Gibb, B. Kolb (1998) A method for vibratome sectioning of Golgi–Cox stained whole rat brain. J Neurosci Methods, 79 , pp. 1–4

Glaser EM,Van Der Loos G (1981) Analysis of thick brain sections by observe-reverse computer microscopy: application of a new, high clarity Golgi–Nissl stain. J Neurosci Methods, 4 , pp. 117–125

Grunwald IC, Korte M, Wolfer D, Wilkinson GA,

Unsicker K, Lipp HP, Bonhoeffer T, Klein R (2001) Kinase-independent requirement of EphB2 receptors in hippocampal synaptic plasticity Neuron, 32 pp. 1027–1040

Grunwald IC, Korte M, Adelmann G, Plueck A, Kullander K, Adams RH, Frotscher M, Bonhoeffer T, Klein R (2004) Hippocampal plasticity requires postsynaptic EphrinBs Nat Neurosci, 7 , pp. 33–40

E. Harlow, D. Lane (Eds.) (1988) Antibodies: a laboratory manual, Cold Spring Harbor Laboratory, N.Y. , p. 449

Harvey CD, Svoboda K (2007) Locally dynamic synaptic learning rules in pyramidal neuron dendrites. Nature, 450:1195-1200.

Hebb DO (1949). The organization of behaviour: a neuropsychological theory. Wiley , New york, USA

Henderson JT, Georgiou J, Jia Z, Robertson J, Elowe S, Roder JC, Pawson T (2001) The receptor tyrosine kinase EphB2 regulates NMDA-dependent synaptic function Neuron, 32 , pp. 1041-1056

Holland SJ, Gale NW, Mbamalu G, Yancopoulos GD, Henkemeyer M, Pawson D (1996) Bidirectional signalling through the EPH-family receptor Nuk and its transmembrane ligands Nature, 383 , pp. 722–725

Holtmaat AJ, Trachtenberg JT, Wilbrecht L, Shepherd GM, Zhang X, Knott GW, Svoboda K (2005) Transient and persistent dendritic spines in the neocortex in vivo. Neuron, 45:279-291.

Huff NC, Frank M, Wright-Hardesty K, Sprunger D, Matus-Amat P, Higgins E, Rudy JW (2006) Amygdala regulation of immediate-early gene expression in the hippocampus induced by contextual fear conditioning. J Neurosci, 26 (5) , pp. 1616–1623

Hughes, John R (1958). Post-tetanic Potentiation. Physiological Reviews 38 (1): 91–113.

Harris E, Cotman C (1986) Long-term potentiation of guinea pig mossy fiber responses is not blocked by N-methyl D-aspartate antagonists. Neurosci Lett 70 (1): 132–7.

Isoda K, Morimoto M, Matsui F, Hasegawa T, Tozawa T, Morioka S (2010) Postnatal changes in serotonergic innervation to the hippocampus of methyl-CpG-binding protein 2-null mice. Neuroscience, 165, pp. 1254–1260

Huber KM, Kayser MS, Bear MF (2000) Role for rapid dendritic protein synthesis in hippocampal mGluR-dependent LTD. Science, 288 , pp. 1254–1257

Kandel ER, Schwartz JH, Jessell TM. (2007). Principi di neuroscienze. Ambrosiana, Milano.

Kang H, Schuman EM (1996) A requirement for local protein synthesis in neurotrophin-induced hippocampal synaptic plasticity. Science, 273 , pp. 1402–1406

Kim JJ, Fabselow MS (1992) Modality-specific retrograde amnesia of fear. Science 256:675–77

Kim JJ, Clark RE, Thompson RF (1995) Hippocampectomy impairs the memory of recently, but not

remotely, acquired trace eye-blink conditioned response. Behav. Neurosci. 109:195–203

Klein R (2009) Bidirectional modulation of synaptic functions by Eph/Ephrin signalling? Nat Neurosci, 12 (1) , pp. 15–20

Knafo S, Ariav G, Barkai E, Libersat F (2004) Olfactory learning-induced increases in spine density along the spine density along the apical dendrites in CA1 hippocampal neuron? Hippocampus, 14 (7) , pp. 819–825

Knowlton BJ, Mangels JA, Squire LR (1996) A neostriatal habit learning system in humans. Science. 273 (5280):1399-402.

Kullander K, Klein R (2002) Mechanisms and functions of Eph and Ephrin signalling? Nat Rev Mol Cell Biol

Kolb B and Whishaw, IQ (1996) Fundamentals of human neuropsychology (4th ed.). New York, NY: W. H. Freeman.

Jensen and Lisman (2005) Hippocampal sequence-encoding driven by a cortical multi-item working memory buffer. Trends Neurosci. Feb;28(2):67-72.

Kubie JL, Suhterland RJ, Miller RU (1999) Hippocampal lesions produce a temporally graded retrograde amnesia on a dry version of the Morris swimming task. Psychobiology 27:313–30

Isiegas C, Park A, Kandel ER, Abel T, Lattal KM (2006) Transgenic inhibition of neuronal protein kinase A activity facilitates fear extinction. J Neurosci, 26, pp. 12700–12707

Labrie V, Duffy S, Wang W, Barger S, Baker G, Roder J (2008) Genetic inactivation of D-amino acid oxidase enhances extinction and reversal learning in mice. Learn Mem 16(1): 28-37.

Lamprecht R, LeDoux J (2004) Structural plasticity and memory. Nat Rev Neurosci, 5, pp. 45–54

Leuner B, Falduto J, Shors TJ (2003) Associative memory formation increases the observation of dendritic spines in the hippocampus? J Neurosci, 23 (2), pp. 659–665

Liebl DJ, Morris CJ, Henkemeyer M, Parada LF (2003) mRNA expression of Ephrins and Eph receptor tyrosine kinases in the neonatal and adult mouse central nervous system. J Neurosci Res, 71 , pp. 7–22

Lin DT, Makino Y, Sharma K, Hayashi T, Neve R, Takamiya K, Huganir RL (2009) Regulation of AMPA receptor extrasynaptic insertion by 41N, phosphorylation and palmitoylation. Nat Neurosci, 12, pp. 879–887

Luo L, and Flanagan JG (2007) Development of continuous and discrete neural maps. Neuron 56, 284–300.

Matus A (2000) Actin-based plasticity in dendritic spines. Science, 290:754-758.

Martin SJ, Clark RE (2007) The rodent hippocampus and spatial memory: from synapses to systems. Cell Mol Life Sci, 64 (2007), pp. 401–431

McGaugh JL (2002) Memory consolidation and the

amygdala: a systems perspective. Trends Neurosci. 25:456–61

Megías M, Emri Z, Freund TF, Gulyás AI (2001) Total number and distribution of inhibitory and excitatory synapses on hippocampal CA1 pyramidal cells. Neuroscience 102 (3): 527–40.

Matsuo N, Reijmers L, Mayford M (2008) Spine-type-specific recruitment of newly synthesized AMPA receptors with learning. Science, 319, pp. 1104–1107

Matsuzaki M, Honkura N, Ellis-Davies GC, Kasai H (2004) Structural basis of long-term potentiation in single dendritic spines. Nature, 429:761-766.

Migani P, Bartlett C, Dunlop S, Beazley L, Roger J (2007) Ephrin-B2 immunoreactivity distribution in adult mouse brain. Brain Res, 1182 , pp. 60–72

Miller GA (1956) The Magical Number Seven, Plus or Minus Two: Some Limits on our Capacity for Processing Information. Psychological Review, 63, 81-97

Milner B, Corkin S, Teiber HL (1968) Further analysis of the hippocampal amnesic syndrome: 14 years follow-up study of H.M.. Neuropsychologia 6:251-234.

Milner B (1972) Disorder of learning and memory after temporal lobe lesions in man. Clin Neurosurg. 19:421-46.

Morris RGM, Garrud P, Rawlins JNP, O'Keefe J (1982). Place navigation impaired in rats with hippocampal lesions. Nature 297 (5868): 681–83.

Muller GE, Pilzecker A (1900) Experimentelle Beitrage zur Lehre von Ged¨chtnis. Z. Psychol. 1:1–300

O'Keefe J, Nadel L (1978) The hippocampus as a cognitive map. Oxford University Press.

Pfeiffer BE, Huber M (2006) Current advances in local protein synthesis and synaptic plasticity J Neurosci, 26 (27), pp. 7147–7150

Poliakov A, Cotrina M, and Wilkinson DG (2004) Diverse roles of eph receptors and ephrins in the regulation of cell migration and tissue assembly. Dev. Cell 7, 465–480.

Papez JW (1937) A proposed mechanism of emotion. Arch Neurol Psychiatry.;38:725–743.

Pak DT, Sheng M (2003) Targeted protein degradation and synapse remodeling by an inducible protein kinase. Science, 302:1368-1373.

Park M, Salgado JM, Ostroff L, Helton TD, Robinson CG, Harris KM, Ehlers MD (2006) Plasticity-induced growth of dendritic spines by exocytic trafficking from recycling endosomes. Neuron, 52, pp. 817-30

Pasquale EB (2005) Eph receptor signalling casts a wide net on cell behaviour. Nat. Rev. Mol. Cell Biol. 6, 462–475.

Pasquale EB (2008) Eph–Ephrin bidirectional signaling in physiology and disease. Cell, 133, pp. 38–52

Penfield, W (1952) Memory Mechanisms. AMA Archives of Neurology and Psychiatry 67:178-198.

Penzes P, Cahill ME, Jones KA, Srivastava DP (2008) Convergent CaMK and RacGEF signals control dendritic structure and function. Trends Cell Biol, 18 , pp. 405–413

Pavlov IP (1927) Conditioned Reflexes: An Investigation of the Physiological Activity of the Cerebral Cortex. Translated and Edited by G. V. Anrep. London: Oxford University Press.

Radulovic J, Kammermeier J, Spiess J (1998) Relationship between fos production and classical fear conditioning: effects of novelty, latent inhibition, and unconditioned stimulus preexposure. J Neurosci, 18 , pp. 7452–7461

Ramòn y Cajal S (1891) Sur la structure de l'ecorce cerebrale de quelque mammiferes. Cellula. 7:123-176.

Ramos JMJ (1998) Retrograde amnesia for spatial information: dissociation between intra and extramaze cues following hippocampus lesions in rats. 10:3295–3301.

Rao A, Kim E, Sheng M, Craig AM (1998) Heterogeneity in the molecular composition of excitatory postsynaptic sites during development of hippocampal neurons in culture?. J Neurosci

Restivo L, Roman FS, Ammassari-Teule M, Marchetti E (2006) Simultaneous olfactory discrimination elicits a strain-specific increase in dendritic spines in the hippocampus of inbred mice? Hippocampus, 16 (5) , pp. 472–479

Restivo L, Vetere G, Bontempi B, Ammassari-Teule M (2009) The formation of recent and remote memory is associated with time-dependent formation of dendritic spines in the hippocampus and anterior cingulate cortex? J Neurosci, 29 (25) , pp. 8206–8214

Scoville WB, Milner B (1957) Loss of recent memory after bilateral hippocampal lesions. J Neurol Neurosurg Psych, 20:11-21.

Skinner BF (1953) Science and human behavior. Oxford, England: Macmillan.

Skinner BF (1974) About Behaviorism Ch. 1 Causes of Behaviour § 3 Radical Behaviorism.ISBN 0-394-71618-3

Silva AJ (2003) Molecular and cellular cognitive studies of the role of synaptic plasticity in memory. J Neurobiol, 54 , pp. 224–237

Squire LR. (1987). Memory and Brain. New York: Oxford Univ. Press

Squire LR, Clark RE, Knowlton BJ (2001) Retrograde amnesia. Hippocampus. 11(1):50-5.

Squire LR (2004) Memory systems of the brain: A brief history and current perspective. Neurobiology of Learning and Memory. 82; 171-177.

Squire LR, Alvarez P (1995) Retrograde amnesia and memory consolidation: a neurobiological perspective. Curr. Biol. 5:169–77.

Squire LR, Bayley PJ (2007) The neuroscience of remote memory. Curr Opin Neurobiol, 17, pp. 185–196

Suárez J, Llorente R, Romero-Zerbo SY, Mateos B, Bermúdez-Silva FJ, De Fonseca FR, Viveros MP (2009) Early maternal deprivation induces gender-dependent changes on the expression of hippocampal CB(1) and CB(2) cannabinoid receptors of neonatal rats. Hippocampus, 19, pp. 623–632

Sutherland RJ, Kolb B, Whishaw IQ (1982) Spatial-mapping- definitive disruption by hippocampal or medial frontal cortical damage in the rat. Neuroscience Letters 31 (3): 271–6

Sutherland RJ, Weisend MP, Mumby D,Astur RS, Hanlon FM, Koerner A, Thomas MJ, Wu Y, Moses SN, Cole C, Hamilton DA, Hoesing JM (2001) Retrograde amnesia after hippocampal damage: Recent vs. remote memories in two tasks. Hippocampus 11 (1): 27–42.

Tang SJ, Reis G, Kang H, Gingras AC, Sonenberg N, Schuman EM (2002) A rapamycin-sensitive signaling pathway contributes to long-term synaptic plasticity in the hippocampus. Proc Natl Acad Sci USA, 99, pp. 467–472

Takasu MA, Dalva MB, Zigmond RE, Greenberg ME(2002) Modulation of NMDA receptor-dependent calcium influx and gene expression through EphB receptors. Science, 295, pp. 491–495

Richard F, Thompson and Jeasok, Kim J (1996) Memory systems in the brain and localization of a memory. Proc. Natl. Acad. Sci. USA Vol. 93, pp. 13438–13444

Tronson NC, Schrick C, Fischer A, Sananbenesi F, Pages G, Pouyssegur J, Radulovic J (2008) Regulatory mechanisms of fear extinction and depression-like behavior. Neuropsychopharmacology, 33, pp. 1570–1583

Trabalza A, Colazingari S, Sgobio C, Bevilacqua A (2012) Contextual learning increase dendrite complexity and EphrinB2 levels in hippocampal mouse neurons. Behav Br Res 227: 175– 183

Tulving and Thomson (1973). Encoding specificity and retrieval processes in episodic memory, in Psycological Review, 80 352-373

Zheng Z, Keifer J (2009) PKA has a critical role in synaptic delivery of GluR1- and GluR4 Containing AMPARs during initial stages of acquisition of in vitro classical conditioning. J Neurophysiol, 10 , pp. 2539–2549

West AE, Griffith EC, Greenberg ME (2002) Regulation of transcription factors by neuronal activity. Nat Rev Neurosci, 3, pp. 921–931

Wilson MA, McNaughton BL (1994). Reactivation of hippocampal ensemble memories during sleep. Science 265 (5172): 676–79.

Xia Z, Storm DR (2005) The role of calmodulin as a signal integrator for synaptic plasticity. Nat Rev Neurosci, 6, pp. 267–276

Yong-Seok L, Silva A (2009) The molecular and cellular biology of enhanced cognition. Nat Rev Neurosci, 10, pp.

126–140

Yoshihara Y, De Roo M, Muller D (2009) Dendritic spine formation and stabilization. Curr Opin Neurobiol (2) , pp. 146–153

Vyas A, Mitra R, Shankaranarayana Rao BS, Chattarji S (2002) Chronic stress induces contrasting patterns of dendritic remodeling in hippocampal and amygdaloid neurons. J Neurosci, 22 (15), pp. 6810–6818

Zola-Morgan SM, Squire LR (1990) The primate hippocampal formation: evidence for a time-limited role in memory storage. Science 250:288–90

Publications

Behavioural Brain Research 227 (2012) 175–183

Contents lists available at SciVerse ScienceDirect

Behavioural Brain Research

journal homepage: www.elsevier.com/locate/bbr

Research report

Contextual learning increases dendrite complexity and EphrinB2 levels in hippocampal mouse neurons

Antonio Trabalza[a,1,2], Sandra Colazingari[a,1], Carmelo Sgobio[b], Arturo Bevilacqua[a,*]

[a] Department of Psychology, Section of Neuroscience, University of Rome "Sapienza", via dei Marsi 78, 00185 Rome, Italy and "Centro di Ricerca in Neurobiologia Daniel Bovet" (CRiN), Rome, Italy
[b] IRCCS Fondazione Santa Lucia, via del fosso di Fiorano 65, 00143, Rome, Italy

ARTICLE INFO

Article history:
Received 9 August 2011
Received in revised form 3 November 2011
Accepted 6 November 2011
Available online xxx

Keywords:
Contextual fear conditioning
Cued fear conditioning
Dendritic spines
Dendritic nodes
EphrinB2
Pyramidal neurons
Hippocampus
Amygdala
Mouse

ABSTRACT

Although the role of hippocampus in memory processing is well assessed, an association of experience-dependent behavioural modifications with hippocampal neuron morphological and biochemical changes deserves further characterisation. Here, we present evidence of dendritic alterations together with rapid accumulation of EphrinB2, a factor known to influence cell plasticity, in pyramidal neurons of the CA1 area of mouse hippocampus, during the formation of recent contextual fear memory. Male C57BL/6N mice exhibited a robust fear response 24 h after contextual and cued fear conditioning. At this time and in the absence of the memory test, *conditioned* mice showed morphological alterations in hippocampal and lateral amygdala neurons. Western blot analysis of extracts from *conditioned* but not *pseudoconditioned* or naive mice showed a specific increase in the amount of EphrinB2 in the hippocampus but not the cortex. However, levels of EphA4 receptor, known to interact trans-synaptically with EphrinB2, did not change upon conditioning in extracts from the same structures. Finally, immunohistochemical analysis of the hippocampus and amygdala of *conditioned* mice showed increased levels of EphrinB2 in pyramidal neurons of the CA1 area, when compared to *pseudoconditioned* and control mice. Such increase was not observed in other hippocampal areas or the amygdala. These results suggest that rapid accumulation of EphrinB2 in hippocampal CA1 neurons is involved in the behavioural and cellular modifications induced by contextual fear conditioning. A similar mechanism does not appear to occur in lateral amygdala neurons, in spite of the robust behavioural and cellular modifications induced in such structure by cued fear conditioning.

1. Introduction

According to the theory of memory consolidation, the formation of recent memory traces depends on the hippocampus [1], and this is achieved via rapid synaptic rearrangements morphologically revealed by an increase in spine density on neuronal dendrites [2–5]. In spite of the substantial body of information on alterations of hippocampal neurons following memory consolidation such as spatial learning, still little is known regarding molecular mechanisms underlying this process, with particular reference to the expression of factors that may be directly involved in neuronal rearrangements.

In the nervous system of adult mammals, among factors known to influence neuronal plasticity and the dynamics of dendritic spines are those belonging to the Ephrin family of receptors-ligands [6,7]. In mammals, Eph receptors are divided in two classes: EphA, with nine members and EphB, with five members [8]. These receptors binding EphrinAs (five members) and EphrinBs (three members) respectively, with the exception of EphA4, which can bind both A and B type ligands [9].

Activity of EphrinBs and EphB receptors, in particular, has been directly associated to molecular mechanisms of synaptic plasticity. In cultured rat hippocampal or cortical neurons, for instance, EphB receptors have been shown to be expressed postsynaptically and to interact with presynaptic EphrinBs, regulating initial steps in the formation of synaptic connections [10,11]. Moreover, the interaction of postsynaptic EphB receptors with EphrinB2 potentiates activity of glutamate NMDA receptors suggesting a possible pathway for the involvement of these factors in synaptic plasticity [12]. At the same time, EphrinBs/EphB receptors may also act in a reverse fashion as observed in the hippocampus, where EphrinB ligands are expressed postsynaptically suggesting their

* Corresponding author. Tel.: +39 0649917624; fax: +39 0649917868.
E-mail address: arturo.bevilacqua@uniroma1.it (A. Bevilacqua).
[1] These authors contributed equally to this study.
[2] Present address: Department of Gene Therapy, Centre for Neuroscience, Division of Experimental Medicine, Imperial College Faculty of Medicine, Hammersmith Hospital Campus, Burlington Danes Building, Du Cane Road, London W12 0NN, UK.

0166-4328/$ – see front matter © 2011 Elsevier B.V. All rights reserved.
doi:10.1016/j.bbr.2011.11.008

involvement in the regulation of synaptic transmission and plasticity by interaction with presynaptic receptors [13]. In situ RNA hybridisation data show that, while EphrinB1 expression is barely detectable in CA areas, both EphrinB2 and EphrinB3 are strongly expressed in CA1, and at a much lesser extent in CA3 [13]. At these synapses, EphrinB2 and EphrinB3 have been found to interact with NMDA receptors, being functionally necessary for LTP and LTD development, as demonstrated in genetically modified mice [14]. Interestingly, immunohistochemical analysis of EphrinB2 in the hippocampus has revealed a uniform distribution of the factor in the neuronal layer of all CA areas [15]. This observation, in strong contrast to previous in situ RNA hybridisation results, suggests the possibility that EphrinB2 mRNA is stored according to a post-transcriptional regulatory pathway that insures new synthesis of the factor depending on neuronal activity.

Eph receptors involved in EphrinB binding at hippocampal CA1 and CA3 synapses include, as of now, both EphB2 and EphA4, both of which are largely expressed and required for LTP [13,14,16].

To shed light into the nature of mechanisms of memory consolidation, we subjected mice to contextual and cued fear conditioning and evaluated their behavioural, morphological and biochemical effects 24 h later. At this time point, while a group of animals underwent the behavioural test, a second group was sacrificed for morphological and biochemical analyses. In detail, the right or left hemi brain of these animals was processed for Golgi–Cox impregnation and analysis of morphological changes induced by fear conditioning on pyramidal neurons located in the hippocampal CA1 area and lateral amygdala; the other hemi brain was used for analysis of conditioning-related biochemical events. This was performed by Western blot analysis of the expression of EphrinB2 and of EphA4 receptor as well as immunohistochemical analysis of EphrinB2 distribution in the hippocampus and amygdala. We show that the formation of recent contextual fear memory parallels an increase in both dendritic complexity of CA1 pyramidal neurons and EphrinB2 abundance in the hippocampus. A similar increase is not observed for the EphA4 receptor. Immunohistochemical analysis of hippocampal EphrinB2 revealed a specific increase in the pyramidal neurons of the CA1 area, observed both in the cell bodies and apical dendrites. While the formation of recent cued memory was associated to an increase in dendritic complexity of lateral amygdala neurons, no variations in the levels of EphrinB2 were observed in these cells. An increase in EphrinB2 amount may thus represent an early marker of learning-induced neuronal morphological modifications in the hippocampus but not the amygdala.

2. Materials and methods

2.1. Animals

Thirty male C57BL/6N mice (Charles River Italia, Calco), 6 weeks of age, were used in all experiments. Animals were housed in a temperature-controlled facility (22 °C ± 1 °C) on a 12/12 h light/dark cycle for 7 days. Housing conditions included the use of standard houseroom cages and unlimited access to food and water. Animal weights at the beginning of experiments ranged from 26 to 30 g. All experimental procedures were conducted in accordance with the official European guidelines for the care and use of laboratory animals (86/609/EEC).

2.2. Open field protocol

Twenty-four hours prior to the fear-conditioning session, basal levels of anxiety and locomotor activity were tested by placing each mouse in a circular open field (60 cm diameter; 30 cm H) for 6 min. Animal behaviour was recorded by a video camera fixed over the chamber and connected to a personal computer. Activity was assayed using software for behaviour analysis (Ethovision 3.0, Noldus Information Technology, Amsterdam, NL), by measuring indexes of distance travelled and thigmotaxis. Six out of the thirty mice of present experiments were not subjected to further treatments and were used as control animals, *naive* to fear conditioning protocols.

2.3. Contextual fear-conditioning protocol

For this procedure, each of the remaining 24 mice was placed in a transparent Plexiglas cage (28 cm × 28 cm × 10 cm, $L \times W \times H$) with a grid floor made of stainless steel rods (conditioning chamber), inside an experimental room (room 1). After 2 min of free exploration, 12 animals (from now on named *conditioned*) were exposed to a conditioned stimulus (CS) consisting of a tone (80 dB, 2000 Hz, 20 s) and to a subsequent unconditioned stimulus (US) consisting of an electric shock (0.3 mA, 1 s), provided immediately after the CS. Mice were left in the cage without additional stimuli for a total time of 5 min. Twelve control mice (from here on named *pseudoconditioned*) were maintained in the cage for a total of 5 min without any stimulus. Activity of each mouse was recorded as described for the open field test. Responses measured consisted of time of immobility (freezing), i.e., a complete lack of movement except for those relative to breathing, expressed in seconds.

Contextual fear memory was tested on 6 animals of both *conditioned* and *pseudoconditioned* groups 24 h after the conditioning session. To this end, each mouse was placed in the conditioning chamber inside room 1 for 5 min. During the test, animals were not subject to any stimulus. Activity, recorded as described for the conditioning session, was analysed in the first 2 min of the test.

2.4. Cued fear-conditioning protocol

One hour after the contextual test session, tested mice were placed in a cue test cage, consisting of a transparent Plexiglas cage (28 cm × 28 cm × 35 cm, $L \times W \times H$) with a plain floor and shaped in a triangle by a diagonal black plastic wall, inside a different experimental room (room 2) with different lights. After 2 min of free exploration, each mouse was exposed to the same tone (80 dB, 2000 Hz) used for the contextual fear-conditioning session for the remaining 3 min of the test. Activity was recorded and assayed as described for the previous tests. Responses measured consisted of time of freezing, expressed in seconds, during the initial 2 min and the remaining 3 min of the test.

2.5. Animal perfusion and brain preparation

Twenty-four hours after the conditioning session, 6 animals of each experimental group, for a total of 18, were anesthetised with chloral hydrate (400 mg/kg, i.p.) and perfused intracardially with ice-cold 0.1 M phosphate-buffered saline (PBS, pH 7.4). Since non-significant interhemispheric differences have been so far reported in the assessment of neuronal morphology upon conditioning (i.e., [5]), we dissected the brains, cut them in two halves along the central fissure, and processed one half for morphological analysis, the other half for *Western blot* and/or immunohistochemical analysis of EphrinB2. Distribution of right/left hemispheres was balanced among groups.

2.6. Golgi–Cox staining and section preparation

Variations in neuronal morphology were assessed by Golgi–Cox staining, as described by Glaser and Van Der Loos [17]. To this end, dissected hemispheres were impregnated using a standard Golgi–Cox solution (1% potassium dichromate, 1% mercuric chloride, 0.8% potassium chromate) and stored in the dark at room temperature for 6 days. They were then transferred to a 30% sucrose solution for 2 days and finally sectioned using a vibratome. Coronal sections (150 μm thick) were mounted on gelatinised slides, stained according to the method described by Gibb and Kolb [18] and cover slipped with Eukitt.

2.7. Quantification of neuronal morphological parameters

Measurements were performed on pyramidal neurons located in the CA1 region of the dorsal hippocampus and in the lateral amygdala, defined according to the Franklin and Paxinos [19] atlas, with a light transmission microscope (Leica DMLB, Leica Microsystems GmbH, Wetzlar, Germany) equipped with an image analysis device and software for morphological analyses and three-dimensional reconstruction system (Neurolucida, MicroBright Fields, Inc., Colchester, VT, USA). Neurons were first identified under low magnification (200×) in the appropriate sections and selected for further analysis according to the following criteria: presence of at least three dendrites without obvious truncations; complete and dark impregnation along the entire length of all dendrites; relative isolation from neighbouring impregnated neurons [20]. Quantitative assessments of complete dendritic structure and spine density of six neurons per animal were then performed under higher magnification (1000×) by an experimenter blind to the experimental conditions. The length and the number of branch nodes of the dendritic trees were quantified tracing the entire apical and basal dendrites. As for spine density assessment, segments of 25 μm were sampled on apical and basal dendrites starting 50 μm from the cell body. On each dendrite, all protrusions with or without bulbous expansions were counted as spines if they were in direct continuity with the dendritic shaft and were used for calculation of spine density. Spine density was automatically calculated by dividing the counted number of spines by the measured dendrite length. At the same time, a precise Sholl analysis was performed by referring spine densities among branch orders and among circular distances from the soma. Values obtained for all neurons from a given animal were averaged to a single value.

2.8. Western blot analysis of EphrinB2

Dissected hemispheres from 3 animals of *conditioned, pseudoconditioned* and control groups were rapidly placed on ice. The whole cortex and the dorsal hippocampus were carefully removed and homogenised in RIPA lysis buffer [21] containing a commercial mixture of protease and phosphatase inhibitors (Sigma–Aldrich, Milano, Italia). Samples were subsequently centrifuged at 10,000 × *g* for 30 min a 4 °C to remove cell debris. Concentration of soluble protein in the supernatants was determined by the standard Bradford colorimetric assay [22]. Aliquots containing 60 μg protein of each sample were diluted in Laemmli sample buffer, boiled at 100 °C for 5 min and subject to 8% polyacrylamide gel electrophoresis in the presence of 0.1% SDS. Coloured molecular weight markers (Sigma–Aldrich, Milano, Italia) were used as size references. Electrophoretic separation was performed for 2 h under a field of 15 V/cm. Proteins were then transferred to a nitrocellulose membrane in a Tris-glycine-methanol buffer, under a 150 mA current applied for 2 h. Finally, the membrane was soaked in protein blocking solution, consisting of a 3% bovine serum albumin (BSA) in a Tris-buffered saline (TBS), for 1 h at RT, and processed for identification of EphrinB2 by use of a specific polyclonal goat antibody (Neuromics, Edina, MN, USA, catalogue number: GT15026), diluted 1/1000 in blocking solution. This antibody was chosen among other commercially available antibodies for both Western blot and immunohistochemical analysis (see below), in light of its proven specificity for EphrinB2 and lack of cross-reactivity with other EphrinB members [15]. The membrane was incubated with the primary antibody or a control solution overnight at 4 °C, washed with blocking solution three times for 10 min and finally incubated for 1 h at RT with a horseradish peroxidase (HRP)-conjugated, rabbit secondary anti-goat antibody (Sigma–Aldrich, catalogue number: A5420) diluted 1/5000 in blocking solution. The membrane was washed with blocking solution three times for 5 min, processed for immunoreactivity detection by a HRP-driven chemiluminescence reaction (Pierce Thermo Scientific, Rockford, IL, USA) and exposed to Kodak XAR-5 autoradiographic film.

After EphrinB2 analysis, each membrane was incubated at 55 °C for 5 min in a 2% SDS, 100 mM β-mercaptoethanol, 62.5 mM Tris–HCl pH 6.7 solution to detach bound antibodies, washed in PBS and processed as described above, using a mouse monoclonal primary antibody specific for β-actin (Santa Cruz Biotechnology, Heidelberg, Germany, catalogue number: sc-8432), diluted 1/1000 and a HRP-conjugated goat secondary anti-mouse antibody (Santa Cruz Biotechnology, catalogue number: sc-2005), diluted 1/5000.

Films were scanned and subjected to a densitometric measure of their intensity, which is proportional to the amount of specific antibody-bound protein present in each sample, by use of an image analysis software (ImageJ, Rasband, W.S., U.S. National Institutes of Health, USA, http://imagej.nih.gov/ij/).

2.9. Western blot analysis of EphA4 receptor

Protein extracts were also processed for EphA4 receptor analysis. Nitrocellulose filters containing electrophoresed proteins were first subject to analysis of EphA4 receptor by use of a specific polyclonal antibody (Santa Cruz Biotechnology, catalogue number: sc-921) diluted 1/500 in blocking solution, and subsequently of β-actin, as described above. Scans and image analysis were performed accordingly.

2.10. Immunohistochemical analysis of EphrinB2

Histochemical evaluation of EphrinB2 content of dorsal hippocampus and amygdala of three animals of each experimental group, i.e. *conditioned, pseudoconditioned* and control (*naive*), was performed by the procedure described by Migani et al. [15]. Dissected hemispheres were rapidly soaked in 4% paraformaldehyde (PFA) in PBS and fixed overnight at 4 °C. They were then transferred to 30% sucrose in PBS, embedded in cutting medium and rapidly frozen at −20 °C. Sections were prepared at −20 °C using a Leitz cryostat (Leica Microsystem GmbH, Wetzlar, Germany). Forty micrometre-thick coronal sections were singularly placed in cell culture wells in 0.5% NaN_3 in PBS and stored at 4 °C until use. Immunohistochemistry was performed simultaneously on free-floating serial sections relative to the hippocampus and amygdala. Sections were post-fixed overnight in 4% PFA in PBS at 37 °C to reduce non-specific immunostaining. After three washes for 5 min in PBS at RT, sections were treated with 3% H_2O_2 in PBS to inhibit endogenous peroxidase activity, washed twice for 10 min in PBS at RT and then incubated in 10% rabbit serum, 5% BSA in PBS (blocking solution), for 18 h at RT to increase the specific staining/background ratio. Sections were incubated at RT with goat primary EphrinB2 specific antibody (Neuromics, Edina, MN, USA, catalogue number: GT15026), diluted 1/400 in blocking solution for 2 h, under gentle rocking, and washed three times in blocking solution for 20 min at RT. They were finally incubated at RT with a rabbit secondary biotin-conjugated anti-goat antibody (Santa Cruz Biotechnology, catalogue number: sc-2774; Sigma–Aldrich, catalogue number: B7014), diluted 1/1000. After three further 10 min washes at RT with PBS, antibody binding was revealed by a biotin–streptavidin–peroxidase system (ABC, Vector Laboratories, Burlingame, CA, USA) and visualised by 5 min incubation in diaminobenzin (DAB)–metal complex (Vector Laboratories, Burlingame, CA, USA). Sections were rinsed in PBS and mounted on glass slides, dehydrated by immersion in increasing alcohol concentrations, treated with xylene and finally mounted with Permount (Sigma–Aldrich). Images were recorded by a digital camera connected to a Nikon 80i (Nikon Italia, Torino, Italia) microscope and a personal computer, and analysed using ImageJ software (Rasband, W.S., U.S. National Institutes of Health, USA, http://imagej.nih.gov/ij/). Illumination and recording settings were kept constant throughout the observations. Images were converted to greyscale and scanned. Quantitative immunohistochemical analyses of different hippocampal regions and of the amygdala were performed on 200× images, calculating optical density (OD) according to the formula $OD = -\log 10(I/I_0)$, where I indicates the intensity of transmitted light and I_0 the intensity of incident light [23]. At least six sections per animal were analysed; in each of them six fields (100 μm diameter) per region were sampled. For a more detailed analysis of hippocampal CA1 areas, the OD values were sampled on 400× images of at least twelve individual neuronal cell bodies per animal. Values obtained for each sample in a given animal were averaged to a single value.

2.11. Statistical analyses

Results were expressed as means ± SEM. Behavioural performances, relative to 6 *conditioned* and 6 *pseudoconditioned* animals, were subject to analysis of variance (ANOVA). Differences in spine densities and branch node numbers were evaluated on 6 animals per group (*conditioned, pseudoconditioned* and control) by a two-way ANOVA. Post-hoc analyses were conducted by Tukey honestly significant differences (HSD) analysis. Apical and basal dendritic compartments were considered separately. Densitometry of Western blot scans, relative to 3 animals per group (*conditioned, pseudoconditioned* and control), was analysed by one-way ANOVA. Immunohistological data, relative to 3 animals per group (*conditioned, pseudoconditioned* and control), were evaluated by two-way ANOVA, followed by post-hoc HSD analysis. Correlation analysis of EphrinB2 immunoreactivity and apical dendritic spine density of hippocampal CA1 neurons was performed by calculating Spearman's rank correlation coefficient rho. Statistical analyses were performed using R: a language and environment for statistical computing (R development core team, R foundation for statistical computing, ISBN 3-900051-07-0, 2008, Vienna, Austria, http://www.R-project.org).

3. Results

3.1. Behaviour

Levels of general locomotor activity and stress/anxiety of all mice prior to conditioning were similar. Levels of animal arousal prior to conditioning were evaluated subjecting all mice to the open field test. Analysis performed on total horizontal activity, centre region activity and peripheral region activity showed no difference among all animals, suggesting that individual levels of stress/anxiety are not responsible for animal performances/cellular features observed as a function of conditioning (data not shown).

Prior to fear conditioning, context exploration activity of all animals was similar in the first 2 min of the training session. During the first 2 min of the training session, in which animals were allowed to explore the experimental chamber prior to conditioning, no differences were observed between mice distributed to the two experimental groups, i.e., *conditioned* and *pseudoconditioned* animals (data not shown).

During the memory retrieval session, conditioned mice showed strong contextual and cued fear responses. Exposed to the same context, animals subjected to the shock 24 h earlier showed greater freezing responses (i.e., the percent of time spent in immobility) during the first 2 min of the test session, when compared to *pseudoconditioned* mice, (*conditioned* animals, 38 ± 9.9 s; *pseudoconditioned* animals: 14.1 ± 1.1 s; training condition effect, $F_{1,10} = 5.76$; $p < 0.05$)(Fig. 1A).

When exposed to a different context, *conditioned* and *pseudoconditioned* animals showed similar exploration activity during the first 2 min of the test session, prior to administration of the tone. On the contrary, during the final 3 min of the test session, in which animals were subject to a continuous tone, a greater freezing response was observed in *conditioned* animals (61.84 ± 6.5 s vs. 30.96 ± 1.7 s of *pseudoconditioned* animals; training condition effect, $F_{1,10} = 20.91$; $p < 0.01$).

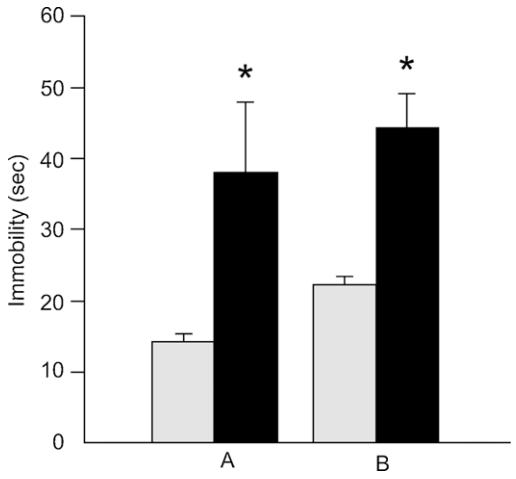

Fig. 1. Behavioural responses to context and cued fear conditioning. (A) Freezing time, expressed in seconds, during the first 2 min (context exposition) of the conditioning test, relative to *pseudoconditioned* (□) and *conditioned* (■) animals (mean ± SEM). Asterisk indicates difference between groups: training condition effect, $F_{1,10} = 5.76$; $p < 0.05$. (B) Freezing time, expressed in seconds, during the last 3 min (cue exposition) of the conditioning test, relative to *pseudoconditioned* (□) and *conditioned* (■) animals (mean ± SEM). Asterisk indicates difference between groups: training condition effect, $F_{1,10} = 20.91$; $p < 0.01$.

3.2. Neuronal morphology

Contextual fear conditioning induced an increase in dendritic arborisation and spine density in pyramidal neurons of the CA1 area of hippocampus and of lateral amygdala. The number of dendritic nodes and the density of dendritic spines were measured in apical and basal dendrites of hippocampal CA1 neurons and lateral amygdala neurons from conditioned, pseudoconditioned and control (naive) mice. While no differences were observed for both dendritic node number and spine density on basal dendrites of hippocampal neurons in the three experimental conditions, structural rearrangements were observed on apical dendrites of neurons from conditioned mice (training condition effect: nodes, $F_{2,26} = 2.453$; $p < 0.001$; spines, $F_{2,26} = 2.172$; $p < 0.01$) (Fig. 2A and B). Structural rearrangements relative both node number and spine density were also observed on basal and apical dendrites of lateral amygdala neurons from conditioned mice, (training condition effect: basal nodes, $F_{2,12} = 1.870$; $p < 0.05$; basal spines, $F_{2,14} = 3.303$; $p < 0.001$; apical nodes, $F_{2,10} = 1.974$; $p < 0.05$; apical spines, $F_{2,16} = 1.759$; $p < 0.05$) (Fig. 3A and B).

3.3. Variations in EphrinB2 levels upon conditioning

Contextual fear conditioning is associated with a rapid increase in levels of EphrinB2 in the hippocampus. Presence of EphrinB2 in the hippocampus and whole cortex of conditioned, pseudoconditioned and naive mice was measured by Western blot analysis and subsequent densitometry, normalised by comparison with ubiquitous β-actin. A single, broad band of molecular mass slightly smaller than 40 kDa, as described for EphrinB2 [24], was detected in protein extracts from both the hippocampus and the cortex. Densitometric measurements showed a strong increase in EphrinB2 levels in the hippocampi of conditioned vs. pseudoconditioned/control mice (training condition effect, $F_{2,6} = 20.063$; $p < 0.01$), while no differences were observed in the cortices (Fig. 4). When presence of EphA4 receptor was analysed in the same conditions, no variations were observed in either structure of conditioned and pseudoconditioned/control animals (Fig. 5).

Contextual fear conditioning is associated with a rapid increase in levels of EphrinB2 in the CA1 area of the hippocampus. The

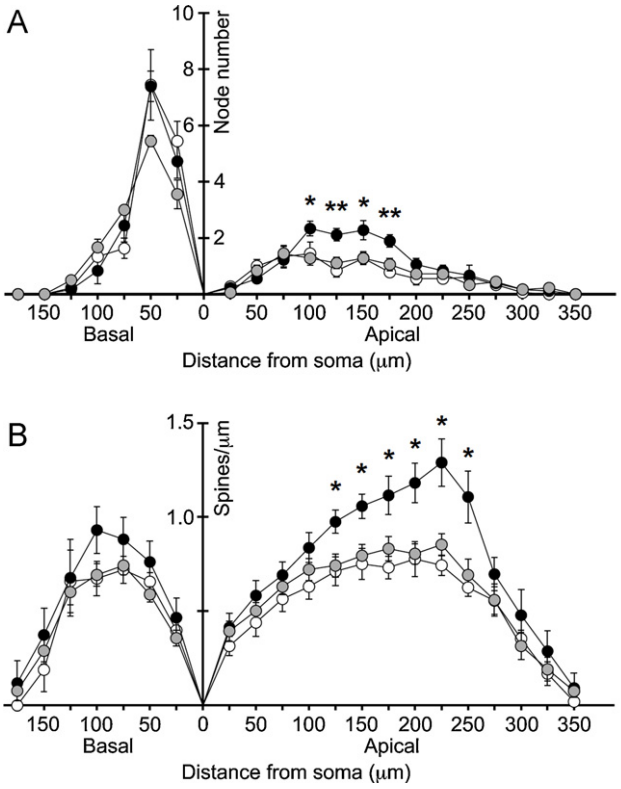

Fig. 2. Dendritic nodes and spines of pyramidal CA1 hippocampal neurons. (A) Values represent the mean number ± SEM of dendritic nodes/25 μm dendritic segment, relative to basal (left panel) and apical (right panel) dendrites of pyramidal CA1 hippocampal neurons from *control* (●), *pseudoconditioned* (○) and *conditioned* (●) animals. Asterisks indicate differences between *conditioned* and *pseudoconditioned/control* animals: $^{*}p < 0.01$; $^{**}p < 0.001$. (B) Values represent the mean number ± SEM of dendritic spines/μm counted on 25 μm dendritic segments, relative to basal (left panel) and apical (right panel) dendrites of pyramidal CA1 hippocampal neurons from *control* (○), *pseudoconditioned* (○) and *conditioned* (●) animals. Single asterisks indicate difference between *conditioned* and *pseudoconditioned/control* animals, $p < 0.01$.

increase in EphrinB2 levels in the hippocampi of conditioned mice was further investigated by immunohistochemical analysis in different areas of such structure, namely CA1, CA3 and dentate gyrus (DG) (Fig. 6A). The same analysis was performed on the amygdalas, the involvement of which in fear conditioning was evaluated by the cued test. Presence of EphrinB2 was observed in the pyramidal cell layer of CA1 and CA3 areas and in the granular layer of DG of all animals, confirming results of Migani et al. [15]. As for presence of such factor in the amygdala, EphrinB2 positive small cells were observed both in the lateral and basolateral nuclei, as already reported by Migani et al. [15]. Analysis of optical density values of conditioned vs. pseudoconditioned/control animals (Fig. 6B) showed an increased abundance of EphrinB2 in the CA1 area (training condition effect, ($F_{2,6} = 6.41$; $p < 0.05$), but not in other hippocampal areas nor in the amygdala. In addition, when the CA1 area of mice belonging to the three experimental groups was observed in detail (Fig. 7A), positive cell distribution was similar. In these neurons, EphrinB2 was localized in the neuronal cell bodies and apical dendrites, independently of the experimental group. Finally, when cell staining of pyramidal neurons in the hippocampi of conditioned animals was compared to that displayed by both pseudoconditioned and control animals by analysis of optical density (Fig. 7B), it was found to be substantially enhanced ($F_{2,6} = 60.8$, $p < 0.001$), suggesting an increase in EphrinB2 expression of individual cells.

A correlation analysis of EphrinB2 immunoreactivity with neuronal morphology revealed the existence of a positive relationship

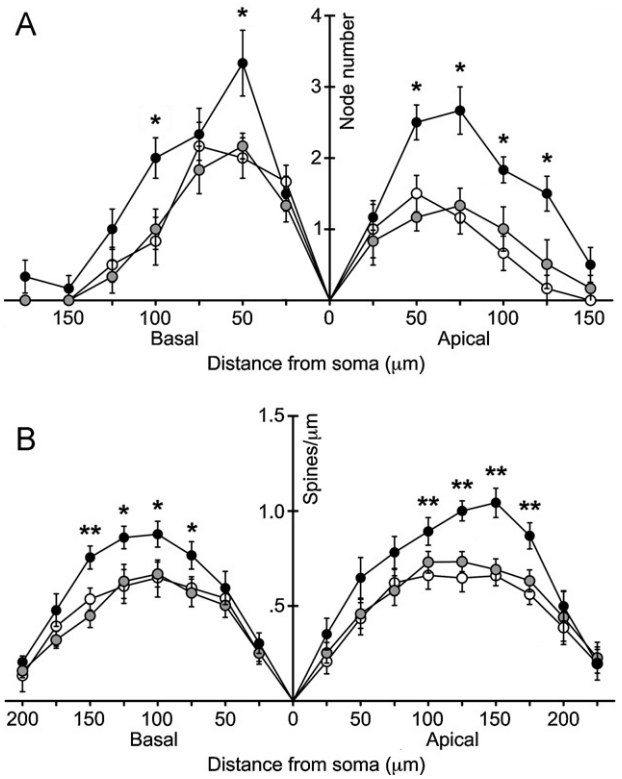

Fig. 3. Dendritic nodes and spines of pyramidal lateral amygdala neurons. (A) Values represent the mean number ± SEM of dendritic nodes/25 μm dendritic segment, relative to basal (left panel) and apical (right panel) dendrites of pyramidal lateral amygdala neurons from *control* (○), *pseudoconditioned* (◌) and *conditioned* (●) animals. Single asterisks indicate difference between *conditioned* and *pseudoconditioned/control* animals, $p < 0.05$. (B) Values represent the mean number ± SEM of dendritic spines/μm counted on 25 μm dendritic segments, relative to basal (left panel) and apical (right panel) dendrites of pyramidal lateral amygdala neurons from *control* (○), *pseudoconditioned* (◌) and *conditioned* (●) animals. Asterisks indicate differences between *conditioned* and *pseudoconditioned/control* animals: $^{*}p < 0.05$; $^{**}p < 0.01$.

between EphrinB2 levels and apical dendritic spine density of pyramidal neurons of the CA1 area of the hippocampus (Spearman's rank correlation rho = 0.9; $p < 0.05$).

4. Discussion

The formation of recent memories is a process that involves the medial temporal lobe, including the hippocampus [25–27,69], and is believed to depend initially on modifications in neuronal synaptic connections, based on learning-induced pathways of protein synthesis [28]. However, the nature of such pathways is still not well understood, in spite of the substantial amount of data produced on morphological modifications of neurons involved in memory formation and consolidation [2–4].

Here, we provide evidence that changes in spine density and dendrite complexity occur in hippocampal neurons during the formation of recent memory and, consistent with the hypothesis of Bailey et al. [28], that such changes are associated to an increase in the levels of EphrinB2 observed in these cells.

Animals were challenged by the context-dependent fear conditioning test, a behavioural paradigm dependent on hippocampal modifications [29], and by the cue-dependent fear conditioning test, which is not affected by hippocampal plasticity but rather depends on the lateral nucleus of the amygdala [30,31].

Prior to the conditioning session, animal performance measured in the open field test was found to be the same for all mice. Accordingly, the basal level of anxiety and arousal could not be taken into

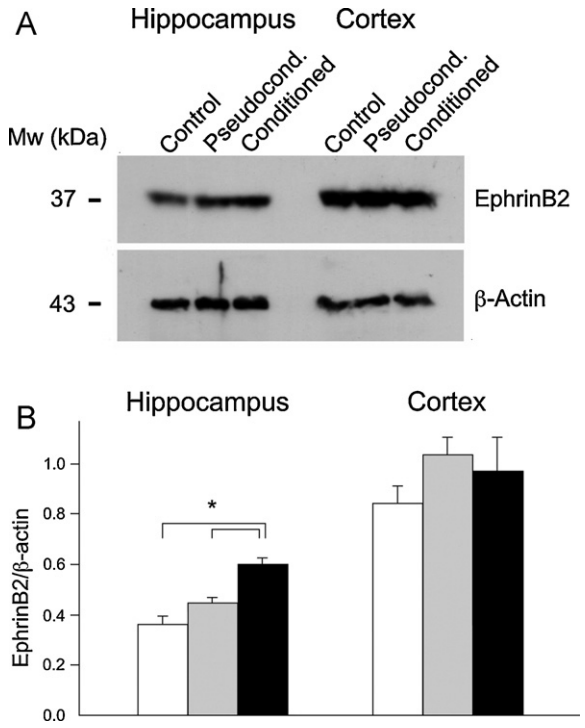

Fig. 4. (A) Representative Western blot of EphrinB2 in protein extracts from the hippocampus and the cortex of *control, pseudoconditioned* and *conditioned* animal. (B) Densitometric analysis of EphrinB2/β-actin abundance in the hippocampus and the cortex of *control* (□), *pseudoconditioned* (◻) and *conditioned* (■) animal. Values represent the mean value ± SEM of extracts from three animals/group. Asterisk indicates difference between *conditioned* and *pseudoconditioned/control* animals, $p < 0.001$.

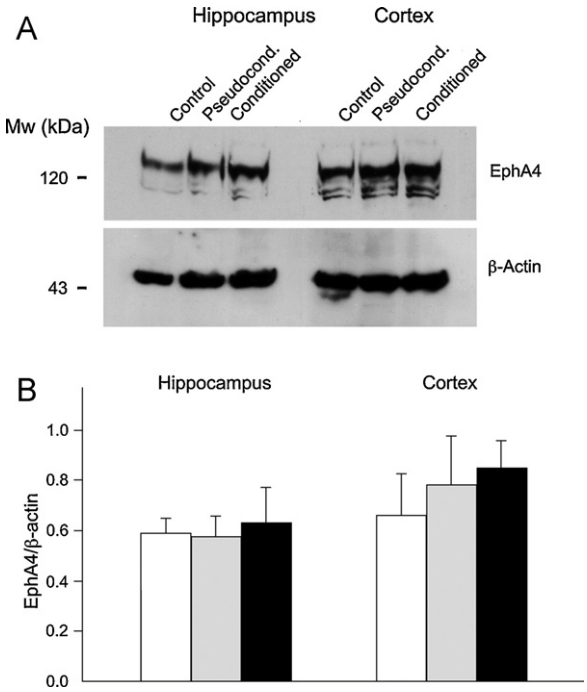

Fig. 5. (A) Representative Western blot of EphA4 in protein extracts from the hippocampus and the cortex of *control, pseudoconditioned* and *conditioned* animal. (B) Densitometric analysis of EphA4/β-actin abundance in the hippocampus and the cortex of *control* (□), *pseudoconditioned* (◻) and *conditioned* (■) animal. Values represent the mean value ± SEM of extracts from three animals/group.

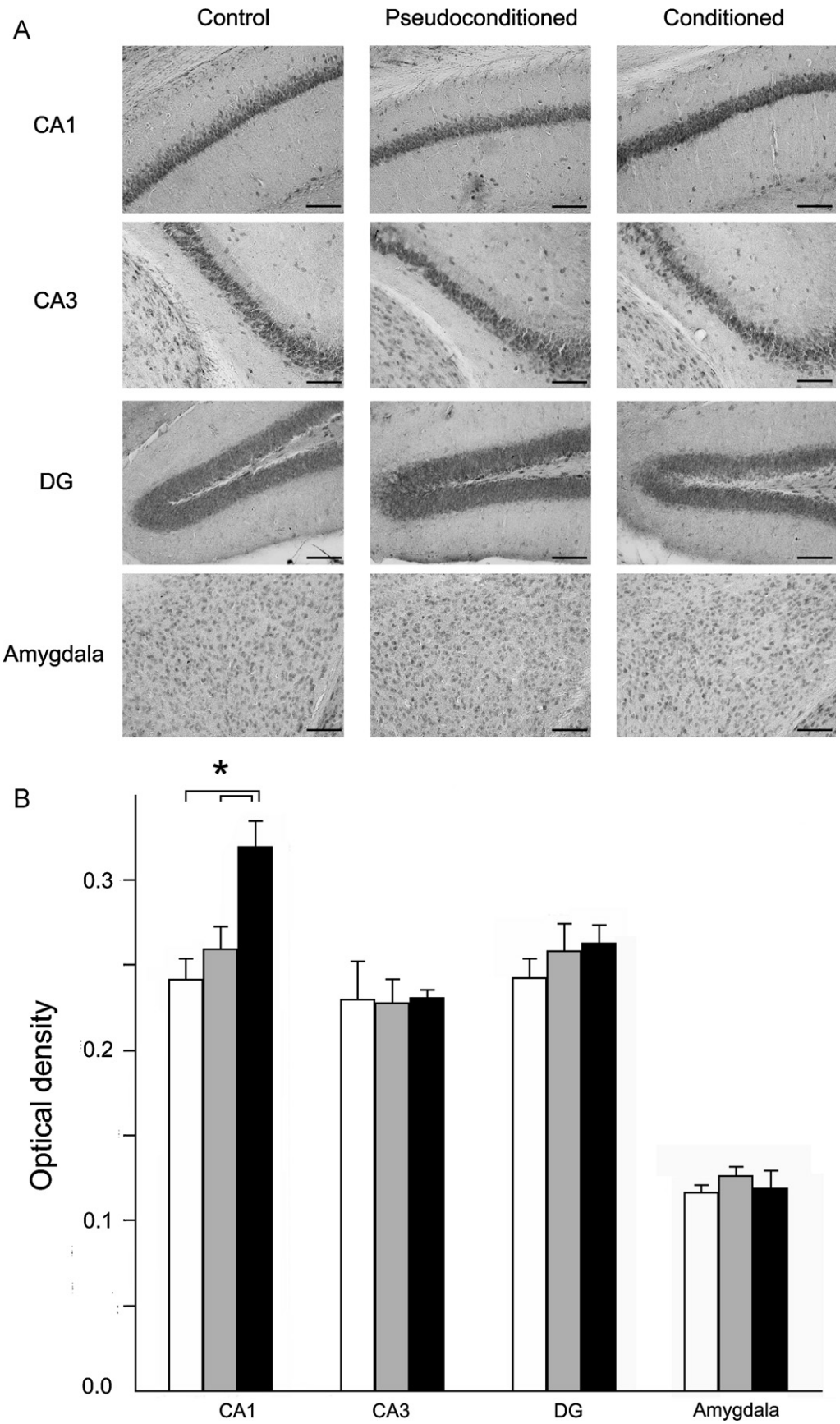

Fig. 6. (A) Representative immunohistochemical localization of EphrinB2 in hippocampal areas CA1, CA3 and DG, and the amygdala of *control*, *pseudoconditioned* and *conditioned* animals. Bars, 100 μm. (B) Densitometric analysis of EphrinB2 in the hippocampus and amygdala of *control* (□), *pseudoconditioned* (□) and *conditioned* (■) animals. Values represent the mean value ± SEM of 3 animals/group. Asterisk indicates difference between *conditioned* and *psedoconditioned*/*control* animals, $p < 0.05$.

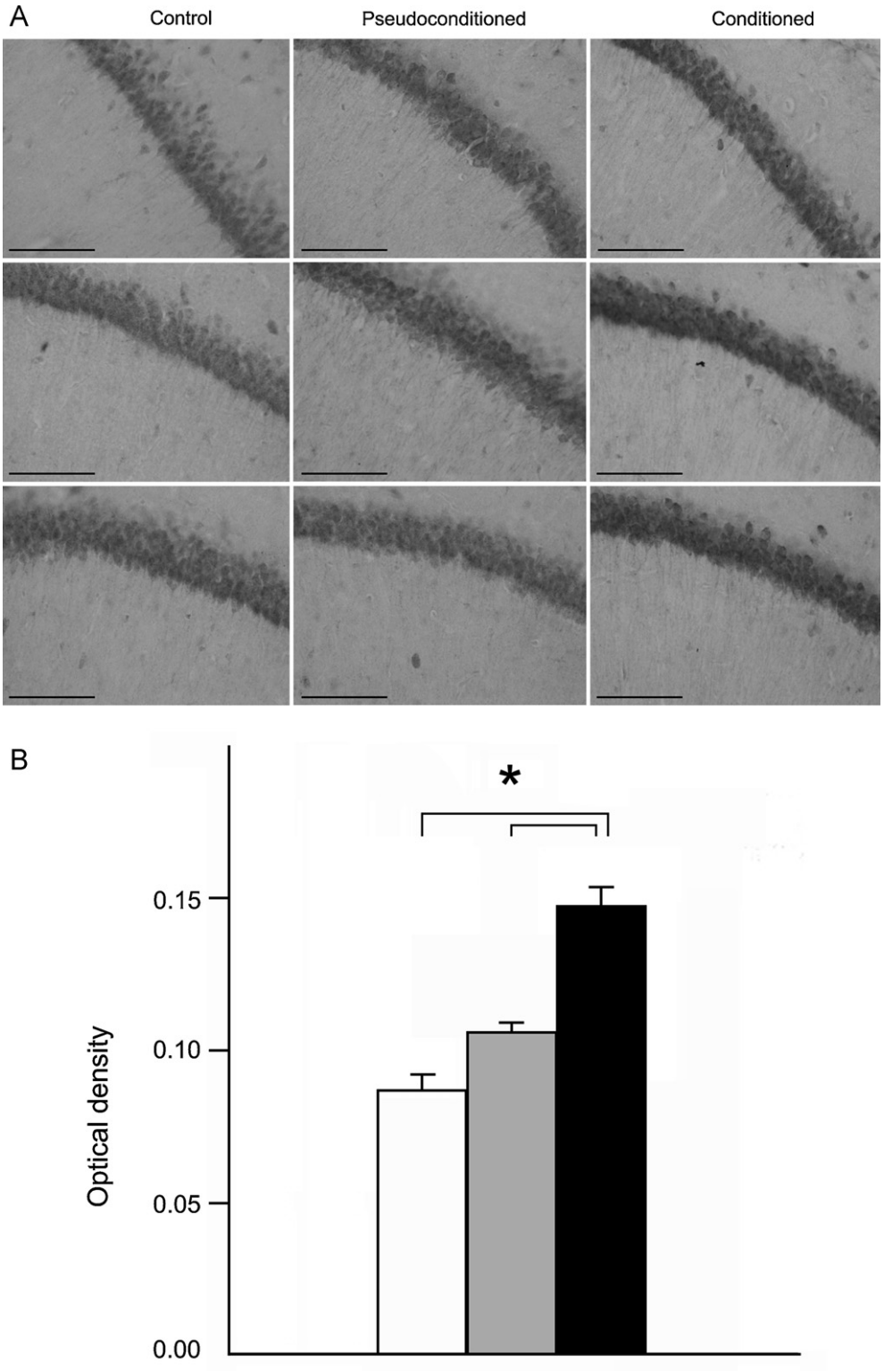

Fig. 7. (A) Representative immunohistochemical localization of EphrinB2 in hippocampal CA1 neurons of *control, pseudoconditioned* and *conditioned* animals. Bars, 100 μm. (B) Densitometric analysis of EphrinB2 in individual CA1 neurons of *control* (□), *pseudoconditioned* (□) and *conditioned* (■) animals. Values represent the mean value ± SEM of 3 animals/group. Asterisk indicates difference between *conditioned* and *pseudoconditioned*/*control* animals, $p < 0.001$.

account to explain different results obtained in the fear conditioning test between various experimental groups. This observation was strengthened by animal behaviour recorded in the first 2 min of the conditioning session, prior to the pairing of CS and US, which did not differ between *conditioned* and *pseudoconditioned* mice (data not shown).

Conditioned animals developed a strong fear response, observed in both the contextual test and the cued test, confirming the involvement of the hippocampus and the amygdala in such behavioural paradigm [32]. The formation of aversive memory was associated with an increase in dendritic node number and dendritic spine density on pyramidal neurons of both the CA1 area of

hippocampus and lateral amygdala. Such an increase was limited to apical dendrites of hippocampal neurons, cells for which various groups [2,3,5] have reported a certain variability in conditioning-dependent modifications relative to basal and apical dendrites, depending on both the specific learning task and/or the experimental procedure employed, and in both basal and apical dendrites of lateral amygdala neurons, as already reported [20].

As for molecular events underlying the formation of recent memories with particular reference to contextual fear conditioning, previous reports have shown that hippocampal CA1 neurons activate signalling pathways controlled by PKA [33], PKC [34], CaMKII [68] and CDK5 [35], and transcription of immediate early genes, such as *cFos* [36,37]. Other pathways, including translation of specific protein products, have not been described yet. Similar mechanisms have been described in lateral amygdala neurons for cued fear conditioning, including PKA [38], PKC [39], MAPK [40] and CaMKII [41] regulated pathways, as well as transcription of early genes [42]. Even in the case of lateral amygdala, new synthesis of specific proteins has not been described so far.

In order to add information on such issue, we investigated possible association of behavioural and cellular modifications induced by fear conditioning in hippocampal and lateral amygdala neurons, to expression of EphrinB2, a cell-adhesion factor known to be strongly expressed in adult brain regions displaying synaptic plasticity [14,15,43], and found to be directly involved in it [14].

Ephrins and Eph receptors belong to a family of tyrosine kinases [44] that cover fundamental roles in the nervous system of vertebrates both during development, by affecting the patterning of axonal connections [45,46,47], and in the adult [6], by modulating, among others, LTP induction [48], the dynamics of dendritic spines [7] and the control of synaptic neuro-glial interactions [49]. EphrinBs, in particular, appear to be involved in both LTP [50] and LTD [13] of hippocampal neuron synapses, and in their maturation process [51], by interaction with their receptors. These factors are expressed both presynaptically and postsynaptically, as observed in hippocampal connections: presynaptic EphrinB members, including EphrinB2, regulate initial steps in the formation of synaptic connections by inducing interaction of postsynaptic EphB receptors with NMDA glutamate receptors [10,11]. Conversely, clustering of postsynaptic EphB2 receptors may enhance interaction with presynaptic Ephrins and increase glutamate release [8]. In hippocampal CA1 and CA3 neurons, EphrinB2 and EphrinB3 are also expressed on postsynaptic membranes and are functionally necessary for LTP and LTD [14].

In the present study, we have focused our attention on EphrinB2. As of now, information on expression of such factor has been gathered by in situ RNA hybridisation and immunohistochemical protein localization. In the hippocampus, EphrinB2 mRNA is abundant in CA1 neurons but poorly expressed in CA3 and DG neurons [13,14]. In contrast to such uneven mRNA distribution, Migani et al. [15] observed similar levels of EphrinB2 protein in neuronal cell bodies of CA1, CA3 and DG. These observations suggest that specific mechanisms may control EphrinB2 synthesis at the translational level, making of such factor a good candidate as a protein product readily induced by conditioning via *de novo* translation of stored messages.

We first identified and quantified hippocampal and cortical presence of EphrinB2 in *conditioned, pseudoconditioned* and control mice by Western blot. A significant increase in the amount of such factor was observed in the hippocampus, but not the cortex, of *conditioned* mice. This result represents the first report of a cell adhesion factor rapidly induced upon conditioning in the structure responsible for spatial learning. Absence of the increase in the cortex 24 h after the conditioning session is reasonable in light of the view that recent memory relies on hippocampal rather than on cortical activity [5].

We then performed localization and quantification of EphrinB2 in the hippocampus of *conditioned, pseudoconditioned* and control mice by immunohistochemistry. In agreement with Migani et al. [15], such method provides a specific, clear localization of EphrinB2 in the pyramidal cell layer of the hippocampus; in addition, various reports have described successful quantification of immunohistochemical data relative to a number of products, including cannabinoid receptors [52], PKC [53], 5-HT [23], the apoptotic protein 14-3-3theta/tau, GFAP and α-internexin [54].

Our immunohistochemical analysis confirms cell distribution of EphrinB2 described by Migani et al. [15], with presence in the pyramidal neuron layer of CA1 and CA3 and in the granular layer of DG of all animals, regardless of spatial conditioning. A detailed analysis of EphrinB2 immunoreactivity allowed us to localize the factor in neuronal cell bodies and apical dendrites. Whether this factor is also present in basal dendrites was not clear and remains to be elucidated. Although maintaining a similar cellular distribution, *conditioned* animals displayed an increased abundance of EphrinB2 in CA1 but not CA3 or DG neurons, which was found to be directly associated with spine density observed on apical dendrites, by Spearman's rank correlation analysis. This suggests that such increase is associated to mechanisms leading to formation of new dendritic spines. Given the high abundance of EphrinB2 mRNA in these cells [13,14,43], it would be tempting to hypothesize that the observed rapid increase is obtained by conditioning-induced translation of stored messages. This, in turn, is consistent with the established view that new protein synthesis is required to maintain the persistence of synaptic strengthening and weakening, independently of transcription [55–58]. We are currently evaluating such hypothesis in our laboratory.

In the amygdala, EphrinB2 positive small cells were observed in the lateral and basolateral nuclei, as reported by Migani et al. [15], but no changes in the amount of such protein were detected in *conditioned* animals. This suggests that, even though such structure is involved in the emotional learning of fear conditioning, molecular mechanisms underlying its plasticity may be different from those observed in the hippocampus.

As for a role of EphA4 receptor in dendritic alterations relative to recent memory formation, which may not depend on new synthesis as apparently suggested by our Western blot analysis, it deserves further study.

Our results on conditioning-induced increase in EphrinB2 abundance in CA1 neurons, although not excluding a similar role in neuronal plasticity for EphrinB3 or other adhesion factors, may represent the basis for further molecular analysis of cell plasticity in the hippocampus and possibly other nervous structures.

Acknowledgements

We are profoundly grateful to Dr. Martine Ammassari-Teule for her invaluable support to this work, help in morphological neuron analysis, and discussion. We also thank Dr. Loukia Katsouri for critical reading of the manuscript. This work was financially supported by PRIN grant 2005055188 to AB.

References

[1] Frankland PW, Bontempi B. The organization of recent and remote memories. Nat Rev Neurosci 2005;6:119–30.
[2] Leuner B, Falduto J, Shors TJ. Associative memory formation increases the observation of dendritic spines in the hippocampus? J Neurosci 2003;23(2):659–65.
[3] Knafo S, Ariav G, Barkai E, Libersat F. Olfactory learning-induced increases in spine density along the spine density along the apical dendrites in CA1 hippocampal neuron? Hippocampus 2004;14(7):819–25.
[4] Restivo L, Roman FS, Ammassari-Teule M, Marchetti E. Simultaneous olfactory discrimination elicits a strain-specific increase in dendritic spines in the hippocampus of inbred mice? Hippocampus 2006;16(5):472–9.

[5] Restivo L, Vetere G, Bontempi B, Ammassari-Teule M. The formation of recent and remote memory is associated with time-dependent formation of dendritic spines in the hippocampus and anterior cingulate cortex? J Neurosci 2009;29(25):8206–14.
[6] Kullander K, Klein R. Mechanisms and functions of Eph and Ephrin signalling? Nat Rev Mol Cell Biol 2002;3(7):475–86.
[7] Yoshihara Y, De Roo M, Muller D. Dendritic spine formation and stabilization. Curr Opin Neurobiol 2009;(2):146–53.
[8] Klein R. Bidirectional modulation of synaptic functions by Eph/Ephrin signalling? Nat Neurosci 2009;12(1):15–20.
[9] Pasquale EB. Eph–Ephrin bidirectional signaling in physiology and disease. Cell 2008;133:38–52.
[10] Rao A, Kim E, Sheng M, Craig AM. Heterogeneity in the molecular composition of excitatory postsynaptic sites during development of hippocampal neurons in culture? J Neurosci 1998;18(4):1217–29.
[11] Dalva MB, Takasu MA, Lin MZ, Shamah SM, Hu L, Gale NW, Greenberg ME. EphB receptors interact with NMDA receptors and regulate excitatory synapse formation? Cell 2000;103(6):945–56.
[12] Takasu MA, Dalva MB, Zigmond RE, Greenberg ME. Modulation of NMDA receptor-dependent calcium influx and gene expression through EphB receptors. Science 2002;295:491–5.
[13] Grunwald IC, Korte M, Wolfer D, Wilkinson GA, Unsicker K, Lipp HP, Bonhoeffer T, Klein R. Kinase-independent requirement of EphB2 receptors in hippocampal synaptic plasticity. Neuron 2001;32:1027–40.
[14] Grunwald IC, Korte M, Adelmann G, Plueck A, Kullander K, Adams RH, Frotscher M, Bonhoeffer T, Klein R. Hippocampal plasticity requires postsynaptic EphrinBs. Nat Neurosci 2004;7:33–40.
[15] Migani P, Bartlett C, Dunlop S, Beazley L, Roger J. Ephrin-B2 immunoreactivity distribution in adult mouse brain. Brain Res 2007;1182:60–72.
[16] Tremblay ME, Riad M, Bouvier D, Murai KK, Pasquale EB, Descarries L, Doucet G. Localization of EphA4 in axon terminals and dendritic spines of adult rat hippocampus. J Comp Neurol 2007;501:691–702.
[17] Glaser EM, Van Der Loos G. Analysis of thick brain sections by observe-reverse computer microscopy: application of a new, high clarity Golgi–Nissl stain. J Neurosci Methods 1981;4:117–25.
[18] Gibb R, Kolb B. A method for vibratome sectioning of Golgi–Cox stained whole rat brain. J Neurosci Methods 1998;79:1–4.
[19] Franklin KBJ, Paxinos G. The mouse brain in stereotaxic coordinates. 2nd ed. San Diego: Academic; 2001.
[20] Vyas A, Mitra R, Shankaranarayana Rao BS, Chattarji S. Chronic stress induces contrasting patterns of dendritic remodeling in hippocampal and amygdaloid neurons. J Neurosci 2002;22(15):6810–8.
[21] Harlow E, Lane D, editors. Antibodies: a laboratory manual. N.Y.: Cold Spring Harbor Laboratory; 1988. p. 449.
[22] Bradford MM. A rapid and sensitive method for the quantitation of microgram quantities of protein utilizing the principle of protein-dye binding. Anal Biochem 1976;72:248–54.
[23] Isoda K, Morimoto M, Matsui F, Hasegawa T, Tozawa T, Morioka S, et al. Postnatal changes in serotonergic innervation to the hippocampus of methyl-CpG-binding protein 2-null mice. Neuroscience 2010;165:1254–60.
[24] Holland SJ, Gale NW, Mbamalu G, Yancopoulos GD, Henkemeyer M, Pawson D. Bidirectional signalling through the EPH-family receptor Nuk and its transmembrane ligands. Nature 1996;383:722–5.
[25] Zola-Morgan SM, Squire LR. The primate hippocampal formation: evidence for a time-limited role in memory storage. Science 1990;250:288–90.
[26] Kim JJ, Fanselow MS. Modality-specific retrograde amnesia of fear. Science 1992;256:675–7.
[27] Martin SJ, Clark RE. The rodent hippocampus and spatial memory: from synapses to systems. Cell Mol Life Sci 2007;64:401–31.
[28] Bailey CH, Kandel ER, Si K. The persistence of long-term memory: a molecular approach to self-sustaining changes in learning-induced synaptic growth. Neuron 2004;44:49–57.
[29] Sanders MJ, Wiltgen BJ, Fanselow MS. The place of the hippocampus in fear conditioning? Eur J Pharmacol 2003;463(1–3):217–23.
[30] Koo JW, Han JS, Kim JJ. Selective neurotoxic lesions of basolateral and central nuclei of the amygdala produce differential effects on fear conditioning. J Neurosci 2004;24:7654–62.
[31] Rodrigues SM, Schafe GE, LeDoux JE. Molecular mechanisms underlying emotional learning and memory in the lateral amygdala. Neuron 2004;44:75–91.
[32] Huff NC, Frank M, Wright-Hardesty K, Sprunger D, Matus-Amat P, Higgins E, Rudy JW. Amygdala regulation of immediate-early gene expression in the hippocampus induced by contextual fear conditioning. J Neurosci 2006;26(5):1616–23.
[33] Isiegas C, Park A, Kandel ER, Abel T, Lattal KM. Transgenic inhibition of neuronal protein kinase A activity facilitates fear extinction. J Neurosci 2006;26:12700–7.
[34] Tronson NC, Schrick C, Fischer A, Sananbenesi F, Pages G, Pouyssegur J, Radulovic J. Regulatory mechanisms of fear extinction and depression-like behavior. Neuropsychopharmacology 2008;33:1570–83.
[35] Sananbenesi F, Fischer A, Wang X, Schrick C, Neve R, Radulovic J, Tsai LH. A hippocampal Cdk5 pathway regulates extinction of contextual fear. Nat Neurosci 2007;10:1012–9.
[36] Radulovic J, Kammermeier J, Spiess J. Relationship between fos production and classical fear conditioning: effects of novelty, latent inhibition, and unconditioned stimulus preexposure. J Neurosci 1998;18:7452–61.
[37] Matsuo N, Reijmers L, Mayford M. Spine-type-specific recruitment of newly synthesized AMPA receptors with learning. Science 2008;319:1104–7.
[38] Goosens KA, Holt W, Maren S. A role for amygdaloid PKA and PKC in the acquisition of long-term conditional fear memories in rats. Behav Brain Res 2000;114:145–52.
[39] Weeber EJ, Atkins CM, Selcher JC, Varga AW, Mirnikjoo B, Paylor R, Leitges M, Sweatt JD. A role for the beta isoform of protein kinase C in fear conditioning. J Neurosci 2000;20:5906–14.
[40] Schafe GE, Atkins CM, Swank MW, Bauer EP, Sweatt JD, LeDoux JE. Activation of ERK/MAP kinase in the amygdala is required for memory consolidation of Pavlovian fear conditioning. J Neurosci 2000;20:8177–87.
[41] Rodrigues SM, Farb CR, Bauer EP, LeDoux JE, Schafe GE. Pavlovian fear conditioning regulates Thr286 autophosphorylation of Ca^{2+}/calmodulin-dependent protein kinase II at lateral amygdala synapses. J Neurosci 2004;24:3281–8.
[42] Scicli AP, Petrovich GD, Swanson LW, Thompson RF. Contextual fear conditioning is associated with lateralized expression of the immediate early gene c-fos in the central and basolateral amygdalar nuclei. Behav Neurosci 2004;118:5–14.
[43] Liebl DJ, Morris CJ, Henkemeyer M, Parada LF. mRNA expression of Ephrins and Eph receptor tyrosine kinases in the neonatal and adult mouse central nervous system. J Neurosci Res 2003;71:7–22.
[44] Friedman GC, O'Leary DDM. Eph receptor tyrosine kinases and their ligands in neural development. Curr Opin Neurobiol 1996;6:127–33.
[45] Winslow JM, Moral O, Valverde J, Shih A, Yuan JQ, Wong SC, Tsai SP, Goddard A, Henzel WJ, Hefti F, Beck KD, Caras IW. Cloning of AL-1, a ligand for an Eph-related tyrosine kinase receptor involved in axon bundle formation. Neuron 1995;14:973–81.
[46] Donoghue MJ, Merlie JP, Sanes JR. The Eph Kinase Ligand AL-1 is expressed by rostral muscles and inhibits outgrowth from caudal neurons. Mol Cell Neurosci 1996;8(2/3):185–98.
[47] Flanagan JG, Vanderhaeghen P. The Ephrins and Eph receptors in neural development. Annu Rev Neurosci 1998;21:390–445.
[48] Gao WQ, Shinsky N, Armanini MP, Moran P, Zheng JL, Mendoza-Ramirez JL, Phillips HS, Winslow JW, Caras IW. Regulation of hippocampal synaptic plasticity by the tyrosine kinase receptor, REK7/EphA5, and its ligand, AL-1/Ephrin-A5. Mol Cell Neurosci 1998;(5–6):247–59.
[49] Murai KK, Pasquale EB. Eph receptor, Ephrins, and synaptic function. Neuroscientist 2004;10(4):304–14.
[50] Contractor A, Rogers C, Maron C, Henkemeyer M, Swanson GT, Heinemann SF. Trans-synaptic Eph receptor–ephrin signaling in hippocampal mossy fiber LTP. Science 2002;296(5574):1864–9.
[51] Henderson JT, Georgiou J, Jia Z, Robertson J, Elowe S, Roder JC, Pawson T. The receptor tyrosine kinase EphB2 regulates NMDA-dependent synaptic function. Neuron 2001;32:1041–56.
[52] Suárez J, Llorente R, Romero-Zerbo SY, Mateos B, Bermúdez-Silva FJ, de Fonseca FR, Viveros MP. Early maternal deprivation induces gender-dependent changes on the expression of hippocampal CB(1) and CB(2) cannabinoid receptors of neonatal rats. Hippocampus 2009;19(7):623–32.
[53] Ferri P, Cecchini T, Ambrogini P, Betti M, Cuppini R, Del Grande P, Ciaroni S. Alpha-tocopherol affects neuronal plasticity in adult rat dentate gyrus: the possible role of PKCdelta. J Neurobiol 2006;66(8):793–810.
[54] Tang SJ, Reis G, Kang H, Gingras AC, Sonenberg N, Schuman EM. A rapamycin-sensitive signaling pathway contributes to long-term synaptic plasticity in the hippocampus. Proc Natl Acad Sci USA 2002;99:467–72.
[55] Kang H, Schuman EM. A requirement for local protein synthesis in neurotrophin-induced hippocampal synaptic plasticity. Science 1996;273:1402–6.
[56] Huber KM, Kayser MS, Bear MF. Role for rapid dendritic protein synthesis in hippocampal mGluR-dependent LTD. Science 2000;288:1254–7.
[57] Cracco JB, Serrano P, Moskowitz SI, Bergold PJ, Sacktor TC. Protein synthesis-dependent LTP in isolated dendrites of CA1 pyramidal cells. Hippocampus 2005;15:551–6.
[58] Pfeiffer BE, Huber M. Current advances in local protein synthesis and synaptic plasticity. J Neurosci 2006;26(27):7147–50.
[68] Silva AJ. Molecular and cellular cognitive studies of the role of synaptic plasticity in memory. J Neurobiol 2003;54:224–37.
[69] Squire LR, Bayley PJ. The neuroscience of remote memory. Curr Opin Neurobiol 2007;17:185–96.

⌘ *Author's Choice*

THE JOURNAL OF BIOLOGICAL CHEMISTRY VOL. 286, NO. 7, pp. 5691–5707, February 18, 2011

PC4/Tis7/IFRD1 Stimulates Skeletal Muscle Regeneration and Is Involved in Myoblast Differentiation as a Regulator of MyoD and NF-κB*[S]

Received for publication, July 13, 2010, and in revised form, November 4, 2010 Published, JBC Papers in Press, December 2, 2010, DOI 10.1074/jbc.M110.162842

Laura Micheli[‡1,2], Luca Leonardi[‡2], Filippo Conti[‡2], Giovanna Maresca[‡], Sandra Colazingari[‡], Elisabetta Mattei[‡], Sergio A. Lira[§], Stefano Farioli-Vecchioli[‡], Maurizia Caruso[‡], and Felice Tirone[‡3]

From the [‡]Istituto di Neurobiologia e Medicina Molecolare, Consiglio Nazionale delle Ricerche, Fondazione S. Lucia, Via del Fosso di Fiorano 64, 00143 Rome, Italy and the [§]Immunology Institute, Mount Sinai School of Medicine, New York, New York 10029

In skeletal muscle cells, the PC4 (Tis7/Ifrd1) protein is known to function as a coactivator of MyoD by promoting the transcriptional activity of myocyte enhancer factor 2C (MEF2C). In this study, we show that up-regulation of *PC4 in vivo* in adult muscle significantly potentiates injury-induced regeneration by enhancing myogenesis. Conversely, we observe that *PC4* silencing in myoblasts causes delayed exit from the cell cycle, accompanied by delayed differentiation, and we show that such an effect is *MyoD*-dependent. We provide evidence revealing a novel mechanism underlying the promyogenic actions of PC4, by which PC4 functions as a negative regulator of NF-κB, known to inhibit *MyoD* expression post-transcriptionally. In fact, up-regulation of *PC4* in primary myoblasts induces the deacetylation, and hence the inactivation and nuclear export of NF-κB p65, in concomitance with induction of *MyoD* expression. On the contrary, *PC4* silencing in myoblasts induces the acetylation and nuclear import of p65, in parallel with a decrease of MyoD levels. We also observe that PC4 potentiates the inhibition of NF-κB transcriptional activity mediated by histone deacetylases and that PC4 is able to form trimolecular complexes with p65 and HDAC3. This suggests that PC4 stimulates deacetylation of p65 by favoring the recruitment of HDAC3 to p65. As a whole, these results indicate that PC4 plays a role in muscle differentiation by controlling the *MyoD* pathway through multiple mechanisms, and as such, it positively regulates regenerative myogenesis.

Skeletal myoblast differentiation is a multistep process characterized by permanent exit from the cell cycle, maturation into mononucleated myocytes, and fusion in multinucleated myotubes. This differentiation program is controlled by the basic helix-loop-helix family of myogenic regulatory factors (MRFs),[4] including *MyoD*, *Myf-5*, *myogenin*, and *MRF4/Myf6/Herculin* (Refs. 1–6 and reviewed in Ref. 7). The MRFs form heterodimers with the ubiquitously expressed basic helix-loop-helix E proteins to bind to a consensus sequence, termed E-box, present in the regulatory regions of many muscle-specific genes (8). Activation of muscle gene expression by MRFs is also dependent on their functional interaction with members of the myocyte enhancer factor 2 (*MEF2*) family of transcription factors, which bind to a conserved A/T-rich sequence often located in close proximity to E-boxes in muscle gene control regions (9, 10).

The gene *PC4*, also known as *Tis7* or *IFRD1* (in rat, mouse, and human, respectively), participates to the process of skeletal muscle cell differentiation. In fact, inhibition of *PC4* function in C2C12 myoblasts, by antisense *PC4* cDNA transfection or microinjection of anti-PC4 antibodies, prevents their morphological and biochemical differentiation (11). Recently, a role for *PC4* in muscle differentiation has been observed also *in vivo*. Muscles from mice lacking *Tis7* display decreased protein and mRNA levels of MyoD, myogenin, and laminin-alfa2 (12). Remarkably, it was observed that myofibers of *Tis7* null 24-month-old mice were reduced in diameter and number and that after muscle crash damage in young mice there was a delay in regeneration, as defined by an alteration of the isometric contractile properties of skeletal muscle. The misregulation of key regulatory proteins and the reduced regeneration occurring in adult muscles of *Tis7* null mice suggest that Tis7 plays an important role in the differentiation of adult muscle stem cells. However, no indication about the underlying molecular mechanism(s) was obtained from the knock-out experiments.

In this regard, we have recently found that *PC4* (as we refer to both the mouse and rat gene) cooperates with MyoD at inducing the transcriptional activity of MEF2C by counteracting the inhibition exerted by histone deacetylase 4 (HDAC4) on MEF2C. This relies on the ability of PC4 to bind selectively MEF2C, thus inhibiting its interaction with HDAC4 (13). Therefore, PC4 appears to act as a positive cofactor of MyoD

* This work was supported in part by Telethon Grant GGP00582, Fondo Investimenti Ricerca di Base Project RBIN04P4ET, and Progetti di Ricerca Interesse Nazionale Project 20074Z3H3N_003.
[S] The on-line version of this article (available at http://www.jbc.org) contains supplemental Figs. S1–S3.
⌘ *Author's Choice*—Final version full access.
[1] Supported by Finanziaria Laziale di Sviluppo Regione Lazio.
[2] These authors contributed equally to this work.
[3] To whom correspondence should be addressed. Tel.: 39-06-501703184; Fax: 39-06-501703313; E-mail: tirone@inmm.cnr.it.

[4] The abbreviations used are: MRF, myogenic regulatory factor; GM, growth medium; DM, differentiation medium; nt, nucleotide; rtTA, reverse tetracycline-regulated TransActivator; CT, control; TG, transgene; P, postnatal day; TA, tibialis anterior; TRITC, tetramethylrhodamine isothiocyanate; TRE, tetracycline-responsive element; HDAC, histone deacetylase; MCK, muscle creatine kinase.

(13). *MyoD* knock-out mice models indicate a unique requirement of *MyoD* during adult muscle regeneration, rather than during embryonic muscle development, where other myogenic regulatory factors can compensate (14). Remarkably, *PC4* is expressed *in vivo* in adult skeletal muscle, although it is barely detectable during embryonic development (15), which suggests a prevalent role for *PC4* in *MyoD*-dependent post-developmental myogenesis.

However, an important question still unanswered is whether *PC4* plays an active part *in vivo* as inducer of adult muscle regeneration. A second question is whether the ability of PC4 to coactivate MyoD is at the origin of the role played by *PC4* in myoblast differentiation or if other mechanisms are involved. To answer these questions, we analyzed the muscle regeneration potential of a mouse model where *PC4* was up-regulated in skeletal muscle, as well as the differentiation process of myoblasts deprived of PC4 expression through RNA interference. We observed that up-regulation of *PC4 in vivo* potentiated injury-induced muscle regeneration and that deprivation of PC4 in myoblasts led to down-regulation of *MyoD* expression, which was responsible for delayed exit from the cell cycle and impairment of terminal differentiation. Furthermore, our data reveal a novel mechanism underlying the promyogenic activity of PC4; in fact, we found that PC4 acts as a repressor of NF-κB transcriptional activity, which is known to inhibit *MyoD* mRNA accumulation. We also found that PC4 represses the activity of NF-κB by enhancing the HDAC-mediated deacetylation of the p65 subunit. Our results indicate that *PC4* can influence muscle regeneration acting as a pivotal regulator of the *MyoD* pathway through multiple mechanisms.

EXPERIMENTAL PROCEDURES

Transgene Constructs—The TRE-*PC4* construct (pUHD10-3-*PC4*) was generated by subcloning the *PC4* (rat sequence) open reading frame (ORF; 1.38 kb (16)) into the EcoRI site of pUHD10-3 (17). The 2.3-kb transgene (PacI-HindIII fragment of pUHD10-3-*PC4*, where the PacI site was added in close proximity to the XhoI site of pUHD10-3) included the *PC4* ORF under the control of seven copies of the tetracycline-responsive element (TRE), followed by the minimal cytomegalovirus (CMV) promoter (PacI-BamHI fragment) and the simian virus 40 (SV40) poly(A) site downstream of the *PC4* ORF (BamHI-HindIII fragment).

The activator transgene, CMV-*βactin*-rtTA, which produces the reverse tetracycline-regulated transactivator (rtTA) that binds and activates TRE-*PC4* in the presence of tetracycline (or of its analog doxycycline), was constructed as described previously, by cloning the rtTA sequence between the CMV enhancer/chicken β-actin promoter and the rabbit β-globin polyadenylation signal (18).

Transgenic Animals and Genotyping—The bitransgenic CMV-*βactin*-rtTA/TRE-*PC4* mouse line is the progeny of two mouse lines, each carrying a transgene as follows: the CMV-*βactin*-rtTA transgene, encoding rtTA driven by the β-actin promoter, and the TRE-*PC4* transgene, carrying the *PC4* coding region under control of TRE (see above). The bitransgenic CMV-*βactin*-rtTA/TRE-*PC4* mouse line used for experiments was isogenic, having been previously interbred for at least six generations. The TRE-*PC4* transgenic line was generated by injecting into zygotes derived from 4- to 8-week-old FVB female mice the purified 2.3-kb PacI-HindIII DNA fragment of TRE-*PC4* (5 ng/ml; see above). Injected embryos were transferred to the oviducts of pseudopregnant FVB foster females aged 2–8 months, as described previously (19). The identification of transgenic founders was conducted by PCR analysis on genomic DNA from tail tips using primers that amplified the whole transgene, being complementary to regions of the vector pUHD10-3-*PC4* upstream and downstream to the *PC4* insert (forward, 5′-CCACTCCCTATCAGTGATAG3–3′; backward, 5′-CTCATCAATGTATCTTATCATGTC-3′). Further controls were also performed by using other sets of primers internal and external to the *PC4* insert. Screening of transgenic mice for routine genotyping was performed by PCR, using the forward primer complementary to a region of the vector immediately upstream to the *PC4* insert (5′-TGACCTCCATAGAAGACACC-3′) and the backward primer within the *PC4* transgene (5′-AATCCCGTTCCTCCACAG-3′). The production and characterization of mice carrying the rtTA transgene under the control of CMV enhancer/chicken β-actin promoter have been described previously (18). Primers used to identify CMV-*βactin*-rtTA transgenic animals amplified 945 bp of the tTA transgene as follows: ftTA2 (5′-TGCTTAATGAGGTCGGAATCG-3′) and rtTA2 (5′-CCAAGGGCATCGGTAAACATC-3′).

Cardiotoxin, Histology, and Quantification of Myofibers and Satellite Cells—To evaluate the muscle regeneration process, we used bitransgenic CMV-*βactin*-rtTA/TRE-*PC4* and control mice (the progeny of bitransgenic mice that did not inherit the TRE-*PC4* transgene), and both were treated with doxycycline (2 μg/ml in drinking water) to equalize any possible effect of doxycyline on regeneration. Injury was performed on the tibialis anterior (TA) muscle of 2-month-old mice by injecting 20 μl of 10 μM cardiotoxin. Regeneration was evaluated in mice with the transgene activated by doxycycline at P30 and analyzed at P60. Mice were killed 5, 7, and 20 days after cardiotoxin injection in TA; then TA muscles were collected and embedded in OCT (Tissue-Tek; Sakura Finetek Europe, The Netherlands), and 10-μm cryosections were cut and processed for histological analysis through immunohistochemistry. At least three animals from each group (control and bitransgenic mice) per time point were analyzed. Images using a 20× lens objective were captured in three sections per group in the regenerative area, and the number of central nucleated myofibers was counted. Results are reported as the average number of fibers per area. In addition, the area of the central nucleated fibers was measured. A minimum of 2000 muscle fibers per group per time point was analyzed. Satellite cells were quantified by counting Pax7-positive cells and the total fibers in sections in the belly of the TA. Five animals for each group were analyzed. Mice were treated with doxycyline from gestation until they were killed at P45.

Isolation and Culture of Primary Myoblasts—Primary myoblasts were isolated as described by Rando and Blau (20). Briefly, adult hindlimb muscles from 2-month-old mice were minced into a coarse slurry using razor blades and enzymati-

cally digested at 37 °C in PBS 1×, 2 mg/ml collagenase/dispase (Roche Diagnostics). The slurry was passed through a 40-μm cell strainer (BD Biosciences). The filtrate was centrifuged at 350 × *g* to sediment the dissociated cells; the pellet was resuspended in growth medium, and the suspension was preplated for 2 h on noncoated dishes. The medium containing floating cells was then centrifuged, and cells were plated on collagen-coated dishes.

Primary myoblasts were grown in Ham's F-10 nutrient mixture (Invitrogen), containing penicillin (200 units/ml) and streptomycin (200 μg/ml), and supplemented with 20% fetal bovine serum (HyClone, Logan, UT) and 5 ng/ml basic FGF (PeproTech Inc., Rocky Hill, NJ). Cells were differentiated in DMEM with 5% horse serum. Tissue culture dishes were coated with 0.01% type I collagen (Sigma). Cells were grown in a humidified incubator at 37 °C in 5% CO_2.

Cell Lines—C2C12 cells from the 16th passage were obtained from H. Blau (Stanford University, Stanford, CA) and propagated in GM (Dulbecco's modified medium (DMEM) with 20% fetal bovine serum) in a humidified atmosphere of 10% CO_2 at 37 °C. Differentiation was obtained by shifting the cultures to DM (DMEM with 2% horse serum), with a change of medium every 24 h. C3H10T1/2 fibroblasts were also grown in GM or DM.

Design of siRNAs—The 19-nucleotide siRNA sequences specific to *PC4/Tis7* (*i.e.* both mouse and rat sequences) were designed by the on-line Design Tool software (MWG, Ebersberg, Germany). Candidate sequences were used to synthesize a pair of 64-mer oligonucleotides that were annealed and cloned in the pSUPER.retro.puro siRNA expression vector, according to the manufacturer's instructions (Oligoengine, Inc., Seattle) (21). The *PC4/Tis7* siRNA sequences were as follows: *PC4*/2, 5′-GAGAGCAGATGTTGGAGAA-3′; *PC4*/7, 5′-GCGCATGTATATTGATAGC-3′. The control sequence from the luciferase gene was 5′-ACGGATTACCAGGGATTTC-3′. The presence of the correct sequence cloned in pSUPER.retro.puro was confirmed by sequencing.

Generation of Recombinant Viruses and Infections—The pSUPER.retro.puro-*PC4*/2, pSUPER.retro.puro-*PC4*/7, pSUPER.retro.puro-LUC constructs, or the empty pSUPER.retro.puro vector (Oligoengine, Inc.) were transfected into the packaging Phoenix helper cells using Lipofectamine 2000 (Invitrogen). The supernatants were collected after 48 and 72 h and used for infection. C2C12 myoblasts or C3H10T1/2 cells were plated in 90-mm dishes (6×10^5 cells) and infected the first time with the viral supernatant after 24 h and then a second time after 48 h. 72 h after plating, the cells were split and selected with puromycin (2 μg/ml) in GM for 4 days. Infected cells were then reseeded to analyze protein and mRNA expression (60-mm dishes; 4×10^5 cells) and cell cycle progression (60-mm dishes; 2×10^5 cells) or for immunofluorescence staining with myosin heavy chain (MHC) (35-mm dishes; 2×10^5 cells) or for transient luciferase reporter transfection experiments (35-mm dishes; $5–7 \times 10^5$ cells).

Plasmids, Expression Vectors, and Retroviruses—pcDNA3-FLAG-*MyoD* was a gift of V. Sartorelli. pCDNA1-*MEF2C*, 4RE-luciferase, and 3×MEF2-luciferase were provided by E. Olson (22, 23). pSCT-*PC4* and HA-*MEF2C* had been previously generated by us (11, 13). pBABE-puro-*MyoD* was obtained from P. Amati, and the generation of pBABE-*MyoD* retroviruses was performed as described previously (24). pcDNA3.1-*Myc-HDAC4* was provided by T. Kouzarides and pcDNA3.1-*Myc-HDAC3* by M. A. Lazar (25).

Immunocytochemistry and Confocal Microscopy—MHC was detected by immunofluorescence staining in C2C12 cell cultures grown on 35-mm dishes and fixed for 10 min at room temperature in phosphate-buffered saline (PBS) containing 3.75% paraformaldehyde. Cells were then washed in PBS, permeabilized by a 5-min incubation in 0.2% Triton X-100 in PBS, washed in PBS, and incubated for 60 min at room temperature with the mouse monoclonal anti-MHC (Developmental Studies Hybridoma Bank, University of Iowa; clone MF20; 1:1). The antigen was revealed by fluorescein isothiocyanate (FITC)-conjugated (Jackson ImmunoResearch, West Grove, PA) secondary antibody. Immunofluorescence was observed by using an Olympus BX51 microscope (Tokyo, Japan) with a Diagnostic Instruments digital camera (model 1.3.0).

Normal and lesioned TA skeletal muscles were dissected from adult mice (2.5 months), embedded in Tissue-Tek OCT (Sakura, Torrance, CA), and frozen in liquid N_2-cooled isopentane. Immunocytochemistry of muscle was performed on serial sections cut transversely at a 9-μm thickness at −25 °C in a cryostat. Cryosections were fixed in 4% formaldehyde, quenched with 100 mM glycine, permeabilized with 0.3% Triton X-100, and blocked in PBS containing 3% normal donkey serum and 0.3% Triton X-100. Sections were then incubated overnight with an antibody against laminin (Sigma; rabbit polyclonal L9393; 1:400) diluted in blocking solution. As for Pax7 immunodetection, TA cryosections fixed in 4% paraformaldehyde were permeabilized in methanol and treated with hot 0.01 M citric acid for 10 min for antigen retrieval. Dividing muscle progenitor cells were detected by visualizing the incorporation of bromodeoxyuridine (BrdU), injected daily (95 mg/kg intraperitoneal) during 4 days before killing mice for analysis (at P10, P15, and P30). BrdU incorporation was detected following pretreatment of sections to denature the DNA, with 2 N HCl for 45 min at 37 °C and then with 0.1 M sodium borate buffer, pH 8.5, for 10 min. Afterward, sections were incubated with a rat monoclonal antibody against BrdU (Serotec, Raleigh, NC; MCA2060; 1:150).

Antigens were revealed by Cy2-conjugated donkey anti-rabbit, TRITC-conjugated donkey anti-mouse or donkey anti-rat secondary antibodies (all from Jackson ImmunoResearch). Nuclei were counterstained by Hoechst 33258. Images of the immunostained sections were obtained by laser scanning confocal microscopy using a TCS SP5 microscope (Leica Microsystems, Wetzlar, Germany). All analyses were performed in sequential scanning mode to rule out cross-bleeding between channels.

Differentiation and Fusion Index—Differentiation index and fusion index were calculated as described previously (26, 27). Differentiation index corresponded to the percent ratio of cells labeled by MHC to the total number of cells, as detected by the staining of nuclei with Hoechst 33258 dye. The fusion

index was measured as percent ratio of the number of nuclei detected in MHC-labeled cells to the total number of nuclei.

Immunoblots and Antibodies—C2C12 myoblasts and C3H10T1/2 fibroblasts, either control-infected or shRNA *PC4*-infected, or primary myoblasts from Tg *PC4* were lysed by sonication in buffer containing 50 mM Tris-HCl, pH 7.4, 150 mM NaCl, 1 mM EDTA, 0.2% Nonidet P-40, with protease inhibitors 1 mM Na_3VO_4, 10 mM 2-glycerophosphate, 10 mM NaF, 5 mM ATP, 5 mM $MgCl_2$. In experiments analyzing the protein acetylation state, deacetylase inhibitors were added (5 mM sodium butyrate and 600 nM trichostatin A). Transgenic mouse tissues were homogenized in Laemmli buffer (170 mM Tris-HCl, pH 6.8, 9% glycerol, 2.1% SDS, 4% 2-mercaptoethanol, with protease inhibitors). Proteins were electrophoretically separated by SDS-PAGE and transferred to nitrocellulose filters, as described previously (28). Immunoblots were performed hybridizing filters to the following mouse monoclonal antibodies: against PC4/Tis7 (Sigma; T2576; 1:400); myogenin (Developmental Studies Hybridoma Bank; clone IF5D7/2; 1:3); MyoD (DakoCytomation, Glostrup, Denmark; M3512; 1:500); Pax7 (Developmental Studies Hybridoma Bank; 1:1); myosin heavy chain (Developmental Studies Hybridoma Bank; clone MF20; 1:3); sarcomeric α-actin (Sigma; A2172; 1:2000); cyclin D1 (Santa Cruz Biotechnology, Santa Cruz, CA; clone 72-13G, sc450; 1:200); pRb (BD Biosciences; clone G3-245, 554136; 1:1000); α-tubulin (Sigma; clone 5C5, A2172; 1:2000); FLAG (Sigma; clone M2, F3165; 1:1000); c-*myc* tag (Santa Cruz Biotechnology; clone 9E10; 1:100); or to the following rabbit polyclonal antibodies against: MEF2C (Cell Signaling Technology Inc., Danvers, MA; 9792; 1:500); MEF2 (Santa Cruz Biotechnology; sc313; 1:200); Myf5 (Santa Cruz Biotechnology; sc302; 1:200); cyclin D3 (Santa Cruz Biotechnology; sc182; 1:200); cyclin A (Santa Cruz Biotechnology; sc596; 1:400); cyclin E (Santa Cruz Biotechnology; sc481; 1:200); p21 (Santa Cruz Biotechnology; sc397; 1:200); p65 (Santa Cruz Biotechnology; sc372; 1:1000); p65 acetyl-K310 (Abcam, Cambridge, UK; ab52175; 1:500); or goat polyclonal antibody against HDAC4 (Santa Cruz Biotechnology; sc5246; 1:200).

Immunoprecipitation—C2C12 myoblasts clone S4 grown in 90-mm dishes, transfected with *Myc-HDAC3* or pcDNA3, were lysed by sonication in buffer containing 50 mM Tris-HCl, pH 7.4, 150 mM NaCl, 1 mM EDTA, 0.2% Nonidet P-40, protease inhibitors, 1 mM Na_3VO_4, 10 mM 2-glycerophosphate, 10 mM NaF, 5 mM ATP, 5 mM $MgCl_2$, 5 mM sodium butyrate, 600 nM trichostatin A. Then 0.3 mg of total protein lysate was immunoprecipitated overnight with agarose-conjugated rabbit polyclonal anti-p65 (Santa Cruz Biotechnology; sc372AC), or with agarose-conjugated control IgG (Santa Cruz Biotechnology; normal rabbit IgG; sc2345).

RNA Extraction, Real Time RT-PCR—Total cellular RNA, obtained from tissues or cells according to the procedure of Chomczynski and Sacchi (29), was reverse-transcribed as described previously (28). Total RNA was analyzed by real time RT-PCR amplification, using TaqMan probe-based fluorogenic 5′-nuclease chemistry in duplicate samples and a 7900HT System (Applied Biosystems, Foster City, CA). Relative quantification was performed by the comparative cycle-threshold method (30). The mRNA expression values were normalized to those of the TATA-binding protein gene, used as endogenous control. Statistical analysis of mRNA expression values was performed by Student's *t* test on data normalized to the endogenous controls but not relativized in fold expression of the calibrator sample. Specific real time RT-PCR primers for mouse mRNA primers of *PC4/Tis7*, muscle and cell cycle genes, and of the endogenous controls were deduced from published murine cDNA sequences and are available on request.

Chromatin Immunoprecipitation (ChIP)—ChIP assays were carried out as described, with modifications in the procedure of sample analysis (31). Briefly, cross-linking of C2C12 cells, either infected with shRNA-expressing viruses or not, was performed with 1% formaldehyde for 10 min at room temperature. Then, chromatin was prepared from cell lysates in SDS lysis buffer (1% SDS, 10 mM EDTA, 50 mM Tris-HCl, pH 8) according to standard protocols (Upstate Biotechnology, Inc.). Cellular lysates were sonicated to obtain DNA fragments of average size of 500–700 bp and immunoprecipitated with anti-MyoD antibody (Santa Cruz Biotechnology; rabbit polyclonal M-318 sc-760), or normal rabbit serum as control. The immunoprecipitated DNA and the input DNA were analyzed in duplicate samples by real time PCR using SYBR Green PCR master mix (Applied Biosystems, Foster City, CA) and a 7900HT System (Applied Biosystems).

The amount of immunoprecipitated promoter sequence was calculated as percentage of input (ratio of the average value of the DNA detected in immunoprecipitated samples to the average value of the DNA present in input lysates; as described by Heard *et al.* (32)). For each cell treatment, we calculated in parallel the percentages of DNA immunoprecipitated by immune and normal serum. PCR primers used to amplify were as follows: (*a*) myogenin promoter (region of 140 nt before the transcription start), 5′-GGAATCACATGTAATCCACTGGAAACG-3′ and 5′-GGCTCAGGTTTCTGTGGCGTT-3′; (*b*) muscle creatine kinase (*MCK*) enhancer (region 1100 nt before transcription star; (33)), 5′-GGATGAGAGCAGCCACTACGG-3′ and 5′-CCAGGCATCTCGGGTGTCC-3′; (*c*) *PC4/Tis7* mouse promoter (region 780 nt before transcription start), 5′-TTTGCGACTGTTGATATAACTCATGTATG-3′ and 5′-CAGTTTGGAGGTCAGTTTGGGATAAG-3′; and (*d*) *NeuroD1* promoter, 5′-GTTAGAAGAGGAACTGGAAAGAGAAAGG-3′ and 5′-TGACAGAGGAGGAGGAGGAATGG-3′.

Cell Cycle Analysis—The distribution of cells in the different phases of the cell cycle was studied by using propidium iodide staining. Cells grown as described above were harvested, washed in PBS, fixed in 70% cold ethanol for at least 1 h, and after removing alcoholic fixative, stained with a solution containing 50 μg/ml propidium iodide (Sigma) and 75 KU/ml RNase (Sigma) in PBS, overnight at room temperature in the dark. Twenty thousand events per sample were acquired by using a FACScan cytofluorimeter (BD Biosciences). The percentages of the cell cycle phases were estimated on linear propidium iodide histograms by using the MODFIT software.

Luciferase Assays—C3H10T1/2 fibroblasts (either naive or infected with the retrovirus targeting *PC4*) were transfected with 4RE-LUC, *MCK*-LUC, or the 3×*MEF2*-LUC reporters, whereas C2C12 cells were transfected with the *NF-κB*-LUC reporter and with the indicated expression constructs by using the Lipofectamine reagent. The pRL-*TK* control reporter (*Renilla* luciferase driven by the thymidine kinase promoter) was included in all transfections. 48 h after transfection, luciferase assays were performed by the Dual-Luciferase reporter assay system (Promega) according to the manufacturer's instructions, as described previously (13). The luciferase activity of each sample (Li) was normalized for differences in transfection, measuring in each transfected cell extract the expression levels of *Renilla* luciferase (Ri). The normalized activity of the reporter gene was thus equal to Li × Li/Ri. The fold activity was then obtained by dividing each average normalized reporter activity value by the average normalized reporter activity units of the corresponding control culture. Statistical analysis between groups was performed by Student's *t* test on normalized reporter activity values.

Isolation of Nuclei—Nuclear extracts were obtained from C2C12 cells cultured in GM or 24 and 48 h after shift to DM, following a described protocol, with minor changes (34). Cells were trypsinized and washed in cold phosphate-buffered saline, then the cellular pellet was resuspended in 200 μl of 10 mM HEPES, pH 7.9, 10 mM KCl, 1.5 mM $MgCl_2$, 0.1 mM EGTA, and 0.5 mM dithiothreitol (DTT) on ice. Cells were passed 10 times through a 26-gauge needle and centrifuged to collect nuclei, which were subsequently resuspended in 50 μl of buffer containing 10 mM HEPES, pH 7.9, 0.4 M NaCl, 1.5 mM $MgCl_2$, 0.1 mM EGTA, 0.5 mM DTT, and 5% glycerol. Afterward, nuclei were sonicated and incubated by gentle shaking at 4 °C for 30 min. Finally, nuclear extracts were pelleted at 14,000 rpm for 5 min at 4 °C, and the supernatant was used for electrophoresis. All solutions contained protease inhibitors, 1 mM Na_3VO_4, 10 mM β-glycerophosphate, 10 mM NaF, 5 mM ATP, 5 mM $MgCl_2$, 5 mM sodium butyrate, and 600 nM trichostatin A.

RESULTS

Up-regulation of PC4 in Vivo Stimulates Skeletal Muscle Regeneration—The first question that we sought to address was whether *PC4* was able to positively control skeletal muscle regeneration *in vivo*. To this aim, we generated a bitransgenic mouse model conditionally overexpressing *PC4* in skeletal muscle. We first generated a transgene carrying the coding region of the rat *PC4* cDNA, under the control of tetracycline-responsive elements (TRE, also named TetO by Kistner *et al.* (35)), referred to as TRE-*PC4*. We obtained three transgenic (Tg) TRE-*PC4* mouse family lines (named B, G, and H).

To activate the expression of the *PC4* transgene, the Tg TRE-*PC4* B, G, and H lines were crossed with a second transgenic mouse, *i.e.* CMV-*βactin*-rtTA, carrying the reverse tetracycline transcriptional activator (rtTA) under control of the CMV enhancer/chicken β-actin promoter, whose expression is mainly restricted to skeletal muscle and heart (18). In this way, we obtained three lineages (named B, G, and H) of the bitransgenic mouse CMV-*βactin*-rtTA/TRE-*PC4* (hereafter referred to as Tg *PC4* for brevity), in which doxycycline (a tetracycline analog), administered to mice at the desired time, triggers the production of the transcription transactivator rtTA, which in turn induces the expression of exogenous *PC4* by binding to the TRE within the TRE-*PC4* transgene (Fig. 1*A*).

We monitored the expression of the *PC4* transgene in the adult skeletal muscle of B, G, and H mouse lines of Tg *PC4* at 2 months of age, following administration of doxycycline from P30. It was found that the doxycycline-dependent induction of PC4 protein expression was about 53-, 77-, and 34-fold above basal levels, respectively (as defined by densitometry, after normalization to the total amount of protein per sample; Fig. 1*B*). No evident phenotypic changes in size, weight, viability, and gross morphology were detected in the three Tg *PC4* mouse lines (data not shown). Therefore, the Tg *PC4* line G, showing the highest induction of transgenic PC4 protein in skeletal muscle, accompanied by a very low basal level of expression in the absence of doxycycline, was chosen for further analysis. In Tg *PC4* line G, the transgenic PC4 protein was greatly expressed in skeletal muscle and to a lower level in heart and liver, barely detectable in kidney, and not expressed in brain and spleen (Fig. 1*C*). An analysis of transgenic *PC4* mRNA expression in the Tg *PC4* mouse line G revealed a pattern similar to that of the PC4 protein, with the highest expression in skeletal muscle (Fig. 1*D*, *left panel*); an equivalent level of *PC4* mRNA expression was detected in tibialis anterior, extensor digitorum longus, or diaphragm muscles (*TA*, *EDL*, and *Dia*, respectively; Fig. 1*D*, *right panel*).

Next, we verified whether the up-regulation of *PC4* had any effect on the expression of muscle genes, by measuring their mRNA levels in the TA muscle of P60 bitransgenic Tg *PC4* mice treated with doxycycline since P30. We observed that the activation of the *PC4* transgene (activated Tg *PC4* mice, $n = 4$, and control Tg *PC4* mice, $n = 4$) significantly induced the mRNA levels of *MyoD* and *myogenin* (1.4-fold, $p = 0.03$, and 1.5-fold, $p = 0.01$, respectively; Fig. 2*A*). Moreover, the Tg *PC4*-activated TA muscle showed significantly increased levels of *Pax7* (3-fold, $p = 0.01$), c-*met* (1.6-fold, $p = 0.01$), *nestin* (1.4-fold, $p = 0.01$), and *Myf-5* (3-fold, $p = 0.02$). Finally, *MEF2C* and *MHC* mRNA levels were also induced following doxycycline treatment, although not significantly (1.2-fold, $p = 0.22$, and 1.7-fold, $p = 0.16$, respectively; Fig. 2*A*). Given that *Pax7*, *Myf-5*, c-*met*, and *nestin* are markers of satellite cells (36–38), our results suggest that activation of the *PC4* transgene in adult muscle leads to an increase in the number and/or activity of these cells. Indeed, although mitotically quiescent for much of the time in adult muscle, satellite cells are sporadically activated to proliferate and differentiate to provide new myonuclei for muscle homeostasis and hypertrophy (36). The possibility that the induction of *PC4* can enhance the satellite cell activity is also suggested by the observation that TA muscles from adult (P60) Tg *PC4* mice treated with doxycycline since P30 were found to contain a slightly, although significantly, lower number of myofibers per area than control TA muscles (11% decrease, $p = 0.007$; Fig. 2*B*, *histograms* on the *left*), which implies a larger fiber size.

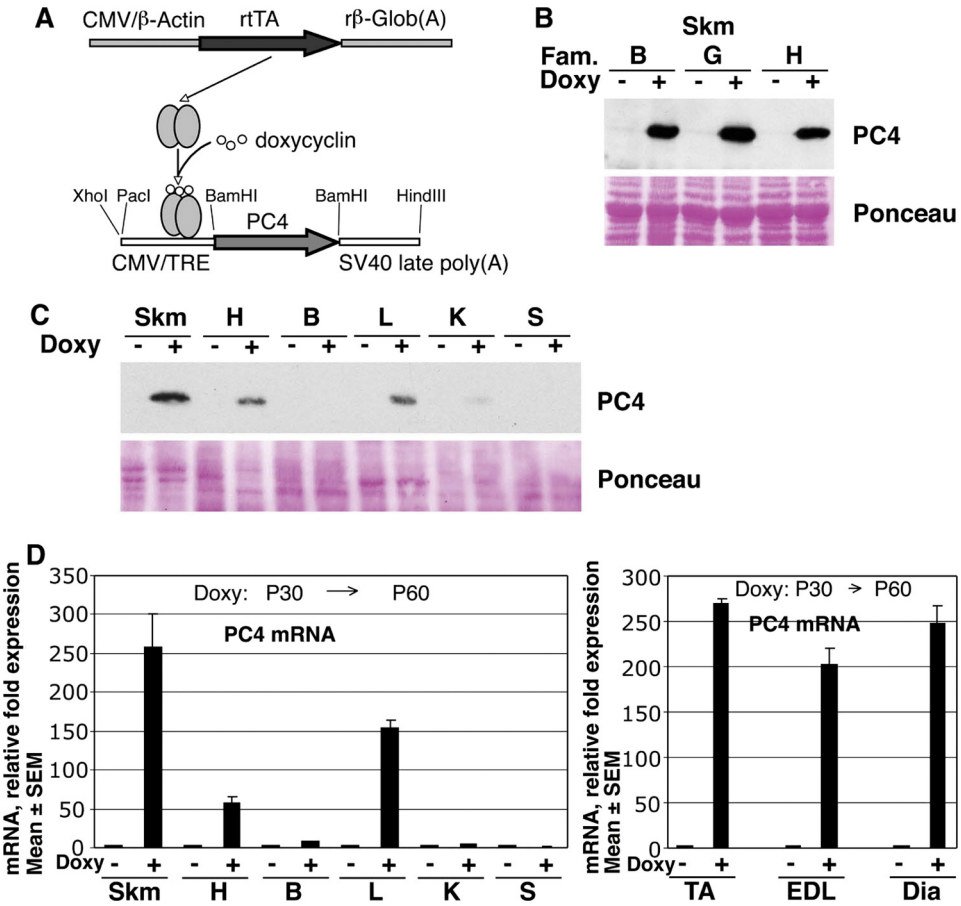

FIGURE 1. **Generation of a conditional bitransgenic mouse expressing *PC4* in skeletal muscle.** *A,* transgene CMV-*β*-*actin*-rtTA contains the CMV enhancer/chicken *β*-actin promoter, followed by the doxycycline rtTA and the rabbit *β*-globin polyadenylation site. The TRE-*PC4* transgene contains TRE fused downstream to the minimal CMV promoter, the *PC4* ORF, and the SV40 late polyadenylation site. The rtTA protein binds the TRE and activates transcription of the *PC4* transgene in the presence of doxycycline. *B,* analysis of the PC4 protein expressed in skeletal muscle by the three lines, B, G, and H, of *PC4* bitransgenic mice, activated or not with doxycycline supplied in the drinking water since P30. *C,* tissue expression analysis of the PC4 protein by Western blot. *D, PC4* mRNA by real time PCR in line G of bitransgenic mice treated or not with doxycycline (*Doxy*). *PC4* mRNA fold expression was calculated relative to the level of expression in untreated mice. Tg *PC4* mice used for experiments were 2 months old and isogenic, being the progeny of at least six generations of interbreeding. *Skm,* skeletal muscle; *H,* heart; *B,* brain; *L,* liver; *K,* kidney; *S,* spleen; *TA,* tibialis anterior; *EDL,* extensor digitorum longum; *Dia,* diaphragm.

Because satellite cells, which are generated during embryonic and fetal muscle development, are mostly active during the early postnatal period to provide myonuclei for skeletal muscle growth (36, 39), we wished also to determine the effects of an earlier induction of *PC4* on satellite cell and myofiber number in adult muscle. To maintain an enhanced expression of *PC4* throughout the time spanning embryonic and postnatal myogenesis until adulthood, we activated Tg *PC4* starting at conception until P45. It turned out that the number of satellite cells per myofiber in TA muscle of P45 Tg *PC4* mice, as determined by quantifying the $Pax7^+$ cells/myofiber, increased significantly with respect to control mice (26% increase, $p = 0.040$; Fig. 2*C*). This effect was accompanied by a significant increase in the number of myofibers per area (29% increase, $p = 0.03$; Fig. 2*B*, *histograms* on the *right*) and a reduction of myofiber cross-sectional area (25% decrease, $p = 0.0001$; supplemental Fig. S1), indicating that a net increase of the total number of satellite cells occurred. As a means to obtain more information about the origin of the *PC4*-dependent increase of satellite cells, we measured also the number of proliferating cells in muscle sections from control and Tg *PC4* mice activated since conception, at the age P10, P15, and P30. Proliferating muscle cells were labeled by injecting mice intraperitoneally with BrdU daily for 4 days preceding the day of analysis. In Tg *PC4* mice, we observed a significant increase of BrdU-positive nuclei per myofiber at P10 (36% increase, $p = 0.04$; supplemental Fig. S2, *A* and *B*), and a less pronounced increase at P15 and at P30. These data suggest an enhancement by PC4 of satellite cells activity during the early postnatal life and, altogether, are consistent with the idea that *PC4* up-regulation leads to enhanced myogenesis.

Next, we sought to assess the effects of *PC4* up-regulation on the process of muscle regeneration during adulthood, *i.e.* independently from any effect on embryonic/postnatal myogenesis. To this aim, we lesioned the TA muscle by cardiotoxin injection in P60 Tg *PC4* bitransgenic mice exposed to doxycycline since P30, and we quantified the number of regenerating fibers in time course experiments. Throughout all the experiments with the bitransgenic Tg *PC4* mouse line, we used as control mice the progeny that did not inherit the TRE-*PC4* transgene. This protocol also allowed the treatment of control mice with doxycycline, thus equalizing any possible effect on regeneration of doxycycline itself. The myofibers

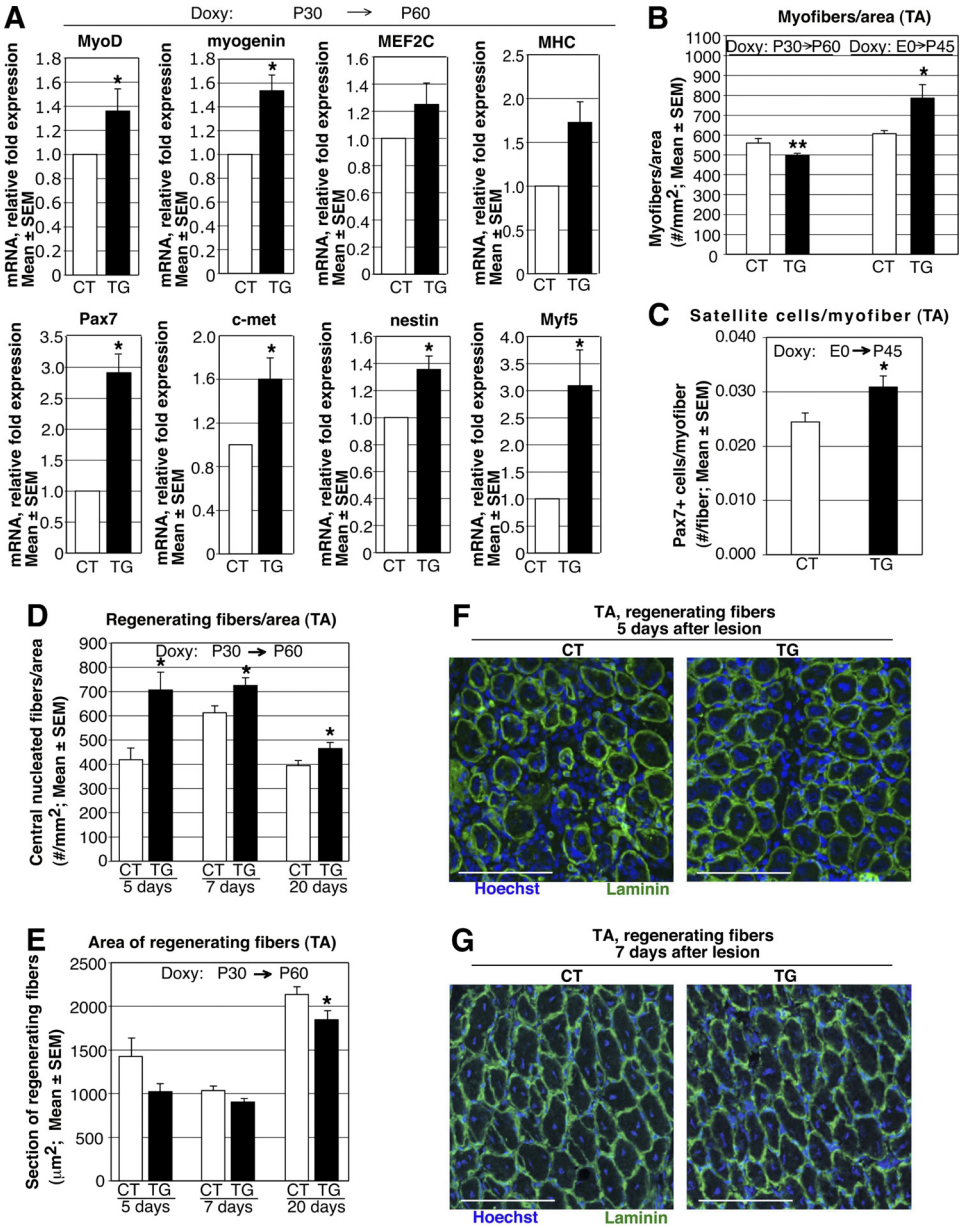

FIGURE 2. ***PC4* up-regulation in skeletal muscle increases myogenic gene expression and satellite cells number and potentiates regeneration.** *A,* induction of *MyoD, myogenin, MEF2C, MHC, Pax7, c-met, nestin,* and *Myf5* mRNA levels in TA muscle from 2-month-old Tg *PC4* mice with transgene activated since P30 (TG), relative to control mice (*CT*). $n = 3$ for each group. *B,* decrease of the number of myofibers per area in cross-sections of TA from P60 Tg *PC4* mice with transgene activated since P30 (*left*); increase of the number of myofibers per area in TA of P45 Tg *PC4* mice with transgene activated since conception (*right*). *C,* increase of the number of satellite cells, measured as $Pax7^+$ cells/myofiber in cross-sections from TA muscle of P45 Tg *PC4* mice with transgene activated since conception. The experiments shown in *B* and *C* were performed with $n = 3$ animals for both CT and TG groups. *D,* increase of the number of regenerating myofibers in TA muscle of P60 Tg PC4 mice with transgene activated at P30, identified by the presence of central nuclei. Injury was induced by injecting cardiotoxin in TA 5, 7, and 20 days before killing mice at P60 for analysis. *E,* cross-sectional area of regenerating myofibers analyzed in *D* showed a decrease in Tg *PC4* mice that became significant in the 20 days post-lesion group. $n = 3$ for CT and $n = 4$ for TG groups 5 and 7 days post-lesion; $n = 3$ for both CT and TG groups 20 days post-lesion. *, $p < 0.05$, or **, $p < 0.01$ CT *versus* the Tg PC4 mice group, Student's *t* test. *F* and *G,* representative confocal microscopy images of the regenerating myofibers at 5 and 7 days after injury, respectively. Immunofluorescence staining for laminin was used to identify the basal lamina surrounding each myofiber; nuclei were visualized by Hoechst 33258. *Bar* indicates 100 μm. *A–G,* CT mice were bitransgenic mice that did not inherit the TRE-*PC4* transgene, exposed to doxycycline (*Doxy*) as the activated bitransgenic mice (TG).

were identified by immunofluorescence staining with anti-laminin antibody, and the nuclei having central localization, an hallmark of regenerating myofibers, were detected by Hoechst 33258. We observed that the lesioned TA muscle of Tg *PC4* mice, at 5, 7, and 20 days after injury presented a number of centrally nucleated myofibers per area significantly higher than the lesioned muscle from control mice (5 days post-lesion: control $n = 3$, Tg *PC4* $n = 4$, $p = 0.016$; 7 days post-lesion: control $n = 3$, Tg *PC4* $n = 4$, $p = 0.011$; 20 days post-lesion: control $n = 3$, Tg *PC4* $n = 3$, $p = 0.03$; Fig. 2, *D*, *F,* and *G*). Consistently, the average cross-sectional area of regenerating fibers, measured in parallel in the same sections, presented in Tg *PC4* mice a tendency to decrease, with a difference from control that attained statistical significance 20 days after the lesion (5 days post-lesion, $p = 0.06$; 7 days post-lesion, $p = 0.06$; 20 days post-lesion, 13% decrease, $p =$

0.02; n = as indicated above; Fig. 2, *E–G*). As a whole, these data indicate that the capability of adult muscle to generate new myofibers following acute damage was significantly potentiated by up-regulation of *PC4*.

RNAi Knockdown of PC4 in Myoblasts Leads to Inhibition of Muscle Differentiation Genes and Induction of Cyclins—The above data establish that *PC4* acts as enhancer of postnatal and regenerative myogenesis but do not ascertain the underlying mechanism. To achieve this goal, we first considered it appropriate to extend previous analyses on the effects of *PC4* deprivation on myoblast differentiation. We targeted *PC4* by RNA interference in the C2C12 myoblast cell line, which was originally derived from satellite cells isolated from adult muscle (40). To identify a retrovirally delivered short hairpin RNA (shRNA) specifically targeting *PC4*, we analyzed several candidate 19-nt *PC4* targeting sequences designed by the MWG on-line Design Tool software (MWG, Ebersberg, Germany). The various sequences were cloned in the pSUPER.retro vector, and the corresponding retroviruses were produced in the Phoenix helper cells. C2C12 myoblasts were then infected with retroviruses expressing the different *PC4* targeting sequences or with the insertless control retrovirus and selected for resistance to puromycin. The analysis of the derived myoblast populations identified two shRNA sequences capable of silencing PC4 protein expression, albeit with different efficiencies, named RS/2 and RS/7 (Fig. 3*A*). Myoblasts infected with RS/2 or RS/7 retroviruses presented in both cases inhibition of MHC expression in cultures kept 48 h in DM, to an extent proportional to the silencing of endogenous *PC4* exerted by each shRNA.

RS/2 shRNA, which inhibited almost completely the expression of endogenous PC4 protein both in proliferating and differentiating myoblasts, was chosen for further experiments. C2C12 myoblasts infected with RS/2 retrovirus also displayed inhibition of endogenous *PC4* mRNA, as determined by Northern analysis (Fig. 3*B*).

In first place, we tested the effect of *PC4* silencing on the morphological differentiation of C2C12 myoblasts. It turned out that the number of cells expressing the late differentiation marker MHC after 72 h in DM was reduced about 40% (see Fig. 3*C*, and differentiation index, Fig. 3*D*; $p < 0.002$). In the absence of *PC4*, myoblasts in DM attained an elongated phenotype but were unable to fuse into multinucleated myotubes (Fig. 3*D*); the fusion index was indeed reduced by more than 50% (Fig. 3*E*; $p < 0.0002$).

An expression analysis of several muscle and cell cycle regulatory proteins was then carried out in C2C12 myoblasts infected with the retrovirus expressing the *PC4*-targeting shRNA, as compared with control myoblasts infected with the empty retrovirus. *PC4*-deprived myoblasts expressed reduced levels of the myogenic regulatory factors MyoD and Pax7 both in GM and DM, respectively, and accumulated decreased levels of early (myogenin, MEF2C) and late muscle proteins (sarcomeric α-actin and MHC; Fig. 4, *left panel*). In contrast, the expression of Myf-5 was induced in differentiating myoblasts lacking PC4. (Fig. 4, *left panel*). We further verified that the shRNA-dependent decrease of muscle genes was specific to the *PC4* targeting sequence, as the pSUPER retrovirus carrying an shRNA sequence targeting luciferase did not inhibit MyoD or MHC levels, similarly to what observed with the insertless virus (supplemental Fig. S3). As for the effects on cell cycle regulatory proteins, *PC4*-deprived myoblasts displayed higher levels of cyclin D1 in proliferating conditions (GM), as well as during the first 24 h in DM compared with control myoblast cultures. Also, cyclin A and cyclin E levels increased in *PC4*-depleted differentiating myoblasts, albeit less evidently than those of cyclin D1, and the retinoblastoma protein (pRb) showed a delayed kinetics of dephosphorylation. However, 48 h after the onset of differentiation, the expression of cell cycle genes attained control levels. No evident change was detected for cyclin D3 and p21 (Fig. 4, *right panel*). Together, these data indicate that *PC4*-deprived, differentiating myoblasts remain in the cell cycle for a longer period and are impaired in their terminal differentiation, as compared with control myoblasts.

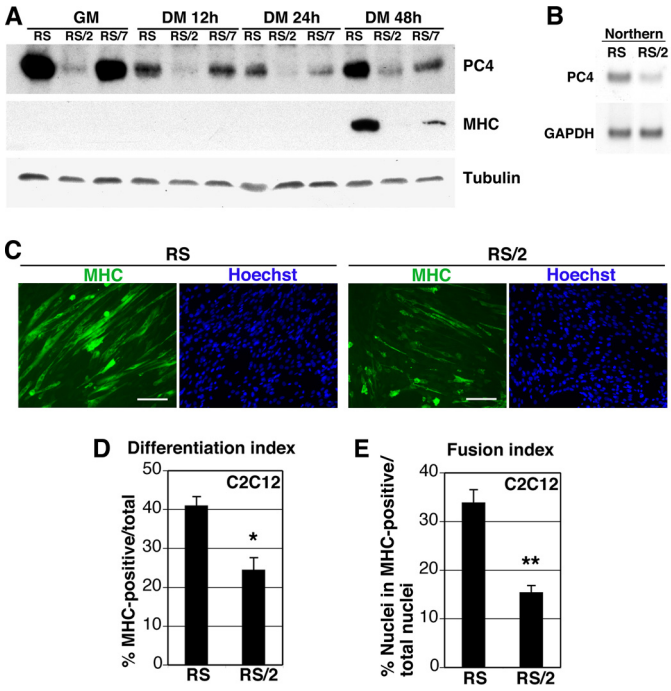

FIGURE 3. **shRNA-mediated inhibition of *PC4* expression impairs myoblast differentiation.** *A,* analysis of PC4 and myosin heavy chain (*MHC*) protein expression in proliferating (GM) or differentiating (DM) C2C12 myoblasts, infected with retroviruses generated by the pSUPER-retro vector expressing the *PC4*-specific shRNA sequences *PC4*/2 and *PC4*/7 (RS/2 and RS/7, respectively) or with the insertless retrovirus (*RS*). After infection, cells were selected for 96 h with puromycin and then cultured in proliferating (GM) or differentiating conditions (DM), as indicated. *B,* Northern analysis of C2C12 myoblasts infected with the retrovirus expressing *PC4* shRNA (*RS/2*) or with the insertless control retrovirus (*RS*). Total RNA was analyzed with a ^{32}P-labeled *PC4* or *GAPDH* probe, as a measure of the amount and integrity of the mRNA. *C,* C2C12 myoblasts, infected with the retrovirus expressing *PC4* shRNA (*RS/2*) or with the insertless control retrovirus (*RS*), were cultured in DM for 96 h; cells were then fixed and stained for immunofluorescence detection with anti-MHC antibody through secondary goat anti-rabbit FITC-conjugated antibody. Nuclei were detected by Hoechst 33258 dye (corresponding photomicrographs on the *right*). *Bar,* 140 μm. RS/2-infected cultures show a clear impairment of differentiation. Differentiation index (percentage of cells labeled by MHC) (*D*) and fusion index (percent ratio of the number of nuclei detected in MHC-labeled cells to the total number of nuclei) (*E*) were both significantly decreased. The numbers of myoblasts analyzed were 2067 and 1920 for RS- or RS/2-infected cultures, respectively. *, $p < 0.01$; **, $p < 0.001$, Student's *t* test.

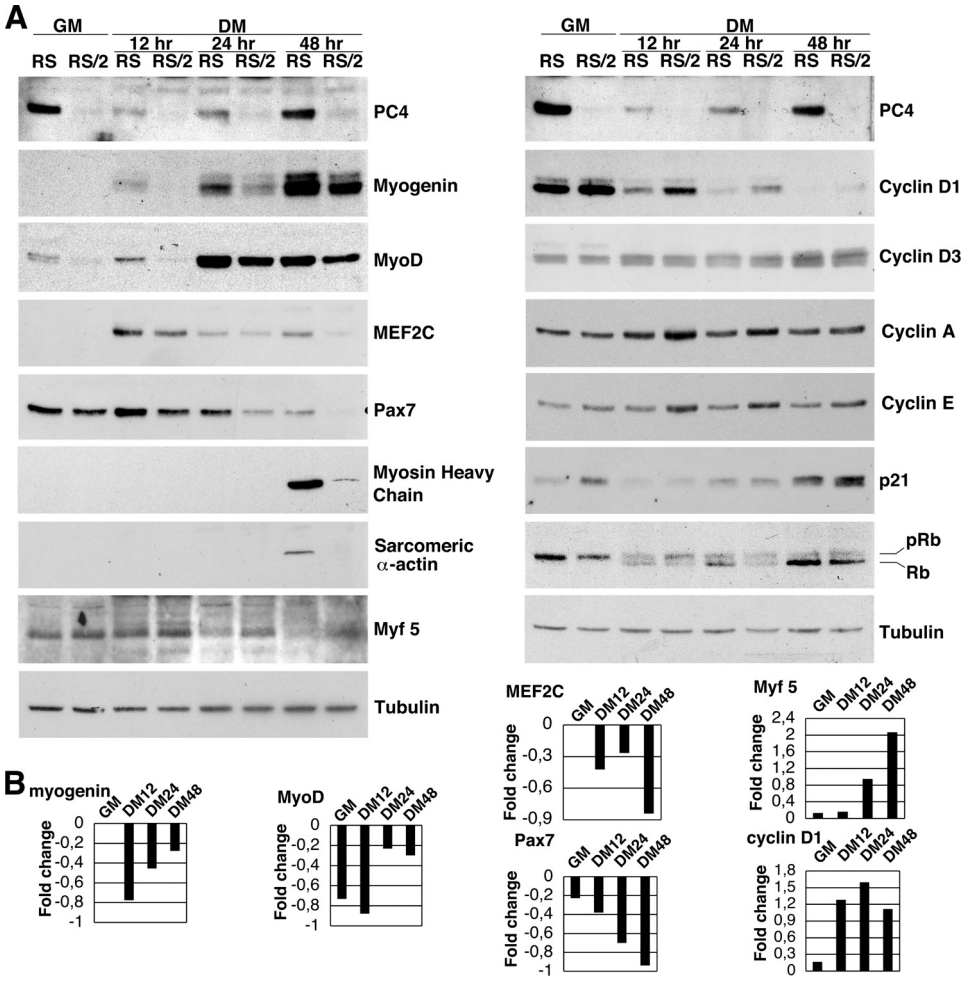

FIGURE 4. **Inhibition of muscle-specific proteins and induction of cell cycle proteins following deprivation of *PC4* in myoblasts.** *A,* expression analysis of the indicated muscle and cell cycle proteins in proliferating or differentiating C2C12 myoblasts deprived of *PC4*. Representative Western blots are shown (out of a total of three experiments). Myoblast cultures infected with the retrovirus expressing the *PC4*-targeting RS/2 shRNA or with the insertless retrovirus were selected with puromycin for 96 h and then cultured in GM or in DM for the indicated times. *B,* densitometry analysis of Western blots is shown in *A*; values are presented as fold change of protein expression in *PC4*-deprived cells relative to RS control cells, after normalization to the corresponding values of α-tubulin expression (the control base line is set to 0).

Next, we defined whether the effects elicited by *PC4* silencing occurred at the mRNA level by measuring the transcripts of muscle and cell cycle genes in C2C12 differentiating myoblasts expressing shRNA against *PC4*, compared with control myoblasts. We observed that in the absence of *PC4*, the mRNA expression of all muscle genes analyzed (*myogenin*, *MyoD*, *MEF2C*, *Pax7*, *MHC*, and *MCK*) was significantly inhibited throughout differentiation, with the exception of *Myf-5*, similarly to what was observed for protein levels (Fig. 5). In contrast, the mRNA levels of cell cycle genes were higher in myoblasts deprived of *PC4*, with a significant increase of cyclin D1 transcripts in proliferating as well as in differentiating myoblasts; such an effect, although less pronounced, occurred also for cyclin E and, to a lesser extent, for cyclin A (Fig. 5).

PC4 Deprivation Delays the Exit from Cell Cycle at the Onset of Differentiation by a MyoD-dependent Mechanism—The above results showed that *PC4* silencing in proliferating myoblasts was associated to an evident inhibition of *MyoD* and *Pax7* expression and to a concomitant increase of cyclin D1 and cyclin E levels (Figs. 4 and 5). This raised the question as to whether the absence of *PC4* affects the cell cycle genes directly or as the consequence of a primary effect on differentiation-controlling genes.

Therefore, we sought to analyze the cell cycle profile of proliferating or differentiating myoblasts lacking *PC4*, as compared with control myoblasts. No significant differences emerged between control and *PC4*-depleted proliferating (GM) myoblast populations with regard to the relative abundance of cells in the G_0/G_1, S, or G_2/M phases of the cell cycle (Fig. 6*A*). This suggests that the deprivation of *PC4* does not affect cell cycle progression. Nonetheless, when the relative abundance of G_0/G_1, S, or G_2/M phase cell populations was analyzed in differentiating cells, it turned out that in the absence of *PC4* the number of cells in the G_0/G_1 phase was significantly reduced after 12 or 24 h in differentiation medium, whereas in parallel, the S phase population was highly increased (Fig. 6*A*). Such increase of the S phase cell population became less evident after 48 h in differentiation medium. As a whole, this indicates that the progressive exit from the cell cycle was significantly delayed in differentiating myoblasts lacking *PC4.*

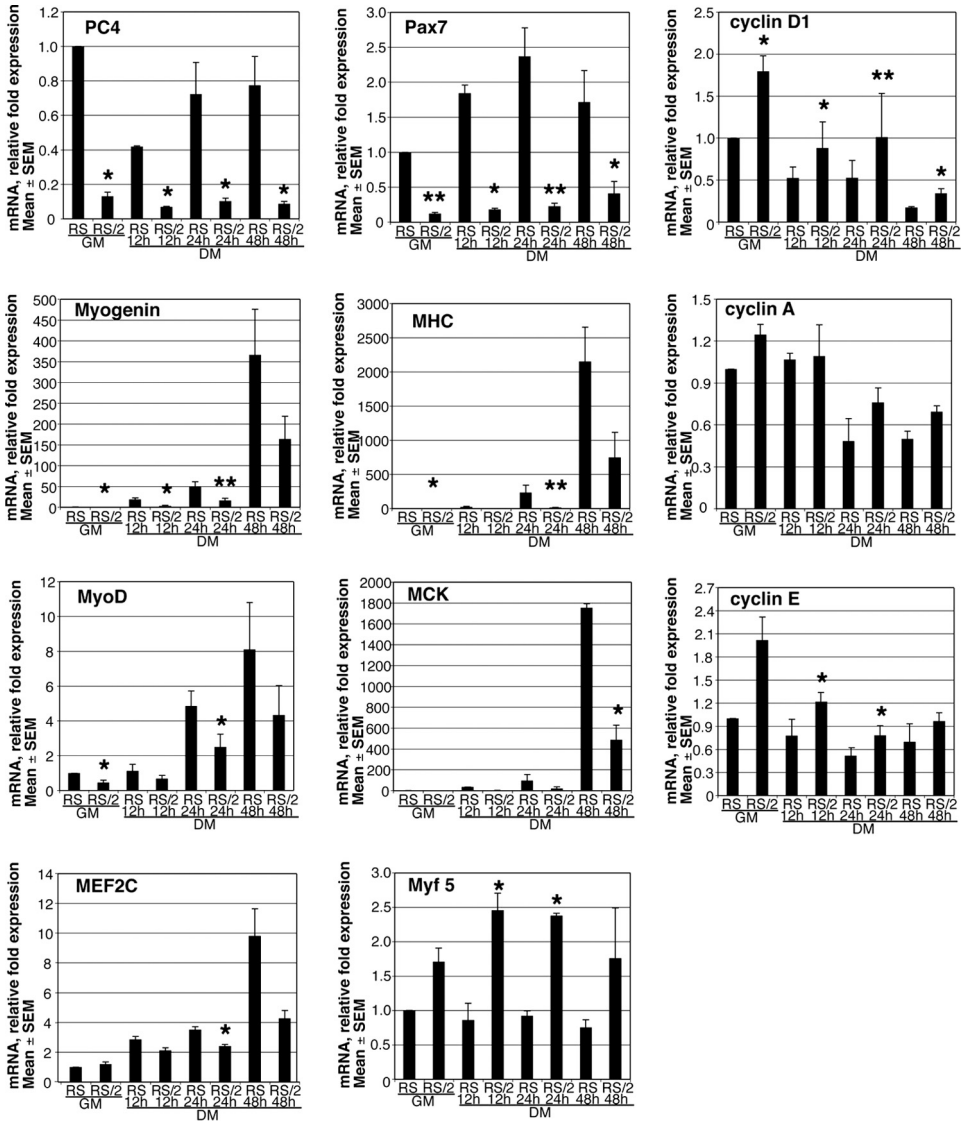

FIGURE 5. **Deprivation of *PC4* results in inhibition of muscle gene mRNA expression and enhanced expression of cell cycle genes.** Real time PCR analysis of the indicated muscle and cell cycle mRNAs from C2C12 myoblasts, infected with the retrovirus expressing the shRNA to *PC4* (RS/2) or with the control retrovirus (*RS*). Cells were cultured in GM or DM as indicated. Average ± S.E. values are from three independent experiments and are shown as fold change relative to control sample (RS-infected cells in GM), which was set to unit. TATA-binding protein mRNA was used as endogenous control for normalization. *, $p < 0.05$; **, $p < 0.01$ *versus* the corresponding time point of control-infected cells (RS), Student's *t* test.

This conclusion is consistent with the increased levels of cyclin D1 and cyclin E, which regulate the transition from G_1 to S phase (41, 42), observed in myoblasts lacking *PC4* 12 and 24 h after the shift to DM (Fig. 4). As MyoD is known to limit cell cycle progression by promoting G_1 arrest (43, 44), we asked whether the prolonged permanence in the cell cycle of *PC4*-deprived differentiating myoblasts was primarily due to the impaired expression of MyoD in these cells.

To this end, we analyzed the effect of *PC4* deprivation in C3H10T1/2 fibroblasts, either in the absence or in the presence of retrovirally transduced exogenous *MyoD* (Fig. 6, *B* and *C*). We found that in the absence of *PC4*, C3H10T1/2 fibroblasts transduced with *MyoD* showed a significant reduction of the cell population in G_0/G_1 phase 12 h after the shift to DM, although the S phase cell population was significantly increased at the same time point (Fig. 6*B*). This result is similar to that obtained in differentiating C2C12 cells (see above Fig. 6*A*). In contrast, no significant effect of *PC4* deprivation was observed in the absence of MyoD on the relative abundance of cell populations in G_1-S-G_2/M in differentiation medium (Fig. 6*C*). This suggests that the delayed exit from cell cycle of *PC4*-deprived myoblasts occurs as the consequence of *MyoD* down-regulation.

PC4 Silencing Impairs the MyoD/MEF2 Transcriptional Function—It is known that *MyoD* can positively regulate its own expression through an autoregulatory loop also involving the activity of MEF2 factors, which in turn are activated by MyoD (45, 46). Our previous data indicate that the overexpression of *PC4* potentiates the activity of *MyoD* by promoting the transcriptional function of MEF2C (13). However, key points still undefined are whether *PC4* is necessary for the activity of *MyoD* and *MEF2C* and whether there are additional pathways responsible for the action of *PC4*.

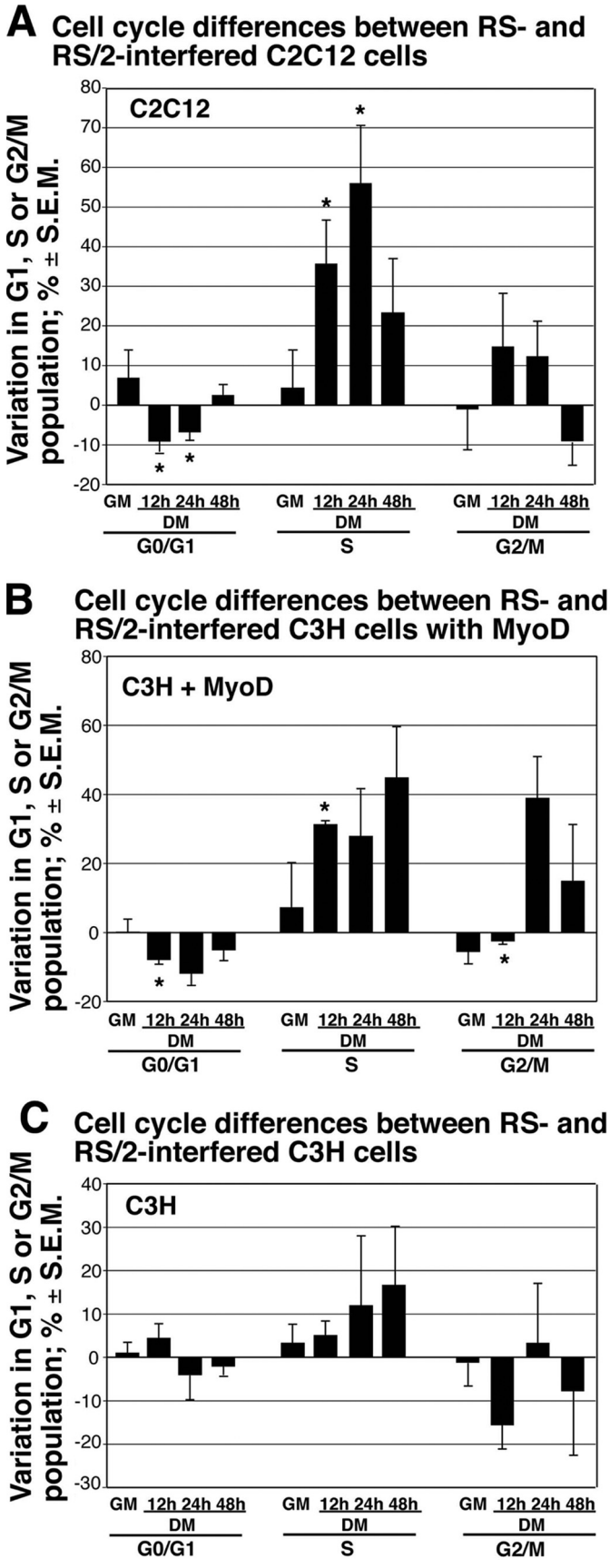

FIGURE 6. **MyoD-dependent delay of cell cycle exit in C2C12 myoblasts deprived of *PC4*.** *A,* flow cytometry analysis of proliferating or differentiating C2C12 myoblasts infected with the retrovirus expressing shRNA to *PC4* (*RS/2*) or with the control retrovirus (*RS*). The infected cells were selected with puromycin for 96 h and then cultured in GM or DM for the indicated times. The DNA content was analyzed after staining with propidium iodide, by flow cytometry. Data from five independent experiments are shown as means ± S.E. of the changes in the percentage of *PC4*-silenced cells in G_0/G_1, S, or G_2/M cycle phase, relative to the percentage of cells infected with the control virus. RS/2-infected cells show a significant decrease of the G_1, and an increase of the S population, 12 and 48 h after shift to DM. *, $p < 0.05$ *versus* the corresponding control group at the same time point, Student's *t* test. *B* and *C,* flow cytometry analysis of C3H10T1/2 fibroblasts deprived of *PC4*, induced or not to differentiate into myotubes by ectopic MyoD. C3H10T1/2 cell cultures were infected with PC4-targeting shRNA retrovirus (*RS/2*) or with control retrovirus (*RS*), selected with puromycin for 96 h, and then infected with a retrovirus expressing *MyoD* (pBABE-*MyoD*) (*B*), or infected with the control retrovirus (pBABE) (*C*). Infected cells were cultured in GM or DM as indicated. Data from three independent experiments are shown as means ± S.E. of the changes in the percentage of *PC4*-silenced cells in the different cell cycle phases, with respect to control cells. The absence of *PC4* causes cell cycle changes similar to those observed in C2C12 myoblasts only in C3H10T1/2 cells expressing *MyoD*. *, $p < 0.05$ *versus* the corresponding control group (RS-infected) of the same time point, Student's *t* test.

Thus, to test if the absence of *PC4* results in an inhibition of MyoD and MEF2 activity, reporter assays were performed in C3H10T1/2 fibroblasts expressing shRNA targeting *PC4* or in control fibroblasts, cotransfected with increasing amounts of an expression construct for MyoD (pCDNA3-FLAG-*MyoD*) and either the 4RE-LUC reporter, carrying four tandemly repeated MyoD binding sites, the *MCK*-LUC reporter, carrying *MCK* enhancer sequences containing both MyoD and MEF2-binding sites, or the 3×MEF2-LUC reporter, carrying three tandemly repeated *MEF2* sites (Fig. 7, *A–C*). It was found that the RNAi-mediated knockdown of *PC4* significantly inhibited the MyoD-mediated transactivation of all tested reporters (4RE-LUC reporter, $p = 0.04$ and 0.01; *MCK*-LUC reporter, $p = 0.02$ and 0.02; 3×*MEF*2-LUC reporter, $p = 0.04$ and 0.004, for 0.1 or 0.2 μg of cotransfected *MyoD*, respectively). However, examination of whole-cell lysates and total RNA from these transfections indicated that deprivation of *PC4* reduced both the mRNA and protein levels of the exogenous FLAG-tagged *MyoD* (Fig. 7, *D* and *E*). This unexpected evidence, although preventing us from answering specifically the initial question as to whether the transcriptional activity of MyoD was inhibited in the absence of *PC4*, revealed that PC4 may stimulate *MyoD* mRNA accumulation, which may represent a novel function of *PC4* (see below).

Furthermore, given that our previous data demonstrated that PC4 coactivates MyoD by enhancing the activity of MEF2C (13), we wished to test whether the RNAi-mediated knockdown of *PC4* could directly affect the transcriptional activity of MEF2C, independently of any effect on *MyoD*. To this aim, we performed reporter assays in C2C12 myoblasts, cultured in proliferating conditions where MyoD is inactive. Myoblasts expressing shRNA to *PC4* or control myoblasts were cotransfected with the MEF2-responsive reporter construct and vectors expressing *MEF2C* and *PC4* or *MEF2C* alone. We observed that the silencing of *PC4* significantly reduced the transactivation mediated by MEF2C alone, as well as that potentiated by PC4 ($p = 0.043$ and $p = 0.008$, respectively; Fig. 7, *F* and *F′*). To further test whether *PC4* could directly control the activity of MEF2C, we cotransfected the *MEF2*-responsive reporter and an expression construct for

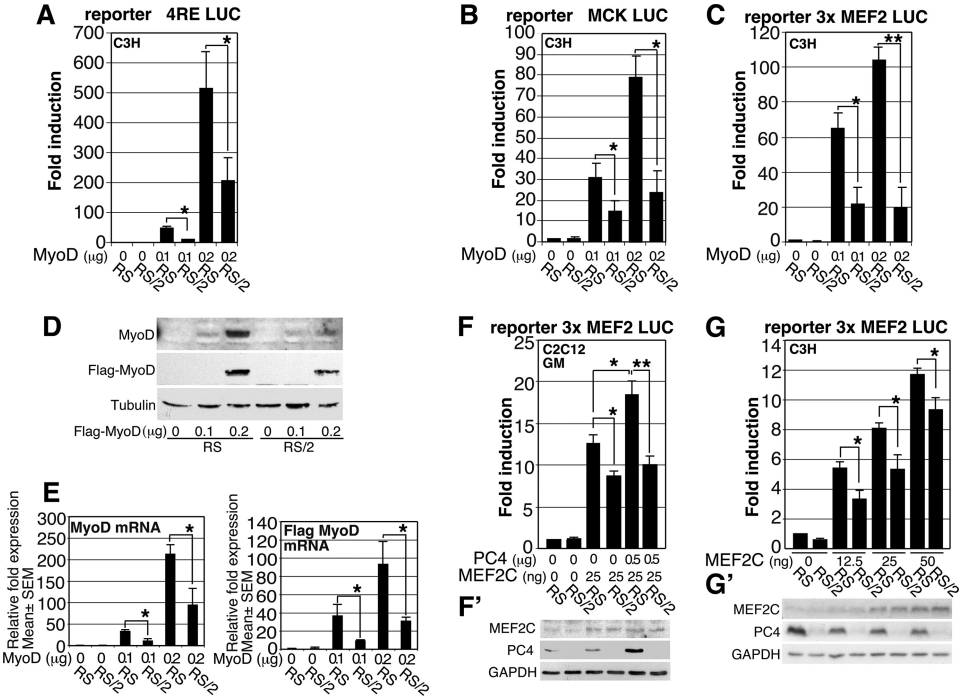

FIGURE 7. **Reduced transcriptional activity of MyoD and MEF2C in the absence of *PC4*.** *A–C,* C3H10T1/2 cell cultures were infected with the shRNA retrovirus expressing shRNA to *PC4* (*RS/2*) or the control retrovirus (*RS*); following selection with puromycin for 96 h, cells were seeded in 35-mm dishes (7×10^5) and cotransfected the next day with the pCDNA3-FLAG-*MyoD* construct (0.1 or 0.2 μg) or the empty vector and either the 4RE-LUC reporter (0.1 μg) (*A*), *MCK*-LUC reporter (0.3 μg) (*B*), or 3×MEF2-LUC reporter (0.2 μg) (*C*). After 24 h, the cultures were shifted to DM and harvested for analysis 48 h later. Luciferase (*LUC*) activity from cell extracts was expressed as fold induction relative to the activity of the RS-infected control sample not transfected with *MyoD* (that was set to unit), and it resulted in significantly reduced cultures deprived of PC4, with respect to control RS cultures. *Bars* represent the average fold induction ± S.E. determined in four independent experiments, each performed in duplicate. *, $p < 0.05$ or **, $p < 0.01$ (Student's *t* test). Parallel C3H10T1/2 cell cultures treated as above were analyzed for endogenous and exogenous MyoD protein expression by Western blot (*D*) and for *MyoD* mRNA expression by real time PCR (*E*), which is shown as average ± S.E. fold expression relative to the RS-infected control sample not transfected with MyoD, set to unit. TATA-binding protein mRNA was used as endogenous control for normalization. *, $p < 0.05$ (Student's *t* test). *F,* C2C12 cells infected with the RS/2 retrovirus targeting *PC4* or the control RS retrovirus were plated in duplicate in 35-mm culture dishes (5×10^4) and cotransfected the following day with the 3×*MEF2*-LUC reporter (0.1 μg), the pCDNA1-*MEF2C* (0.025 μg), and the pSCT-*PC4* (0.5 μg) expression vectors, as indicated. Cells were maintained in GM and harvested 48 h after transfection. Luciferase activities are expressed as fold induction relative to the activity of the RS-infected control sample not transfected with *MEF2C* or *PC4*. *Bars* represent the average fold induction ± S.E. from three independent experiments performed in duplicate. *, $p < 0.05$; **, $p < 0.01$ (Student's *t* test). *F′,* parallel cultures were analyzed for MEF2 protein expression by Western blot. *G,* C3H10T1/2 cells infected with the RS/2 or the control RS shRNA retroviruses were transfected with the 3×*MEF2*-LUC reporter (0.1 μg) and increasing concentrations of pCDNA1-MEF2C expression vector, as indicated. Cells were maintained in GM and harvested 48 h after transfection. Luciferase activities are expressed as fold induction relative to the activity of the RS-infected control sample. *Bars* represent the average fold induction ± S.E. from four independent experiments performed in duplicate. *, $p < 0.05$ (Student's *t* test). *G′,* parallel cultures were analyzed for MEF2 protein expression by Western blot.

MEF2C in C3H10T1/2 cells, which do not express *MyoD*, where *PC4* had been silenced or not. It turned out that the absence of *PC4* caused a significant reduction of the activity of the *MEF2*-responsive reporter at increasing concentrations of *MEF2C* ($p = 0.002$, $p = 0.003$ and $p = 0.004$, respectively; Fig. 7, *G* and *G′*). Therefore, the data of Fig. 7 show that the absence of *PC4* can directly impair the transactivating activity of MEF2C.

PC4 Inhibits the Activity of NF-κB by Inducing HDAC-dependent Deacetylation of p65—The above results indicated that the *PC4* silencing inhibited the levels of *MyoD* transcript in C2C12 cells (Fig. 5), as well as the MyoD levels produced from a transfected expression construct under the control of a heterologous promoter (Fig. 7, *D* and *E*). This suggested that *PC4*, besides regulating *MyoD* transcription through MEF2C, might be implicated also in a second mechanism controlling *MyoD* mRNA accumulation. Noteworthy, it has been shown that NF-κB can suppress *MyoD* expression at the post-transcriptional level through a destabilization element in the *MyoD* transcript (47). This observation raised the intriguing hypothesis that *PC4* could have an impact on *MyoD* through *NF-κB*. Thus, we investigated a possible functional interaction between PC4 and NF-κB by analyzing in C2C12 cells the effect of an overexpression or deprivation of PC4 on the transactivation potential of NF-κB. To this aim, a luciferase reporter gene fused to two tandem repeats of the κB site (2×NF-κB-LUC (48)) was transfected in C2C12 myoblasts with or without an expression vector for *PC4,* and its activity was measured in proliferating conditions (GM) or after 48 h in differentiating conditions (DM; Fig. 8*A*). We observed that the overexpression of *PC4* significantly inhibited the endogenous activity of *NF-κB*, both in proliferating and in differentiating myoblasts ($p = 0.02$ for both conditions; Fig. 8*A*, *left*). Moreover, *PC4* overexpression was also able to inhibit significantly the tumor necrosis factor α (TNF)-induced activity of *NF-κB* in proliferating but not in differentiating conditions ($p = 0.04$ and $p = 0.11$, respectively; Fig. 8*A*, *right*). The expression of equal levels of PC4 protein produced under the corresponding conditions (*i.e.* GM and DM) by the transfected *PC4* expression construct was checked by Western blot

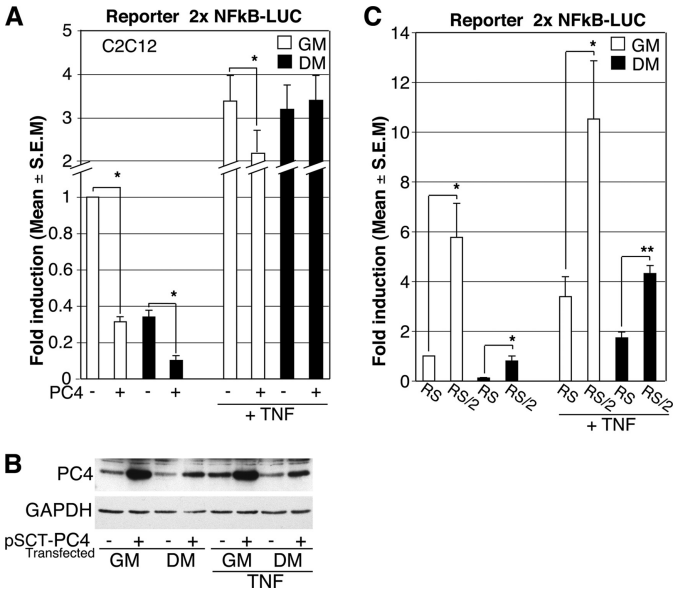

FIGURE 8. **PC4 represses the NF-κB transactivation function.** *A,* C2C12 cells were plated in duplicate 35-mm culture dishes (7×10^4 cells) and co-transfected the next day with the *NF-κB*-LUC reporter (0. 1 μg) and either the pSCT-*PC4* expression construct or the empty pSCT vector (0.5 μg). Cells were either maintained in GM or switched to DM 24 h after transfection and harvested 48 h later. TNF (10 ng/ml) was added 6 h before harvesting, where indicated. Luciferase activity from cell extracts is expressed as fold induction relative to the activity of the GM control sample (transfected with the empty vector and not treated with TNF). *Bars* represent the average fold induction ± S.E. determined from five independent experiments, each performed in duplicate. *, $p < 0.05$ (Student's *t* test). *B,* C2C12 cells transfected as in *A* were analyzed for PC4 protein expression by Western blot. *C,* C2C12 cells infected with the RS/2 retrovirus expressing shRNA to *PC4* or the control retrovirus (*RS*) were plated in duplicate 35-mm culture dishes (7×10^4 cells) and transfected the next day with the NF-κB-LUC reporter (0.1 μg). Cells were either maintained in GM or switched to DM 24 h after transfection and harvested 48 h later; where indicated, TNF (10 ng/ml) was added 6 h before harvesting. Luciferase activity is expressed as fold induction relative to the activity of the GM RS-infected control sample not treated with TNF. *Bars* represent the average fold induction ± S.E. determined from five independent experiments performed in duplicate. *, $p < 0.05$; **, $p < 0.01$ (Student's *t* test).

(Fig. 8*B*). Conversely, C2C12 myoblasts where the expression of *PC4* had been silenced by shRNA presented a significant stimulation of *NF-κB* activity both in proliferating and differentiating conditions ($p = 0.02$ and $p = 0.01$, respectively; Fig. 8*C*, *left*), also following stimulation by TNF ($p = 0.049$ in GM; $p = 0.005$ in DM; Fig. 8*C*, *right*). These findings reveal that *PC4* can function as a negative regulator of NF-κB transcriptional activity.

NF-κB consists of five members, RelA(p65), RelB, c-Rel, p50, and p52, that form homo- and heterodimers, with the p65/p50 complex being the most common. In inactive conditions, NF-κB is bound to IκB inhibitor proteins that mask its nuclear translocation signal and sequester it in the cytoplasm (49). Following phosphorylation of IκBα by IκB kinase, the p65/p50 dimers are released from IκBα and translocate to the nucleus (50, 51). The concomitant acetylation of p65 by P300/CBP acetyltransferases prevents its reassociation with the IκBα inhibitor and the ensuing nuclear export (52, 53). Therefore, the acetylation state of p65 critically controls the nuclear localization, and hence the activity, of p65. It has been shown that the p65 subunit of NF-κB is constitutively present in the nuclei of proliferating myoblasts, whereas nuclear p65 levels decline during their differentiation (54). Given that the deacetylation of p65 mediated by HDACs negatively modulates the activity of NF-κB (52, 55), and we and others demonstrated that PC4 binds HDACs (13, 56), we sought in the first place to assess whether *PC4* could enhance the HDAC-mediated inhibition of *NF-κB* activity in proliferating myoblasts. We observed that *PC4* significantly potentiated the inhibition exerted by *HDAC4* or *HDAC3* of the endogenous activity of *NF-κB* ($p < 0.05$ for both *HDACs*; Fig. 9, *A* and *B*). The amount of proteins produced by the transfected *PC4*, *HDAC4*, and *HDAC3* expression constructs was checked by Western blot (Fig. 9, *A′* and *B′*). Next, we determined by Western blot analysis of nuclear extracts the levels of nuclear p65 and its state of acetylation in proliferating or differentiating myoblasts lacking *PC4*, compared with control myoblasts. The levels of c-Jun were also determined to normalize for nuclear protein amounts, whereas those of cytoplasmic glyceraldehyde-3-phosphate dehydrogenase (GAPDH) served as control for purity of nuclear extracts (Fig. 9*C*). It was found that *PC4*-deprived myoblasts displayed increased levels of nuclear p65, acetylated in lysine 310, in either culture condition, although most evidently in proliferating myoblasts, which was accompanied by down-regulation of MyoD levels (Fig. 9*C*). This finding, together with the above reported ability of PC4 to synergize with HDACs in inhibiting NF-κB activity, strongly suggests that PC4 negatively regulates through HDACs the acetylation state of p65 and consequently its activity and localization. Notably, acetylation of p65 at lysine 310 is thought to be necessary for the full transactivation function of p65 (57).

We further checked the ability of PC4 to control the acetylation state of p65 in primary myoblasts freshly isolated from the adult muscle of Tg *PC4* mice at P45. The expression of the *PC4* transgene was induced *in vivo* since conception and was kept active in cultured myoblasts. We found that the up-regulation of *PC4* led to a decrease of nuclear p65 acetylated in lysine 310 in proliferating primary myoblasts (although in differentiating myoblasts acetylated p65 was not detectable, given the very low levels of p65 in this condition). Concomitantly, we observed an increase of MyoD levels. This result confirms that PC4 exerts a negative control on p65 acetylation and hence on its activity, in correlation with an induction of MyoD expression, and suggests that such action is effective *in vivo* (Fig. 9*D*).

Finally, we sought to investigate whether PC4 can form molecular complexes with p65 and HDAC3. To this aim, lysates of C2C12 myoblasts (clone S4 constitutively overexpressing PC4; Ref. 13) transfected with *myc-HDAC3* were immunoprecipitated with the anti-p65 antibody and subjected to Western blot analysis with an anti-PC4 antibody or with an anti-Myc antibody to reveal HDAC3. As shown in Fig. 9*E*, PC4 was found to associate with p65 in complexes also containing HDAC3, both in proliferation and in differentiation conditions (*i.e.* GM and DM). This result suggests the possibility that PC4 may stimulate p65 deacetylation by facilitating the recruitment of HDAC3 to p65.

MyoD Binds to the PC4 Gene Promoter—In a previous study, we have shown that the expression of *MyoD* in fibro-

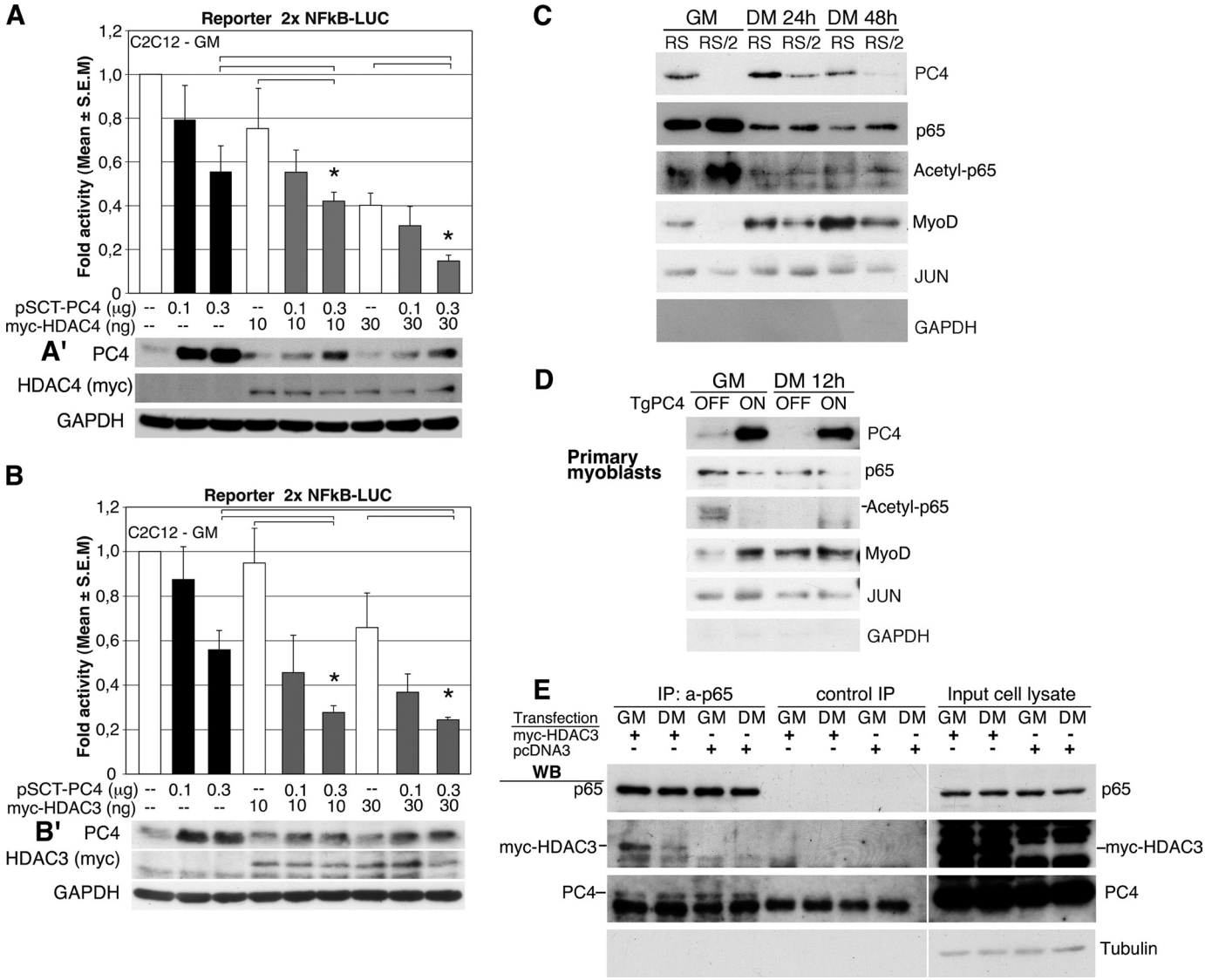

FIGURE 9. **PC4 represses the NF-κB transactivation function by promoting HDAC-dependent deacetylation of p65.** *A* and *B*, PC4 synergizes with HDAC4 or HDAC3 in inhibiting NF-κB activity. C2C12 cells, plated in duplicate 35-mm culture dishes (7×10^4 cells), were cotransfected the next day with the *NF-κB*-LUC reporter (0.1 μg), the pSCT-*PC4* (0.1–0.3 μg), and the pcDNA3-*myc-HDAC4* (10–30 ng) (*A*) or pcDNA3-myc-HDAC3 expression constructs (10–30 ng) (*B*). The pSCT and/or pcDNA3 empty vectors were included where necessary to normalize for DNA content. Cells were maintained in GM and harvested 48 h after transfection. Luciferase activity from cell extracts is calculated as fold change relative to the activity of the GM control sample transfected with the empty vectors. *Bars* represent the average fold activity ± S.E. determined from four independent experiments performed in duplicate. *, $p < 0.05$ *versus* the corresponding condition, as indicated (Student's *t* test). *A′* and *B′*, C2C12 cells transfected as in *A* and *B* were analyzed for PC4, myc-HDAC4, or myc-HDAC3 protein expression by Western blot. *C,* increased acetylation and nuclear localization of p65 in C2C12 cells deprived of *PC4*. Western blot analysis of nuclear extracts from C2C12 cells infected with the RS/2 retrovirus expressing shRNA to PC4 or the control retrovirus (*RS*), cultured in proliferating (GM) or differentiating conditions (DM 24 or 48 h). The same filter was probed with antibodies against PC4, p65, p65 acetylated at lysine 310 or MyoD, as well as c-Jun and GAPDH, markers of nuclear and cytoplasmic localization, respectively. *D,* decreased acetylation and nuclear localization of p65 in primary myoblasts isolated from adult muscle of the Tg *PC4* mouse. Nuclei were prepared from primary myoblasts derived from the Tg *PC4* mouse, cultured in proliferating (GM) or differentiating conditions (DM 12 h). *PC4* transgene was induced by administration of doxycycline to Tg *PC4* mice since conception and by addition of doxycycline to the medium (20 ng/ml) of primary myoblasts. The same filter was probed with antibodies against PC4, p65, p65 acetylated at lysine 310, MyoD, c-Jun or GAPDH. *E,* PC4 forms complexes with HDAC3 and p65. C2C12 cells (clone S4 constitutively overexpressing PC4) were transfected with pcDNA-*Myc-HDAC3* or the empty vector and cultured in GM or DM for 48 h as indicated. Cell lysates were immunoprecipitated with either anti-p65 antibody or control rabbit IgG, covalently bound to agarose beads. Immuno-complexes (*IP: a-p65* and *control IP*) and input cell lysates were analyzed by Western blotting (*WB*) with anti-Myc, anti-PC4 or anti-p65 antibodies. Input lysates: 1/15 of lysates used for immunoprecipitation.

blasts mediates the induction of *PC4* mRNA expression during the ensuing process of myogenic differentiation by stimulating the activity of the *PC4* gene promoter through a mechanism independent of MyoD binding to E-box motifs (13). We were now interested to define whether MyoD is nonetheless recruited to the *PC4* promoter. To this end we performed ChIP experiments in C2C12 myoblasts using an anti-MyoD antibody and amplifying a fragment of the mouse *PC4* gene (Tis7) promoter region. We observed that the MyoD protein was significantly recruited to the *PC4*/*Tis7* promoter, whereas the binding of MyoD to the *NeuroD1* negative control promoter was not above background levels (Fig. 10, *A* and *B*). This indicates that MyoD directly regulates *PC4* mRNA expression during differentiation. Notably, however, the MyoD protein was found to associate to the *PC4*/*Tis7* promoter not only during differentiation but also in prolifer-

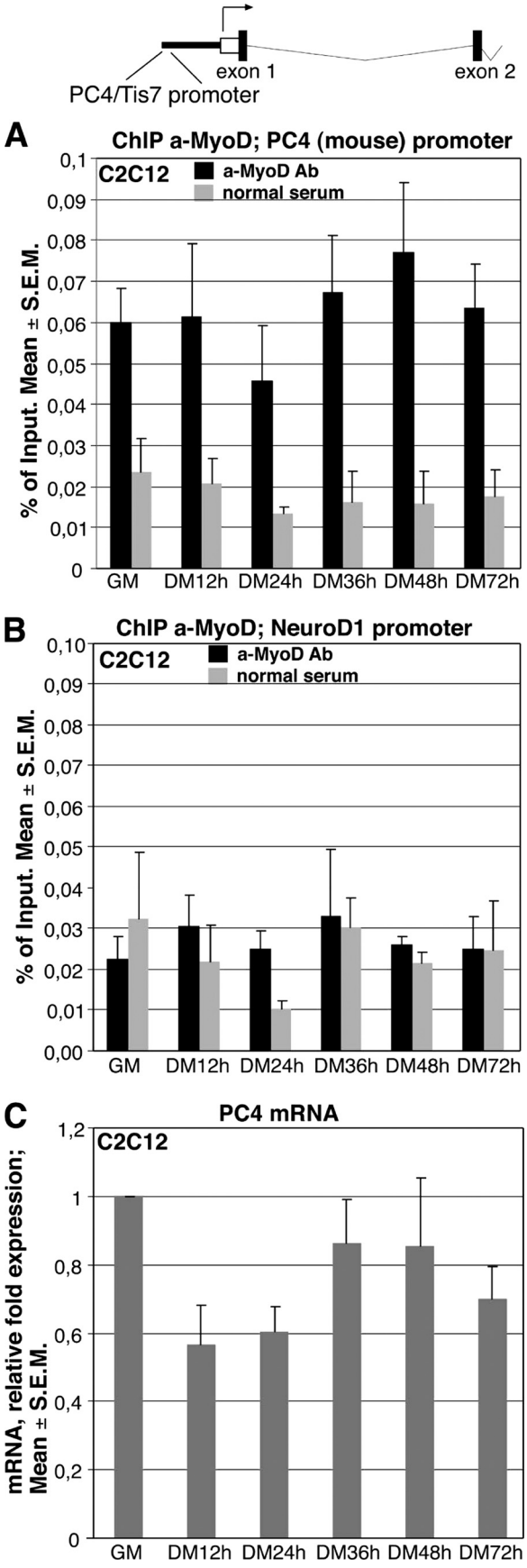

FIGURE 10. **MyoD is recruited to the *PC4* gene promoter.** *A,* ChIP analysis of MyoD binding to the mouse *PC4* promoter in proliferating (GM) or differentiating (DM) C2C12 myoblasts. The scheme *above* the graph illustrates the first exon of the mouse *PC4/Tis7* gene and the promoter region analyzed, located 780 nt before the transcription start. The amounts of *PC4* promoter region retrieved from immunoprecipitates obtained with anti-MyoD antibody (*black columns*) or with normal rabbit serum (*gray columns*) are expressed as percentage of the amounts of promoter region from input cell lysates. The same amount of chromatin was immunoprecipitated in ChIPs with a-MyoD or normal rabbit serum. *B,* ChIP analysis of MyoD binding to the *NeuroD1* promoter in C2C12 myoblasts, performed as negative control. *C, PC4* mRNA levels, detected by real time PCR in duplicate cultures of myoblasts analyzed by ChIP, expressed as fold values relative to the mRNA amount present in GM cultures. *A–C,* the average ± S.E. values are from three experiments.

ating myoblasts, *i.e.* in GM, where *MyoD* is transcriptionally inactive and *PC4* is expressed at levels similar to those of differentiating myoblasts (Fig. 10*C*). Indeed, as we have previously shown, *PC4* mRNA expression is positively regulated in proliferating conditions by serum growth factor-dependent mechanisms (13). The constitutive binding of MyoD to the *PC4* promoter suggests that *PC4* may belong to the category of genes directly activated by *MyoD* during differentiation through a feed-forward mechanism (58).

DISCUSSION

In this study, using gain and loss of function approaches, we show that *PC4* up-regulation in skeletal muscle *in vivo* stimulates regeneration and that the mechanism underlying this effect involves the control of MyoD by *PC4* through NF-κB.

In fact, in transgenic mice conditionally up-regulating *PC4* in adult skeletal muscle, we observed a significantly induced expression of *MyoD* and *myogenin* as well as that of several satellite cells markers, together with a remarkable increase of adult muscle regeneration following acute chemical damage. Conversely, the deprivation of *PC4* in adult satellite cell-derived C2C12 myoblasts produced the opposite effects, *i.e.* a dramatic impairment of myoblast fusion and greatly reduced expression of both *MyoD* and downstream differentiation markers, accompanied by an up-regulation of G_1-S cyclins, in particular cyclin D1. The induction of cyclin levels, detected in proliferating as well as differentiating conditions, led to a prolongation of the proliferative state of *PC4*-deprived myoblasts in differentiation medium. This effect was MyoD-dependent, because it was not observed in *PC4*-deprived C3H10T1/2 fibroblasts cultured in similar conditions, unless these cells were rendered myogenic through ectopic *MyoD* expression. This conclusion is consistent with the known ability of MyoD to inhibit cell cycle progression through several mechanisms, including induction of the retinoblastoma growth suppressor gene (*Rb*) and the cyclin-dependent kinase inhibitor *p21*, or its interaction with cyclin-dependent kinase 4 (CDK4) assembled to cyclin D1 (43, 44, 59–61). Furthermore, it is worth noting that proliferating $MyoD^{-/-}$ myoblasts cultured from knockout mice display increased levels of cyclins D and E that remain high after mitogen withdrawal (60), which is similar to what we observe in myoblasts expressing decreased MyoD levels as the consequence of *PC4* ablation.

Thus, the functional ablation of *PC4* in C2C12 differentiating myoblasts results in delayed exit from the cell cycle and impaired differentiation and fusion as the consequence of *MyoD* down-regulation. Furthermore, in this study we show that the down-regulation of MyoD by *PC4* relies on multiple mechanisms.

We have previously demonstrated that PC4 stimulates the transcriptional activity of MEF2C through displacement of HDAC4 from the MADS domain of MEF2C, because of its ability to bind both HDAC4 and MEF2C (13). MEF2 factors are known to participate in the autoregulatory loop exerted by MyoD on its own transcription (45, 46). Our present data indicate that the down-modulation of MyoD levels observed in the absence of *PC4* depends, at least in part, on a reduced activity of MEF2C.

Because, however, in the absence of *PC4* the most evident decrease of MyoD levels occurred in proliferating myoblasts, *i.e.* when MEF2C is not expressed (62), the deprivation of *PC4* also inhibited the levels of *MyoD* transcript produced from a transfected expression construct under the control of a heterologous promoter, and a further *PC4*-dependent mechanism controlling *MyoD* mRNA levels post-transcriptionally is conceivably operating in myoblasts. A key observation made in our study is that the deprivation of *PC4* or its overexpression in myoblasts significantly stimulates or inhibits, respectively, the transcriptional activity of NF-κB, revealing that *PC4* is a negative regulator of NF-κB. This is a noteworthy finding, because NF-κB is known to function as an inhibitor of skeletal myogenesis through several mechanisms (47, 54, 63, 64), including suppression of *MyoD* mRNA expression at the post-transcriptional level (47).

We show that *PC4* synergizes with HDAC4 and HDAC3 to inhibit the NF-κB transcriptional activity. It is known that the activity of NF-κB is critically controlled by acetylation. In particular, HDAC3, by deacetylating the p65 subunit of NF-κB, favors its binding to the IκBα repressor, with consequent nuclear export and relocalization into the cytoplasm of the p65-IκBα complex (52, 53, 55). Thus, we hypothesized that PC4 may facilitate the recruitment of HDAC3 to p65. Indeed, our immunoprecipitation experiments show that PC4 can form trimolecular complexes with HDAC3 and p65. Strong support for the idea that PC4 may favor the recruitment of HDACs to p65, thus promoting deacetylation and hence inactivation of p65, comes from the observations that primary myoblasts overexpressing transgenic *PC4* display reduced levels of acetylated p65, although deprivation of PC4 in myoblasts results in an increase of acetylated p65. In further agreement with the model proposed, we also find that overexpression of *PC4* causes a parallel decrease of nuclear p65, although the absence of *PC4* leads to accumulation of p65 in the nucleus, where p65 exerts its action. Notably, up-regulation of transgenic *PC4* in primary myoblasts induces MyoD levels in concomitance with deacetylation of p65 and a decrease of p65 levels in the nucleus, indicating that PC4 can control MyoD through p65 also *in vivo*.

In activated neutrophils, PC4 has been recently shown to associate with NF-κB p65 and HDAC1 (65). However, we identify here for the first time PC4 as a negative regulator of NF-κB activity, and in skeletal muscle this is relevant because the activation of NF-κB activity has been linked with disease states such as cachexia and various dystrophinopathies, although disruption of the NF-κB pathway inhibits skeletal muscle atrophy (66–68). In particular, a recent study has shown that in Duchenne muscular dystrophy mouse models (mdx) and patients, NF-κB signaling is persistently elevated in dystrophic muscles, and its down-regulation results in improved pathology and muscle function in mdx mice, thus implicating NF-κB as a potential therapeutic target for Duchenne muscular dystrophy (69). Thus, *PC4* may behave as a pivotal regulator of muscle differentiation and regeneration, in physiological and pathological condition, acting as an upstream regulator of MyoD levels by corepressing NF-κB activity through HDACs.

It is also noteworthy that in the absence of *PC4* Myf5 levels increase, consistently with the notion that inactivation of *MyoD* in mice leads to up-regulation of *Myf5* (70). This may only partially compensate for *MyoD* down-regulation; in fact, Myf5 appears to substitute for MyoD during embryogenesis but not during regeneration in adult muscle (14, 70).

We also provide evidence that *PC4* transcription is directly regulated by MyoD; in fact, although we have previously shown that MyoD can transactivate the *PC4* promoter, here we report that MyoD is recruited to the promoter region of the endogenous *PC4* gene (13). Altogether, these findings point to the existence of a positive regulatory loop between MyoD and *PC4*, where *PC4* links the MyoD activity to that of NF-κB and MEF2C, acting as repressor or enhancer, respectively. Given that in both cases PC4 acts through HDACs, it follows that, depending on the target to which is associated, PC4 can act as coactivator or corepressor.

Interestingly, the activation of Tg *PC4* since embryogenesis induced significant increases in the number of satellite cells (*i.e.* $Pax7^+$ cells) and myofibers in adult mice, suggesting that *PC4* is also relevant during early postnatal muscle growth. In fact, satellite cells are myogenic progenitors set apart during late fetal development to give rise to proliferating myoblasts for postnatal muscle growth, in addition to homeostasis and repair of adult skeletal muscle (36, 39). Our data also show that PC4 positively regulates the expression of *Pax7 in vivo*. It has been suggested that the expression of *Pax7* may favor the self-renewal of satellite cells (71, 72). However, because it has been shown that Pax7 acts genetically upstream of *MyoD* (71, 73, 74), it seems unlikely that the PC4-dependent increase of *Pax7* expression is mediated through *MyoD*; instead, one possibility is that up-regulation of *PC4* during embryonic and postnatal development, by enhancing the *MyoD*-dependent process of differentiation, may also trigger the activity and the renewal of the pool of satellite cells.

Considering the dramatic decrease in the number of myogenic cells occurring in muscle degenerative pathologies such as Duchenne dystrophy, our data highlighting the ability of *PC4* to potentiate the regenerative process suggest that *PC4* might be further investigated as a therapeutic target.

REFERENCES

1. Braun, T., Bober, E., Winter, B., Rosenthal, N., and Arnold, H. H. (1990) *EMBO J.* **9,** 821–831
2. Braun, T., Buschhausen-Denker, G., Bober, E., Tannich, E., and Arnold, H. H. (1989) *EMBO J.* **8,** 701–709
3. Davis, R. L., Weintraub, H., and Lassar, A. B. (1987) *Cell* **51,** 987–1000
4. Edmondson, D. G., and Olson, E. N. (1989) *Genes Dev.* **3,** 628–640
5. Miner, J. H., and Wold, B. (1990) *Proc. Natl. Acad. Sci. U.S.A.* **87,** 1089–1093

6. Rhodes, S. J., and Konieczny, S. F. (1989) *Genes Dev.* **3,** 2050–2061
7. Berkes, C. A., and Tapscott, S. J. (2005) *Semin. Cell Dev. Biol.* **16,** 585–595
8. Lassar, A. B., Davis, R. L., Wright, W. E., Kadesch, T., Murre, C., Voronova, A., Baltimore, D., and Weintraub, H. (1991) *Cell* **66,** 305–315
9. Naya, F. J., and Olson, E. (1999) *Curr. Opin. Cell Biol.* **11,** 683–688
10. Black, B. L., Molkentin, J. D., and Olson, E. N. (1998) *Mol. Cell. Biol.* **18,** 69–77
11. Guardavaccaro, D., Ciotti, M. T., Schäfer, B. W., Montagnoli, A., and Tirone, F. (1995) *Cell Growth Differ.* **6,** 159–169
12. Vadivelu, S. K., Kurzbauer, R., Dieplinger, B., Zweyer, M., Schafer, R., Wernig, A., Vietor, I., and Huber, L. A. (2004) *Mol. Cell. Biol.* **24,** 3514–3525
13. Micheli, L., Leonardi, L., Conti, F., Buanne, P., Canu, N., Caruso, M., and Tirone, F. (2005) *Mol. Cell. Biol.* **25,** 2242–2259
14. Megeney, L. A., Kablar, B., Garrett, K., Anderson, J. E., and Rudnicki, M. A. (1996) *Genes Dev.* **10,** 1173–1183
15. Buanne, P., Incerti, B., Guardavaccaro, D., Avvantaggiato, V., Simeone, A., and Tirone, F. (1998) *Genomics* **51,** 233–242
16. Tirone, F., and Shooter, E. M. (1989) *Proc. Natl. Acad. Sci. U.S.A.* **86,** 2088–2092
17. Gossen, M., and Bujard, H. (1992) *Proc. Natl. Acad. Sci. U.S.A.* **89,** 5547–5551
18. Wiekowski, M. T., Chen, S. C., Zalamea, P., Wilburn, B. P., Kinsley, D. J., Sharif, W. W., Jensen, K. K., Hedrick, J. A., Manfra, D., and Lira, S. A. (2001) *J. Immunol.* **167,** 7102–7110
19. Hogan, B., Costantini, F., and Lacy, E. (1995) *Manipulating the Mouse Embryo: A Laboratory Manual,* 2nd Ed, Cold Spring Harbor Laboratory Press, Cold Spring Harbor, NY
20. Rando, T. A., and Blau, H. M. (1994) *J. Cell Biol.* **125,** 1275–1287
21. Brummelkamp, T. R., Bernards, R., and Agami, R. (2002) *Science* **296,** 550–553
22. Molkentin, J. D., Black, B. L., Martin, J. F., and Olson, E. N. (1996) *Mol. Cell. Biol.* **16,** 2627–2636
23. Lu, J., McKinsey, T. A., Zhang, C. L., and Olson, E. N. (2000) *Mol. Cell* **6,** 233–244
24. Fimia, G. M., Gottifredi, V., Bellei, B., Ricciardi, M. R., Tafuri, A., Amati, P., and Maione, R. (1998) *Mol. Biol. Cell* **9,** 1449–1463
25. Guenther, M. G., Barak, O., and Lazar, M. A. (2001) *Mol. Cell. Biol.* **21,** 6091–6101
26. Soddu, S., Blandino, G., Scardigli, R., Coen, S., Marchetti, A., Rizzo, M. G., Bossi, G., Cimino, L., Crescenzi, M., and Sacchi, A. (1996) *J. Cell Biol.* **134,** 193–204
27. Jacquemin, V., Butler-Browne, G. S., Furling, D., and Mouly, V. (2007) *J. Cell Sci.* **120,** 670–681
28. Guardavaccaro, D., Corrente, G., Covone, F., Micheli, L., D'Agnano, I., Starace, G., Caruso, M., and Tirone, F. (2000) *Mol. Cell. Biol.* **20,** 1797–1815
29. Chomczynski, P., and Sacchi, N. (1987) *Anal. Biochem.* **162,** 156–159
30. Livak, K. J., and Schmittgen, T. D. (2001) *Methods* **25,** 402–408
31. Farioli-Vecchioli, S., Tanori, M., Micheli, L., Mancuso, M., Leonardi, L., Saran, A., Ciotti, M. T., Ferretti, E., Gulino, A., Pazzaglia, S., and Tirone, F. (2007) *FASEB J.* **21,** 2215–2225
32. Heard, E., Rougeulle, C., Arnaud, D., Avner, P., Allis, C. D., and Spector, D. L. (2001) *Cell* **107,** 727–738
33. Buskin, J. N., and Hauschka, S. D. (1989) *Mol. Cell. Biol.* **9,** 2627–2640
34. Baeza-Raja, B., and Muñoz-Cánoves, P. (2004) *Mol. Biol. Cell* **15,** 2013–2026
35. Kistner, A., Gossen, M., Zimmermann, F., Jerecic, J., Ullmer, C., Lübbert, H., and Bujard, H. (1996) *Proc. Natl. Acad. Sci. U.S.A.* **93,** 10933–10938
36. Chargé, S. B., and Rudnicki, M. A. (2004) *Physiol. Rev.* **84,** 209–238
37. Yablonka-Reuveni, Z., Day, K., Vine, A., and Shefer, G. (2008) *J. Anim. Sci.* **86,** E207–E216
38. Sartorelli, V., and Fulco, M. (2004) *Sci. STKE 2004,* re11
39. Sabourin, L. A., and Rudnicki, M. A. (2000) *Clin. Genet.* **57,** 16–25
40. Blau, H. M., Chiu, C. P., and Webster, C. (1983) *Cell* **32,** 1171–1180
41. Weinberg, R. A. (1995) *Cell* **81,** 323–330
42. Welcker, M., and Clurman, B. (2005) *Curr. Biol.* **15,** R810–R812
43. Crescenzi, M., Fleming, T. P., Lassar, A. B., Weintraub, H., and Aaronson, S. A. (1990) *Proc. Natl. Acad. Sci. U.S.A.* **87,** 8442–8446
44. Sorrentino, V., Pepperkok, R., Davis, R. L., Ansorge, W., and Philipson, L. (1990) *Nature* **345,** 813–815
45. Thayer, M. J., Tapscott, S. J., Davis, R. L., Wright, W. E., Lassar, A. B., and Weintraub, H. (1989) *Cell* **58,** 241–248
46. L'honore, A., Rana, V., Arsic, N., Franckhauser, C., Lamb, N. J., and Fernandez, A. (2007) *Mol. Biol. Cell* **18,** 1992–2001
47. Guttridge, D. C., Mayo, M. W., Madrid, L. V., Wang, C. Y., and Baldwin, A. S., Jr. (2000) *Science* **289,** 2363–2366
48. Rossi, A., Kapahi, P., Natoli, G., Takahashi, T., Chen, Y., Karin, M., and Santoro, M. G. (2000) *Nature* **403,** 103–108
49. Hayden, M. S., and Ghosh, S. (2008) *Cell* **132,** 344–362
50. Traenckner, E. B., Pahl, H. L., Henkel, T., Schmidt, K. N., Wilk, S., and Baeuerle, P. A. (1995) *EMBO J.* **14,** 2876–2883
51. Karin, M., and Ben-Neriah, Y. (2000) *Annu. Rev. Immunol.* **18,** 621–663
52. Ashburner, B. P., Westerheide, S. D., and Baldwin, A. S., Jr. (2001) *Mol. Cell. Biol.* **21,** 7065–7077
53. Chen, L. F., Mu, Y., and Greene, W. C. (2002) *EMBO J.* **21,** 6539–6548
54. Bakkar, N., Wang, J., Ladner, K. J., Wang, H., Dahlman, J. M., Carathers, M., Acharyya, S., Rudnicki, M. A., Hollenbach, A. D., and Guttridge, D. C. (2008) *J. Cell Biol.* **180,** 787–802
55. Chen, Lf, Fischle, W., Verdin, E., and Greene, W. C. (2001) *Science* **293,** 1653–1657
56. Vietor, I., Vadivelu, S. K., Wick, N., Hoffman, R., Cotten, M., Seiser, C., Fialka, I., Wunderlich, W., Haase, A., Korinkova, G., Brosch, G., and Huber, L. A. (2002) *EMBO J.* **21,** 4621–4631
57. Chen, L. F., and Greene, W. C. (2003) *J. Mol. Med.* **81,** 549–557
58. Tapscott, S. J. (2005) *Development* **132,** 2685–2695
59. Martelli, F., Cenciarelli, C., Santarelli, G., Polikar, B., Felsani, A., and Caruso, M. (1994) *Oncogene* **9,** 3579–3590
60. Kitzmann, M., and Fernandez, A. (2001) *Cell. Mol. Life Sci.* **58,** 571–579
61. Zhang, J. M., Zhao, X., Wei, Q., and Paterson, B. M. (1999) *EMBO J.* **18,** 6983–6993
62. McDermott, J. C., Cardoso, M. C., Yu, Y. T., Andres, V., Leifer, D., Krainc, D., Lipton, S. A., and Nadal-Ginard, B. (1993) *Mol. Cell. Biol.* **13,** 2564–2577
63. Guttridge, D. C., Albanese, C., Reuther, J. Y., Pestell, R. G., and Baldwin, A. S., Jr. (1999) *Mol. Cell. Biol.* **19,** 5785–5799
64. Wang, H., Hertlein, E., Bakkar, N., Sun, H., Acharyya, S., Wang, J., Carathers, M., Davuluri, R., and Guttridge, D. C. (2007) *Mol. Cell. Biol.* **27,** 4374–4387
65. Gu, Y., Harley, I. T., Henderson, L. B., Aronow, B. J., Vietor, I., Huber, L. A., Harley, J. B., Kilpatrick, J. R., Langefeld, C. D., Williams, A. H., Jegga, A. G., Chen, J., Wills-Karp, M., Arshad, S. H., Ewart, S. L., Thio, C. L., Flick, L. M., Filippi, M. D., Grimes, H. L., Drumm, M. L., Cutting, G. R., Knowles, M. R., and Karp, C. L. (2009) *Nature* **458,** 1039–1042
66. Monici, M. C., Aguennouz, M., Mazzeo, A., Messina, C., and Vita, G. (2003) *Neurology* **60,** 993–997
67. Hunter, R. B., and Kandarian, S. C. (2004) *J. Clin. Invest.* **114,** 1504–1511
68. Baghdiguian, S., Martin, M., Richard, I., Pons, F., Astier, C., Bourg, N., Hay, R. T., Chemaly, R., Halaby, G., Loiselet, J., Anderson, L. V., Lopez de Munain, A., Fardeau, M., Mangeat, P., Beckmann, J. S., and Lefranc, G. (1999) *Nat. Med.* **5,** 503–511
69. Acharyya, S., Villalta, S. A., Bakkar, N., Bupha-Intr, T., Janssen, P. M., Carathers, M., Li, Z. W., Beg, A. A., Ghosh, S., Sahenk, Z., Weinstein, M., Gardner, K. L., Rafael-Fortney, J. A., Karin, M., Tidball, J. G., Baldwin, A. S., and Guttridge, D. C. (2007) *J. Clin. Invest.* **117,** 889–901
70. Rudnicki, M. A., Braun, T., Hinuma, S., and Jaenisch, R. (1992) *Cell* **71,** 383–390
71. Zammit, P. S., Relaix, F., Nagata, Y., Ruiz, A. P., Collins, C. A., Partridge, T. A., and Beauchamp, J. R. (2006) *J. Cell Sci.* **119,** 1824–1832
72. Oustanina, S., Hause, G., and Braun, T. (2004) *EMBO J.* **23,** 3430–3439
73. Seale, P., Ishibashi, J., Holterman, C., and Rudnicki, M. A. (2004) *Dev. Biol.* **275,** 287–300
74. Relaix, F., Rocancourt, D., Mansouri, A., and Buckingham, M. (2005) *Nature* **435,** 948–953